2006

Telomere Structure and Shortening in Telomerase-Deficient Trypanosoma brucei: Implications for Anitgenic Variation

Oliver Dreesen

Telomere structure and shortening in telomerase-deficient
Trypanosoma brucei:
Implications for antigenic variation

A Thesis Presented to the Faculty of

The Rockefeller University

in Partial Fulfillment of the Requirements for

the degree of Doctor of Philosophy

by

Oliver Dreesen

June 2006

Telomere structure and shortening in telomerase-deficient

Trypanosoma brucei:

Implications for antigenic variation

Oliver Dreesen, Ph.D.

The Rockefeller University 2006

Abstract:

A variety of parasites persist in their host through sequential expression of variant surface antigens. Intriguingly, the genes encoding these antigens are frequently found adjacent to the telomeres. Telomeres are nucleoprotein complexes consisting of tandem DNA repeats and proteins that bind to them. Their function is to protect chromosome ends from the DNA repair machinery that would otherwise recognize them as double-stranded breaks. With the help of the ribonucleoprotein telomerase they compensate for the gradual sequence loss that would otherwise arise from the inability of conventional DNA polymerases to replicate chromosome ends.

In *Trypanosoma brucei,* the causative agent of African trypanosomiasis, the surface coat consists of a dense layer of Variant Surface Glycoproteins (VSG). The actively transcribed *VSG* is found in one of ~20 telomeric Expression Sites (ES). Antigenic variation can occur by transcriptional switching, reciprocal translocations, or duplicative gene conversion events between ES. In recent African isolates, duplicative gene conversion occurs at a high frequency and predominates, but the switching frequency decreases dramatically upon laboratory-adaptation. Very little is known about the regulation of antigenic variation.

To address whether telomeres are involved in antigenic switching we created telomerase-deficient *T. brucei*. Telomerase-deficient parasites exhibited progressive telomere shortening at a rate of 3–6 bp/PD, which correlates with the end replication problem and G-overhang length. Upon reaching a critical length, short silent ES telomeres stabilized. Telomere decline was accompanied by loss of minichromosomes and rearrangements at intermediate chromosomes. Essential megabase chromosomes remained stable.

After extensive telomere attrition, the active ES telomere stabilized, but the transcribed *VSG* was gradually lost from the population and replaced by a new *VSG* through duplicative gene conversion. We present a model in which subtelomeric break-induced replication-mediated repair at a short ES telomere leads to duplicative gene conversion and expression of a new *VSG*.

By restoring telomerase, we studied telomere elongation dynamics. At the active ES, the rate of telomere elongation is inversely proportional to the initial telomere length. At silent ES, the rate of elongation remains constant. We propose a model where transcription-dependent chromatin remodeling permits telomere elongation by telomerase. We show that telomere growth at a rate of 6–8 bp/PD appears to be a unique feature of *T. brucei*.

Lastly we demonstrate that fast-switching African *T. brucei* isolates have dramatically shorter telomeres than laboratory strains. We present a speculative model in which telomere growth and breakage affect the rate of antigenic switching.

To Willy and Dorly Kühnis-Schöb

Acknowledgments:

First and foremost, I thank George Cross for his unlimited support during the past few years. It has truly been a pleasure to do my graduate studies in his laboratory. George was Dean of The Rockefeller University when I was admitted to the graduate school. During my recruitment weekend, he emphasized that Rockefeller is committed to creating scientific and intellectual leaders for the future. These words stayed with me during the past years; and I hope that I came a step closer to attaining this goal. I think George is an exceptional leader, critical but fair, demanding and encouraging and always willing to discuss my ideas. George gave me complete freedom, but, at the same time, his questions and comments guided me in the right direction. He provided me with every resource necessary to pursue my studies, whether it was intellectual guidance, "ancient" African trypanosome isolates, a new computer, or an introduction to investigators around the world. Not to mention the chocolates that he brought to the lab, the margaritas or beers he treated me to at the Faculty club, and the fact that he came to cheer me on during the 2005 NYC marathon. I hope to work again with a leader as inspiring and excellent as George.

I thank Titia de Lange for her guidance during my graduate work. Over the last 15 years, a large number of breakthroughs in the telomere field took place in her laboratory. Some of these breakthroughs include the discovery of the first human telomere binding proteins and their function in chromosome end protection and telomerase regulation, the telomere end structure (t-loop), and the link between telomere dysfunction and senescence and apoptosis. Many people can do the obvious experiments, but her work is filled with creativity and imagination. This makes Titia a model scientist for me. In preparation of my FAC meetings and my thesis defense, I always tried to imagine what kind of questions she might ask me. Now that I graduated, these insightful questions will be missed – but Titia's way of doing science will always be an inspiration for me.

Table of contents:

List of abbreviations:

ES	Expression Site
ESAG	Expression Site Associated Gene
ESB	Expression Site Body
BIR	Break-Induced Replication
DSB	Double-stranded Break
IC	Intermediate Chromosomes
MBC	Megabase Chromosomes
MC	Minichromosomes
NHEJ	Non-Homologous End Joining
PD	Population Doublings
PFGE	Pulsed Field Gel Electrophoresis
RAGE	Rotating Agarose Gel Electrophoresis
TERT	Telomerase Reverse Transcriptase
TRD	Telomere Rapid Deletions
VSG	Variant Surface Glycoprotein

List of Figures:

Chapter I

Introduction

Chapter II

T. brucei telomerase, telomere shortening and G-overhang structure

Chapter III

Consequences of telomere shortening at the silent ES

Chapter I

Historical perspective of African sleeping sickness and Trypanosoma brucei

African Sleeping Sickness is caused by the protozoan parasite *Trypanosoma brucei* and kills ~100,000 people per year. Roughly 60 million people live in disease-endemic areas (1,2). Studies on Sleeping sickness commenced in the late 18th century by Captain Sir David Bruce of the British army. Bruce was born in Melbourne, Australia in 1855, trained as a bacteriologist with Robert Koch in Berlin and became a resident medical officer in Malta. In 1883, he devoted his skills to the study of Malta fever, an infection that was widespread around the Mediterranean (3). Within a few years, he succeeded in isolating the causative agent, a gram-negative, non-motile bacteria named *brucella,* from deceased patients. By culturing and infection of laboratory animals, Bruce proved that *brucella* is the causative agent of Malta fever. In 1894, to his bitter disappointment, Bruce was relocated to Pietermaritzburg in Zululand. His goal was to investigate a mysterious disease that the locals called "nagana"="loss of spirit" in ravaged cattle. After a several week journey into fly land, Bruce set up his one-man laboratory in a mud-hut on top of Umbombo hill. The laboratory was 2,000 feet above sea level and free of flies, which proved very helpful to Bruce's investigation.

First, Bruce noted the appearance of a "Haematozoa" in the blood of infected cows. Secondly, he observed that healthy cows, taken into the low country, developed the disease as did the two dogs that accompanied Bruce on his daily excursions. Upon inspection of their blood, Bruce discovered roughly 20 μm slender, flagellated parasites that "wriggle madly like little snakes". Healthy cattle fed on herbage from fly-infested lower country remained fit, putting in doubt earlier suspicions that the parasite was transmitted through infected feed. He then mapped the prevalence of infected and non-infected animals to confined geographic locations. The former were found predominantly in fly-infested bush and scrub country, whereas the latter lived in open areas with less vegetation. This finding led him to his pioneering study of the tsetse. He demonstrated that, an hour after feeding on infected cattle, a few "alive and kicking haematozoa" were present in the tsetse stomach. Tsetse that fed on infected

game animals transmitted the parasite to healthy animals, which subsequently became sick. He fulfilled Koch's postulates when he successfully infected a dog with blood from an infected antelope. Bruce demonstrated for the first time that an insect can transmit a protozoan parasite from a sick to a healthy animal. In humans the parasite causes sleeping sickness, an infection that can last from weeks to years and is fatal. During early stages of an infection, the parasite is found predominately in blood, lymph and peripheral organs. At later stages, the parasite crosses the blood-brain barrier and causes neurological disorders, including disruption of the circadian rhythm and loss of orientation, symptoms that gave the disease its notoriety and name. It remains unclear what prompts this parasite to cross the blood-brain barrier.

T. brucei gambiense is prevalent in central and western parts of Africa where it causes chronic infections. In eastern and southern areas, *T. brucei rhodesiense* causes more acute infections.

How does the parasite maintain its presence in the bloodstream of its mammalian host and successfully evade the immune response? The first clue to this puzzle came from the work of Sir Ronald Ross, who won the Nobel Prize in 1902 for proving that the anopheles mosquito is the transmitting vector of the malaria parasite, *Plasmodium falciparum*. Ross studied the parasitemia in the bloodstream of a patient in Zimbabwe during the course of an infection. He observed that the number of parasites in the bloodstream fluctuated dramatically; waves of parasitemia followed one another, until the patient died. He correctly speculated that the parasite might evade the immune response by frequently changing its surface (Ross and Thomson, 1910).

The variant surface glycoprotein surface coat

The first glimpse of the parasite surface was provided in the late 1960's (4). Electron microscopy revealed that the surface of the parasite is coated with a dense protein layer consisting of Variant Surface Glycoproteins (VSG) (Figure 1A) (5).

A)

B)

Megabase
Chromosomes
(MBC)

Intermediate
Chromosomes (IC)

Minichromosomes (MC)

$(TTAGGG)_4$

C)

ES Promoter

7 6 5 4 8a 8b 3 2 1 VSG

50 bp
Repeats

*ESAG*s

70 bp
Repeats

Telomere
Repeats
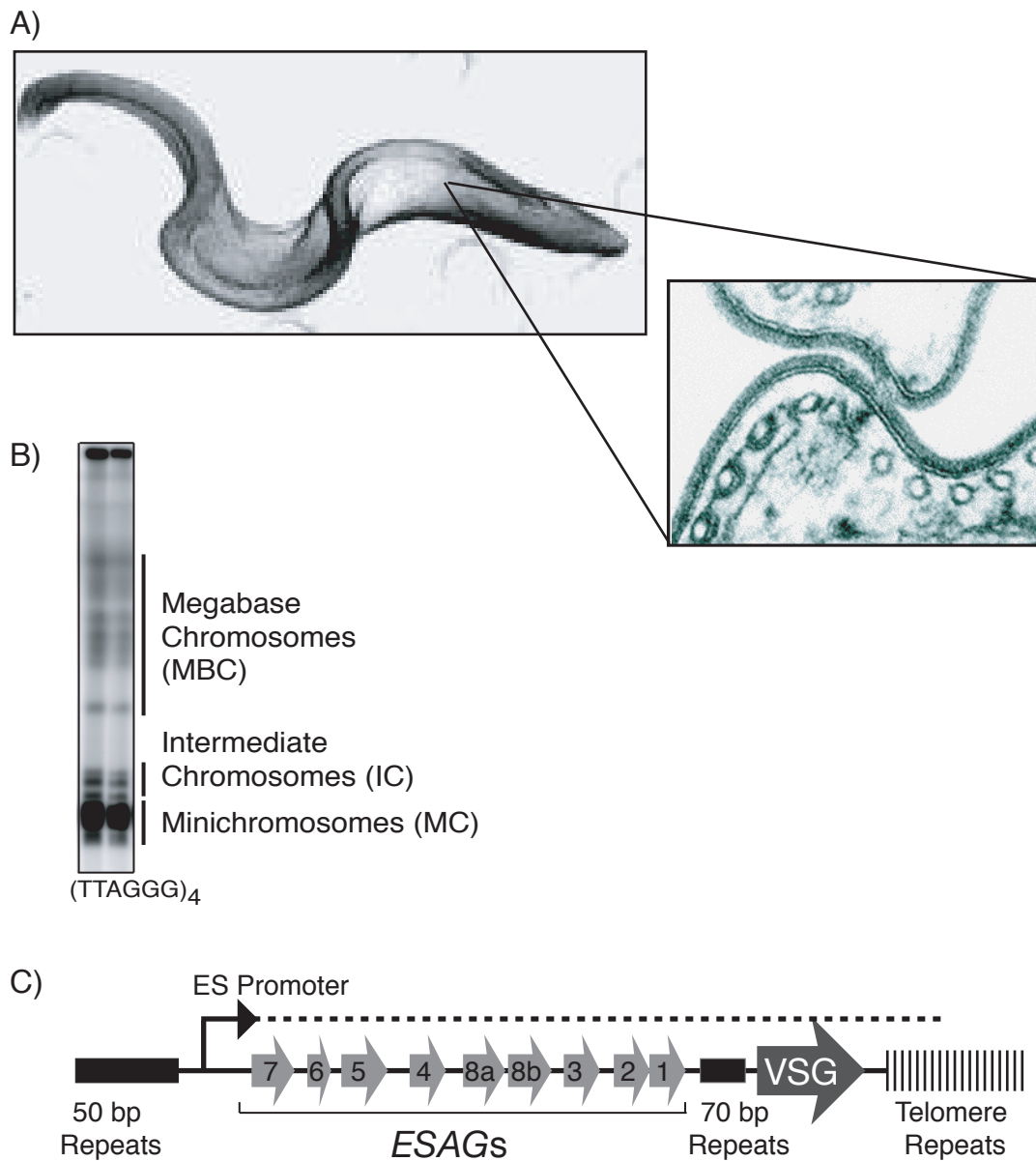
Figure 1
T. brucei, its surface coat and VSG Expression Sites (ES)

A) Upper panel: Scanning Electron Micrograph (EM) of bloodstream form *T. brucei*.
Lower panel: EM cross section. ~10^7 Variant Surface Glycoproteins (VSG) form a
dense, homogeneous surface coat.

B) *T. brucei* chromosomes, separated by Pulsed-Field Gel Electrophoresis (PFGE)
and visualized by hybridization with a $(TTAGGG)_4$ probe. Under these conditions,
11 Megabase Chromosomes (MBC) and 5-7 Intermediate Chromosomes (IC) are
well separated, whereas ~100 Minichromosomes (MC) are concentrated at the bottom
of the gel.

C) Characteristic features of *T. brucei VSG* Expression Sites (ES): ES are located at
the physical ends of chromosomes, flanked by telomeric TTAGGG-repeats. The
upstream boundary of an ES consists of 50 bp repeat arrays. Transcription is initiated
at the ES promoter. Each ES contains Expression Site Associated Genes (*ESAG*s).

Subsequent experiments suggested that the surface coat consisted of a homogenous layer of $\sim 10^7$ VSG molecules, thus, different waves of parasitemia represented different VSG (6). This work, for the first time, confirmed Ronald Ross' notion that the parasite evades the host immune response by sequential expression of different surface epitopes, a process known as antigenic variation.

Characterization of VSG proteins

Throughout the late 70's and 80's, VSG proteins were characterized in great detail, and 2.9Angstrom X-ray crystal structures exists for the N-terminal domains of two VSGs (5-7). VSGs range in size from 433 to 470 amino acids with a molecular mass of roughly 60–70 kDa. The rod-like VSG molecule contains two characteristic alpha-helices of ~70 A and the top of the molecule is formed by the ends of both helices and consists of three-stranded beta-sheets. VSG are inserted into the cell surface lipid bilayer via attachment of a glycosylphatidylinositol- (GPI) anchor (8,9). The notion that VSG are densely packed on the parasites surface came from the observation that monoclonal antibodies raised against purified VSG molecules could not be used on living trypansosomes. Thus, in a densely packed coat of rod shaped VSG molecules, most of the VSG molecule is inaccessible to the antibody whereas the top is exposed (10). The X-ray structure of VSG supports this notion.

In the early 1980's, it was estimated that the genome of *T. brucei* contains roughly 1,000 *VSG* genes, but only one is expressed at a given time (11). Most *VSG* genes lie in large arrays within the subtelomeric region, a location that is known to be a hotspot for ectopic recombination. This might ensure that *VSG* participate in recombination events, which increases antigenic diversity and prevents herd immunity (12).

The genome of T. brucei

The ~35 Mb genome of *T. brucei* consists of 11 large diploid megabase chromosomes (MBC) that range in size from 1–5.2 Mb, several intermediate chromosomes (IC)

(200–700 kB) and ~100 minichromosomes (MC) (25–150 kB) that can be readily separated by Pulsed Field Gel Electrophoresis (PFGE) (Figure 1B) (13-15). Hybridization studies and the recent sequencing of the *T. brucei* genome demonstrated that MBC contain housekeeping genes and a majority of *VSG* Expression Sites (ES). Homologous MBC pairs can differ in size up to 15%, which has been suggested to be due to repetitive sequences (16). There are ~5–7 IC that appear to contain ES and little else, and ~100 MC that mainly consist of 177-bp tandem repeats, silent *VSG* genes and telomeres (15,17,18). MC are thought to provide a reservoir of *VSG* genes that can be activated by duplicative transposition. Despite their similarity and number, MC are mitotically stable and faithfully segregate during several years of continuous propagation (19,20).

The architecture of telomeric VSG expression sites

The first clues as to how the parasite can exclusively express one VSG were provided in 1982, when it was shown that the actively expressed *VSG* is susceptible to digestion with the exonuclease Bal 31. This result demonstrated that the *VSG* is located in an Expression Site (ES) close to the chromosome end (21). Hybridization studies, using sequences upstream of the *VSG,* suggested that there might be ~14–25 conserved ES containing different *VSG*s (22). Subsequent work from several laboratories established that there are ~20 telomeric ES (23,24). ES are ~50 kB long polycistronic transcription units that are flanked by 50-bp repeats and the telomeres (25) (Figure 1C). With the exception of RsaI, these 50-bp repeats are devoid of restriction enzyme recognition sites and present in long arrays on MBC and IC (26). It remains unknown whether 50-bp repeats play any role in ES regulation, however, this topic is under investigation in our laboratory (L. Figueiredo, personal communication).

Downstream of the ES promoter are at least 8 conserved Expression Site Associated Genes (*ESAG*s) (Figure 1C) (22,25,27). The function of most *ESAG*s remains unclear, notably ESAG 1, a membrane associated glycosylated protein, ESAG 2 and 3, which have putative transmembrane domains, and ESAG 5 (28). More is known about

ESAG 4, a membrane-associated adenylate cyclase, ESAG 8, an RNA binding protein, and ESAG 10 which is not present in all ES, but could encode a putative Biopterin transporter (29-32). ESAG 6 and 7 form a heterodimeric transferrin receptor and localize to the flagellar pocket (33,34). ESAG 6 and 7 show slight sequence divergence between different ES, and it has been suggested that usage of different ES could optimize transferrin uptake from the serum of different mammals (28,35-37). The *VSG* is located ~50 kB downstream of the ES promoter and is flanked by imperfect 70-bp repeats and hexameric TTAGGG-repeats.

Monoallelic transcription of VSG ES

As mentioned above, with the exception of the *VSG* gene and the slight sequence variation among *ESAG*s, ES share the same DNA elements. However, the cell is capable of fully transcribing one of ~20 ES in a mutually exclusive fashion. Monoallelic transcription of a particular gene family is not unique to trypanosomes and has been described in several organisms. Smell is perceived by olfactory neurons, which interact with particular odorant molecules in the nasal cavity (38). Each neuron exclusively expresses one of ~1,000 G-protein-coupled olfactory receptors, which interacts with one odorant molecule and transmits the signal into the olfactory bulb (glomeruli) (39). Two main models have been discussed. First, a unique regulatory sequence upstream of the expressed receptor gene promoter could recruit the transcription machinery. Second, a transcription factor, only present in a privileged subnuclear compartment could limit expression to one gene. Alternatively, this factor could be present in limiting amounts, thus ensuring exclusivity (40). I want to highlight some similarities and differences between the two systems: *VSG* genes are transcribed from a telomeric ES, whereas olfactory receptor genes are not. A second *VSG* gene can be inserted in tandem in the active ES locus, resulting in parasites with a mixed surface coat (41). Olfactory neurons express only one gene, even if multiple copies are integrated in tandem arrays (42). The region around the promoter is conserved in all *T. brucei* ES and no particular regulatory element has been found in olfactory receptor genes.

Below, several mechanisms that could ensure transcription of a single *VSG* in *T. brucei* are discussed. It is possible that these mechanisms work in conjunction and add additional layers of regulation to ensure monoallaelic transcription.

Telomere position effect

In 1990 it was shown that subtelomeric regions of yeast chromosomes are subject to transcriptional repression: a Telomere Position Effect (TPE) (43). At some yeast chromosome ends, this repression spreads from the telomere towards the centromere and is dependent on telomere-associated factors such as Sir 2/3/4 and the Ku70/80 heterodimer (44-46). At native telomeres, silencing varies among chromosome ends and is more pronounced at confined subtelomeric region such as the core X element (47,48). TPE also exists also in *T. brucei*. A neomycin cassette under the control of an rDNA or ES promoter was inserted at different locations along a silent ES. Similarly to yeast, levels of transcriptional repression increased when the cassette was moved towards the telomeres (49). A recent result demonstrated that transcriptional repression is increased when the reporter gene was placed in the context of an ES rather than located at a short seeded telomere at the rDNA locus (50). Unfortunately, the precise genomic location of the seeded telomere was not determined in these clones. The telomere was seeded onto a broken chromosome and it is conceivable that this chromosome end was not properly sequestered into a cluster where silencing factors might be present. It was concluded that telomeres mediate repression independent of ES context, but additional repression operates within *VSG* ES (50).

In yeast, transcriptional repression extends ~5 kB towards the centromere; in *T. brucei*, the ES promoter is located ~50 kB away from the telomere, and it is unclear whether TPE is responsible for transcriptional attenuation of the ES promoter (24). Furthermore, *T. brucei* homologues of the KU70/80 heterodimer and SIR2, proteins implicated in yeast TPE, do not play any role in ES silencing in *T. brucei* (51) (Hoek and Cross, unpublished results).

Expression site body

It has been suggested that monoallelic transcription could be achieved by sequestering one ES into a subnuclear compartment that would provide essential transcription elongation factors (52).

Transcription at all ~20 ES promoters is mediated by α-amanitin resistant RNA polymerase I (53,54). At 19 silent ES, transcription ceases ~600–700 bp downstream of the promoter (24,55). In general, POL I mediated transcription is restricted to the nucleolus, where it transcribes rDNA genes. By *in situ* hybridization, active ES transcripts were found at a distinct locus outside the nucleolus, suggesting that full ES transcription might occur in a special nuclear subcompartment (52).

Further evidence to support this hypothesis was provided by raising monoclonal antibodies against the large subunit of RNA POL I. Furthermore the active ES was tagged with 256 tandem copies of the lac operator sequence in a strain that contained a tetracycline-inducible GFP-LacI fusion protein. By immuno-fluorescence microscopy, the GFP-LacI co-localized with POL I signal to a confined spot outside the nucleolus: the Expression Site Body (ESB). Taken together, these results suggest that monoallelic transcription could be achieved by sequestering the actively transcribed ES into a distinct subnuclear compartment, called the ESB (56). It remains to be determined whether this privileged compartment facilitates full ES transcription by providing factors essential for transcriptional elongation.

J-base DNA modification

During restriction mapping of various ES, it was shown that PstI and PvuII (and sometimes HindIII and SphI) restriction endonucleases only partially cleave in silent ES. It was suggested that this could be the consequence of a DNA modification that mediates silencing of ES (57,58) By hydrolysis of nuclear DNA, ^{32}P-postlabelling and two-dimensional thin layer chromatography (2D-TLC) experiments, a novel DNA base called β-D-glucosyl (hydroxymethyl) uracil was identified (59). This base,

called J, consists of a glycosylated thymine and is unique to kinetoplastid protozoan parasites. J-base is enriched in the repetitive sequences that flank every ES: the upstream 50-bp repeats and the downstream telomeres (60). Enrichment was independent of the transcriptional status of the ES. However, J is absent from the active ES, whereas in silent ES, J concentration increases closer to the telomeres.

J biosynthesis is likely to occur in two steps, involving a thymine-hydroxylase (TH) and a glucosyl-transferase (GH). The genes encoding these proteins remain to be identified. More is known about J-binding proteins (JBP1 and JBP2) (61,62). Recent work suggested that JBP2, a SWI2/SNF2-like ATPase, remodels chromatin and makes DNA accessible to TH and GH. JBP1 then binds, maintains and propagates the modification along the DNA (62). J is also present in protozoa that do not undergo antigenic variation and a possible connection between J and ES silencing in *T. brucei* remains speculative.

Chromatin structure

Early studies demonstrated that the actively expressed *VSG* gene is sensitive to DNase I and single-stranded endonuclease digestion (63,64). This hypersensitivity is possibly a consequence of the heavy transcription that occurs in the active ES locus. Hypersensitivity to DNase treatments is often indicative of *cis*-acting regulatory DNA elements (65). To test whether such elements are present in active or silent ES, a neomycin luciferase marker cassette was inserted downstream of the ES promoter (55). Cells were permeabilized and treated with increasing concentrations of micrococcal nuclease. The DNA was isolated and digested with BamHI, which produced a 50 kB fragment containing the neo gene at the 3´ end. By southern blotting using the neomycin marker gene as a hybridization probe, two hypersensitive regions were identified: one was in the core of the promoter and the other ~600 bp upstream. However, no difference was found between active and silent ES, providing further support to the idea that the transcription machinery is present at both silent and active ES promoter (24,55).

To evade the host immune response and maintain an infection, parasites must sequentially express a large repertoire of VSG. Switching of the surface coat gives rise to new variants that survive eradication by the host immune response and dominate in a successive wave of parasitemia. In the past 25 years, the molecular mechanisms underlying antigenic switching in *T. brucei* have been elucidated in some detail (Figure 2). Many antigenic switches occur concomitantly with a genomic rearrangement, such as a duplicative gene conversion (66,67). Two pieces of evidence linked the duplicated *VSG* copy to the active ES: the appearance of a duplicated band correlated with the presence of its corresponding mRNA and the duplicated copy was more sensitive to DNase digestion, suggesting a more accessible open chromatin structure (68,69). In conclusion, the duplicated copy of a silent *VSG* can replace the transcribed *VSG* in an actively transcribed ES (Figure 2A) (68).

Secondly, reciprocal translocations, often encompassing large parts of two ES, can lead to activation of a new *VSG* (70-72) (Figure 2B). Depending on which strands are cleaved during Holliday junction resolution, reciprocal and non-reciprocal (duplicative) translocations can originate from the same recombination intermediate.

Thirdly, simultaneous inactivation / activation of transcription at two ES results in an *in situ* switch and expression of a new *VSG* (Figure 2C) (72). In the context of the proposed ESB, one ES could simply replace another in this privileged compartment.
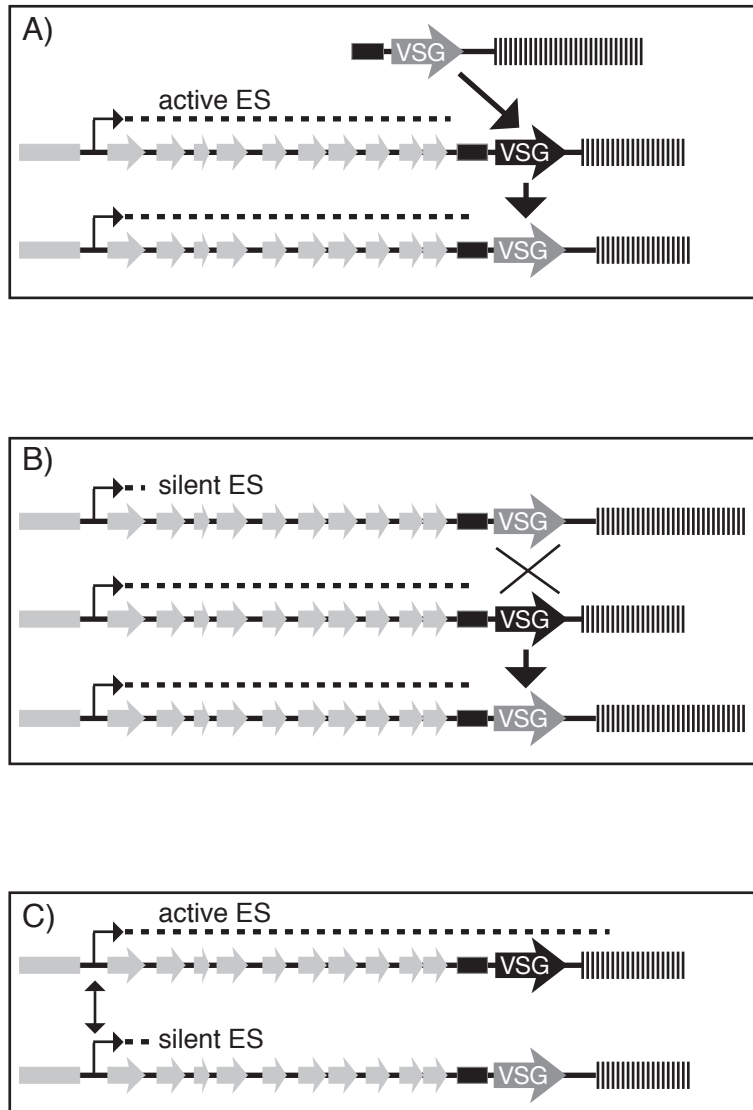
Figure 2

Molecular mechanisms underlying antigenic variation

A) Duplicative gene conversion of a silent *VSG* into the transcribed ES

B) Telomere exchange: reciprocal translocation between silent and active ES

C) Transcriptional switching between two ES

It remains heavily debated which of the three mechanisms dominates or is most relevant to wild-type trypanosomes. Arguably the most extensive analysis to address this question comes from David Barry's lab (73). This study established that in pleomorphic wild-type isolates, 10 out of 11 antigenic switches occurred through duplicative gene conversion (Figure 2A). Although the number of analyzed clones might limit the interpretability of this result, it is the most extensive study that analyzed switching in a "wild-type" setting.

Methods to measure antigenic variation

Perhaps the most pressing question in trypanosome biology in the past several years is what regulates the frequency of antigenic variation. This question remains largely unanswered, in part because of experimental difficulties to efficiently measure the VSG switching rates. Essentially all available methods aim to selectively kill parasites expressing a particular VSG in a clonal population. Several methods have been developed to achieve this.

First, laboratory mice can be immunized by exposure to a particular VSG. This can be achieved by infecting the mouse with a sub-lethal number of parasites expressing a particular VSG or by injection of purified VSG protein (74). Subsequently, vaccinated mice are challenged with a clonal population of parasites expressing the VSG used for immunization. The immune system selectively kills all parasites that have not undergone an antigenic switch and switchers can be outgrown in mice or *in vitro* (70,75). From the number of infected mice, the frequency of switching can be deduced.

Secondly, negative selection against a particular VSG can be achieved by *in vitro* complement-mediated immuno-lysis, using a specific antibody against the expressed VSG (75-78). Nevertheless, parasites that aggregate in clumps can survive this treatment and give rise to false positives (79). In both cases, the procedure is laborious and difficult, requiring numerous repetitions to achieve statistical significance.

A third negative selection procedure is to place the thymidine kinase thymidylate kinase (TK) gene from the herpes simplex virus (HSV-1) downstream of the promoter of the active ES. TK phosphorylates nucleoside analogs that can be added to the culture medium and kill cells by competitive inhibition of DNA polymerase (78,80). Thus, addition of nucleoside analogs selects for parasites that have switched off the ES that contains the TK gene. Although activation of another ES occurred, in 70% of switching events studied, this selection procedure led to an aberrant loss of the TK gene and the active ES (and in most cases the 50-bp repeat arrays). The minority (18%) of switched parasites had activated another ES by *in situ* switching. Since the switching frequency in these parasites was relatively high (10^{-5}/ cell division) the authors argued that inactivation of the active ES is an essential step for the activation of another (78). Regardless, the relevance of these findings is questionable since such aberrant switching events have not been observed in nature.

A recent report employed RNAi against the actively transcribed *VSG* to select for switched parasites (81). Although in principal a very elegant idea, the reported switching frequency was dramatically higher than anticipated (10^{-4}/ division). Several groups, using different techniques consistently obtained much lower switching rates for the same strain (10^{-6}–10^{-7} / division) (74-76,82). These discrepancies should be resolved before this method can be used.

Positive selection for switched parasites can be achieved by insertion of a drug resistance marker into a silent ES (82). Subsequent exposure of the parasites to high drug concentrations selects for parasites that have activated the marked ES. This method has been used widely by us and other labs, yet the procedure could result in a lower switching frequency since activation of only one out of ~20 operational ES is selected for (82-84).

Despite these difficulties, deletion of genes implicated in DNA repair / recombination have been tested for their effect on antigenic switching. Mre11 or KU70/80-deficient

parasites did not exhibit a decreased rate of antigenic switching (85,86). An exception was the deletion of Rad51, a protein involved in strand invasion between homologous sister chromatids (87). Deletion of *T. brucei* Rad51 decreased the rate of antigenic switching by roughly 10-fold (88). Although the reduction in switching was mild and results varied between experiments, it is the only report where deletion of a gene affected antigenic variation. The mild phenotype could be explained by the fact that the genome of *T. brucei* contains 5 other Rad51 homologues, which might partially compensate for the deletion of one (89). Further studies using double mutants of Rad51 homologues might clarify their role during gene conversion-based antigenic switching.

In contrast to the decrease of antigenic switching in Rad51-deficient *T. brucei*, deletion of the VSG co-transposed region (CTR) caused a dramatic increase in antigenic switching (76). This result led to the speculation that the CTR could alter chromatin structure and destabilize the active ES.

Antigenic variation in wild-type African isolates versus laboratory-adapted strains

The frequency of antigenic variation differs dramatically between African pleomorphic wild-type isolates and laboratory-adapted strains. African isolates switch at a rate of 10^{-2}–10^{-4}/ cell division, whereas laboratory-adapted strains undergo antigenic variation at ~10^{-6}–10^{-7} / cell division (74,82,90,91). The high switching frequency of pleomorphic strains was not suitable for investigators to study the molecular mechanisms underlying antigenic switching. Thus, African isolates were subjected to rapid syringe passaging, a procedure during which parasites are grown in laboratory mice in the absence of any immune selection (90). Repeated mouse passaging over several months led to parasites that had a 10,000-fold reduction in switching frequency and became optimized to grow in laboratory mice (92). These experiments were confirmed with several wild-type strains, excluding the possibility that switch reduction is due to genetic differences among wild-type isolates (75,90,91). To this day, the molecular changes that occur during rapid syringe passaging have not been addressed. Identification and characterization of these

14

changes are crucial for improving our understanding of the regulatory machinery that drives antigenic variation.

Expression of surface antigens at telomeric expression sites – a coincidence?

The expression of variant surface proteins from telomeric ES is not restricted to *T. brucei*. Several other parasites, such as *P. falciparum* (the causative agent of malaria), *B. burgdorferi* (lyme disease) and *P. carinii* (pneumonia) transcribe extracellular or environmental sensing proteins from telomeric expression cassettes (93-95). Why are these surface antigens expressed from telomeric ES and do telomeres play a role in regulating antigenic variation? Subtelomeric regions are known to be a hotspot for recombination (96). Frequent recombination among members of a gene family creates diversity and increases the organisms chance to successfully adapt to a new environment.

Telomeres and telomere structure: t-loop

Telomeres ("telos" from the Greek word "far away" or "at end") are the physical ends of linear chromosomes. *Tetrahymena* chromosome ends were the first to be sequenced and are capped by tandem arrays of TTGGGG (97). Six years later the sequence of *T. brucei* telomeres was elucidated. Like their human counterparts, they consist of ~5–15 kB of TTAGGG repeats (98,99).

In the last decade, several structural features of telomeres have been identified. By electron microscopy, it was demonstrated that telomeres from mouse and human cells form a terminal loop structure called t-loop (100). During t-loop formation the telomere terminus loops back and invades the duplex telomere repeat array (Figure 3A). t-loops are conserved in *T. brucei*, in micronuclear DNA of *Oxytricha fallax* and

A)
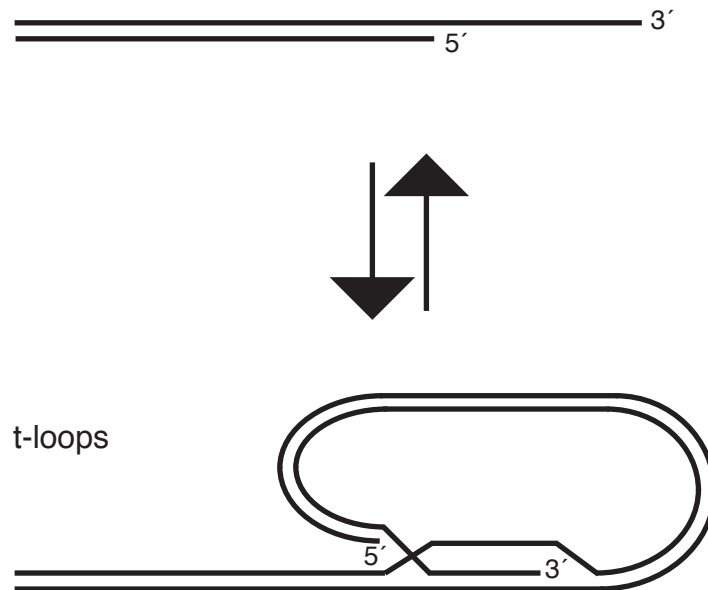
t-loops

B)

Figure 3

Telomere structure: G-overhang and t-loop

A) Telomeres terminate in a 3´ G-rich single-stranded overhang.
By invasion of the duplex upstream region, telomeres can assemble
into a t-loop structure.

B) Electron microscopy of *T. brucei* t-loops. The size of *T. brucei*
t-loops can vary from 0.6 kB (right panel) to more than 6 kB (left panel).
Picture credit: Munoz-Jordan *et al*., 2001

the common garden pea *P. sativum* (101-103). In mammalian cells, the size of the t-loop correlates with the length of a particular telomere (100). In contrast to human HeLa cells (median size 14 kB) and *Oxytricha* (5–19 kB), *T. brucei* t-loops are small. Their size ranges from 0.3 to 8.0 kB, whereas 65% of t-loops are <1.5 kB (Figure 3B) (101). The relevance of these size differences is unclear; however, it suggests that there is a machinery that controls the size of t-loops (101). In mammalian cells, parts of this machinery have been identified. TRF1, a telomere binding protein has the propensity to parallel align two telomere fragments *in vitro* (104). This step might be necessary to facilitate strand invasion during t-loop formation. TRF2, a telomere protection factor, can reconstitute t-loops *in vitro* (105).

Telomeres must ensure genome integrity by protecting chromosome ends from nucleolytic degradation and illegitimate activation of DNA damage checkpoint pathways (106-108). By tucking away the very end of the telomere, t-loops offer a formidable solution to protect chromosome ends from the DNA damage response machinery, and prevent illegitimate ligation of individual chromosomes.

Invasion of the upstream duplex telomere during t-loop formation requires another structural feature of telomeres, the G-strand overhang. In 1993, it was discovered that *S. cerevisiae* telomeres acquire long, single stranded G-strand 3´ overhang (G-overhangs) late in S-phase (109). G-overhangs are a conserved feature of linear chromosomes and they play an important role in telomere replication (110,111).

The End Replication Problem: telomere shortening and G-overhang length

In the early 1970's, Watson and Olovnikov proposed that during semi-conservative replication, removal of the RNA primer, required to initiate lagging strand synthesis, results in a terminal gap that cannot be filled by conventional DNA polymerases. As a consequence of this "End Replication Problem" telomeres should become shorter with each replicative cycle (Figure 4) (112,113). Harley and co-workers confirmed this prediction by showing that telomeres of somatic cells (cultured fibroblasts)
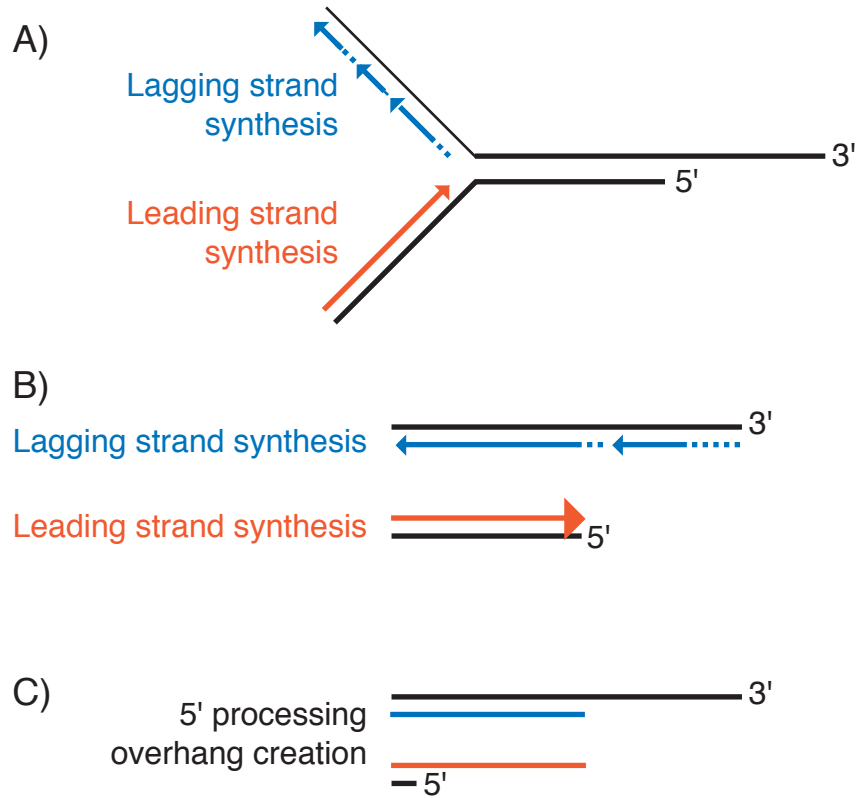
Figure 4
The End Replication Problem

A) During semi-conservative DNA replication, a replication fork approaches the chromosome end. Lagging strand synthesis (shown in blue) requires an RNA primer to initiate synthesis of an Okazaki fragment.

B) Leading strand synthesis (shown in red) can result in a blunt ended chromosome end. Removal of the RNA primer leaves the lagging strand with a terminal gap that cannot be filled by conventional polymerases.

C) 5´ end processing leads to creation of a terminal G-overhang on both newly replicated strands. As a result telomeres shorten during each replicative cycle. The figure illustrates how the rate of shortening correlates with the length of the G-strand overhang.

shortened during continuous *in vitro* culture (114). Furthermore it was demonstrated that elderly have shorter telomeres than young people (115). If telomere shortening could merely be attributed to removal of the lagging strand RNA primer, telomeres should shorten at a rate of ~6 bp/population doubling (PD). However, telomere shortening in human cells was more than 100 bp/PD. What could account for this difference? As mentioned before, telomeres end in a 3´ protrusion called the G-overhang. By parallel in-gel hybridization of two native DNA gels, using radiolabeled $(CCCTAA)_4$ and $(TTAGGG)_4$ probes, and by counting the number of single-strand binding proteins attached to telomere fragments under EM, it was shown that human telomeres end in long (150–200 nt) G-overhangs (110,111,116,117). Furthermore, the rate of telomere shortening correlated with the length of the telomere terminal G-overhang (116,118). The length of G-overhangs and their presence on both leading and lagging strand telomeres suggests, that they are not simply formed by RNA primer removal, and their creation involves nucleolytic degradation of the C-strand (111,119).

In *S. cerevisiae,* G-overhangs are short during most of the cell cycle (12–14 nt) (120). Exclusively during S-phase, G-overhangs become long and can be detected by in-gel hybridization (109). Like in human cells, the rate of telomere shortening in telomere maintenance-deficient yeast correlates precisely with the length of the G-strand overhang (121,122).

In conclusion, G-overhangs are a conserved feature of eukaryotic linear chromosomes. The length of the overhang correlates with the telomere shortening rate, and several lines of evidence suggest that G-overhang formation involves nucleolytic degradation of the C-strand. Yet, the components involved in nucleolytic degradation remain elusive.

Telomerase

Conventional polymerases are incapable of replicating linear chromosomes without gradual telomere erosion. Particularly in unicellular organisms and in germ or cancer cells, which have the ability to multiply indefinitely, the gradual shortening of

telomeres during each replicative cycle needs to be compensated for. In Drosophila, the gradual shortening of chromosome ends is compensated for by frequent transposition of HeT-A and TART telomere-associated retrotransposons onto chromosome termini (123). Another solution to solve this problem was identified in extracts of the ciliate *Tetrahymena thermophila* and named telomere terminal transferase or telomerase (124). This purified enzymatic activity had the ability to add nucleotides onto the 3´ end of oligonucleotides *in vitro* (124). Further experiments showed that RNase treatment abolished its activity, suggesting that telomerase is a ribonucleoprotein (125).

Telomerase RNA

Identification and sequencing of the telomerase RNA component revealed the presence of a short templating region, complementary to the telomeric G-overhang terminus (126). In subsequent years, the telomerase RNA component from many organisms was cloned and provided insight into telomerase function (122,127). The length of the telomerase RNA ranges from 150 nt in ciliates to 382–559 nt in vertebrates to >1300 nt in yeast and its primary sequence is highly divergent (122,128,129) #376]. The templating region generally corresponds to 1.5 telomeric repeats. Exceptions are human, mouse and *K. lactis*, whose templating regions are 11, 8 and 30 nt, respectively. (130,131). Despite the differences in length and primary sequence, a core secondary structure is well conserved within vertebrates and yeast (129,132-134). The secondary structures of various telomerase RNAs was predicted by using mFOLD, a program that calculates the lowest free-energy estimates for helix stability. These predictions were experimentally tested by RNase H cleavage assays (135). The conserved core encompasses the templating domain, used for overhang pairing and nucleotide synthesis, a double stranded boundary element 5´ of the template region, which is thought to interact with, and initiate translocation of TERT, and a pseudoknot structure, essential for telomerase activity and interaction (133). Mutational analysis of yeast telomerase RNA revealed structure motifs critical for the interaction with another member of the telomerase complex, Est1p and the KU70/80

heterodimer (136,137). Importantly, mutations in the human telomerase RNA gene have been linked to dyskeratosis congenita, a disease that causes premature hair loss, osteoporosis, bone marrow failure and abnormal skin pigmentation (138). Tissues that require constant self-renewal are more susceptible to telomerase dysfunction (139).

Telomerase Reverse Transcriptase TERT

After the identification of the first telomerase RNA, various groups joined the race to identify the protein component of telomerase. In an impressive set of experiments, Joachim Lingner succeeded in purifying a small amount of telomerase from *Euplotes aediculatus,* a ciliate that contains both a micro- and a macronucleus (140). The macronucleus contains ~4 x10^7 DNA molecules, each representing a single gene flanked by telomeres (141,142). Thus, *Euplotes* requires large quantities of an enzyme that can synthesize telomeric repeats (~3 x10^5 molecules of telomerase). A biotinylated oligonucleotide complementary to the telomerase RNA component was immobilized on an avidin column and used as bait to pull down telomerase. The ribonucleoprotein was eluted by addition of a displacement oligonucleotide (140). A partial protein sequence of the purified fraction was elucidated using nanoelectrospray tandem mass spectrometry. It revealed that the 123 kDa telomerase protein component contained sequence hallmarks of reverse transcriptases (143). Point mutations in the catalytic reverse transcriptase domain led to telomere shortening in yeast, and proved involvement of the reverse transcriptase in telomere length maintenance. The telomerase reverse transcriptase open reading frame complemented yeast *est2* mutants (est = ever shorter telomeres). EST1-4 were identified in a screen for mutants that had shortened telomeres (121). Telomerase from fission yeast and human was identified shortly after (144,145).

Telomerase reverse transcriptase has several well-conserved domains: a telomerase specific T-motif and the reverse transcriptase domains 1, 2, A, B, C, D and E (Figure 5A, underlined). The telomerase N-terminus contains several less conserved domains (II and III) that are essential for *in vivo* activity, yet dispensable for reconstituting activity *in vitro* (146). Parts of the N-terminus are also necessary for substrate (G-

overhang) binding and interaction with the telomerase RNA (147). Analysis of affinity purified telomerase from human HeLa cells suggested that the enzyme exists as a homodimer *in vivo* (molecular mass of the complex: ~600 kDa; TERT =127 hTR = 150 kDa) (148,149). Regions within N- and C-terminus of telomerase have been implicated in dimerization (150,151).

Despite the tremendous attention that telomerase has received in recent years, it remains unclear how it precisely extends the telomere terminal 3´ overhang. Human telomerase is a processive enzyme; several repeats can be added during one replicative cycle. The templating domain of the telomerase RNA is very short (11 nt), thus, to achieve processivity, the enzyme must dissociate from its DNA substrate and re-anneal to continue nucleotide synthesis. The states of this reaction cycle for *T. brucei* telomerase are illustrated in Figure 5B. *In vitro* activity studies and cloning of *T. brucei* telomere termini suggested that the *T. brucei* telomerase RNA component template region consists of 5´-CCCTAACCC-3´. (1) telomerase binds to the telomere terminal 3´ G-overhang. An RNA–DNA hybrid between the 3 nt RNA templating region and the telomere 3´ end is formed. (2) Using the RNA as a template, the reverse transcriptase copies nucleotides onto the 3´ end. Upon reaching the 5´ boundary of the templating region, the enzyme dissociates. It is also possible that the enzyme dissociates during nucleotide addition. (3). Subsequent translocation places the terminus again at the active site of nucleotide synthesis. Another round of telomere repeat synthesis is initiated (4). Very little is known about these reaction steps, in particular the transition states remain speculative.

In vitro telomerase assays revealed differences between telomerase from various organisms. Human and ciliate telomerase are very processive and can add numerous repeats to an oligonucleotide substrate (152,153). In contrast, yeast telomerase is relatively non-processive, stalls after the addition of every nucleotide and completes only one round of RNA template replication (131). Interestingly, upon addition of one

A)

B)

(1) TTAGGGTTAGGGTTAGGGTTAGGG
AATCCCAATC

CCCAAUCCC

(2) TTAGGGTTAGGGTTAGGGTT
AATC
CCCAAUCCC

TTAGGGTTAGGGTTAGGGTTAGGG
AATC
CCCAAUCCC

(3) TTAGGGTTAGGGTTAGGGTTAGGGTTAGGG
AATCCCAATC

CCCAAUCCC

(4) TTAGGGTTAGGGTTAGGGTTAGGGTTAGGGTTAGGG
AATCCCAATC
CCCAAUCCC
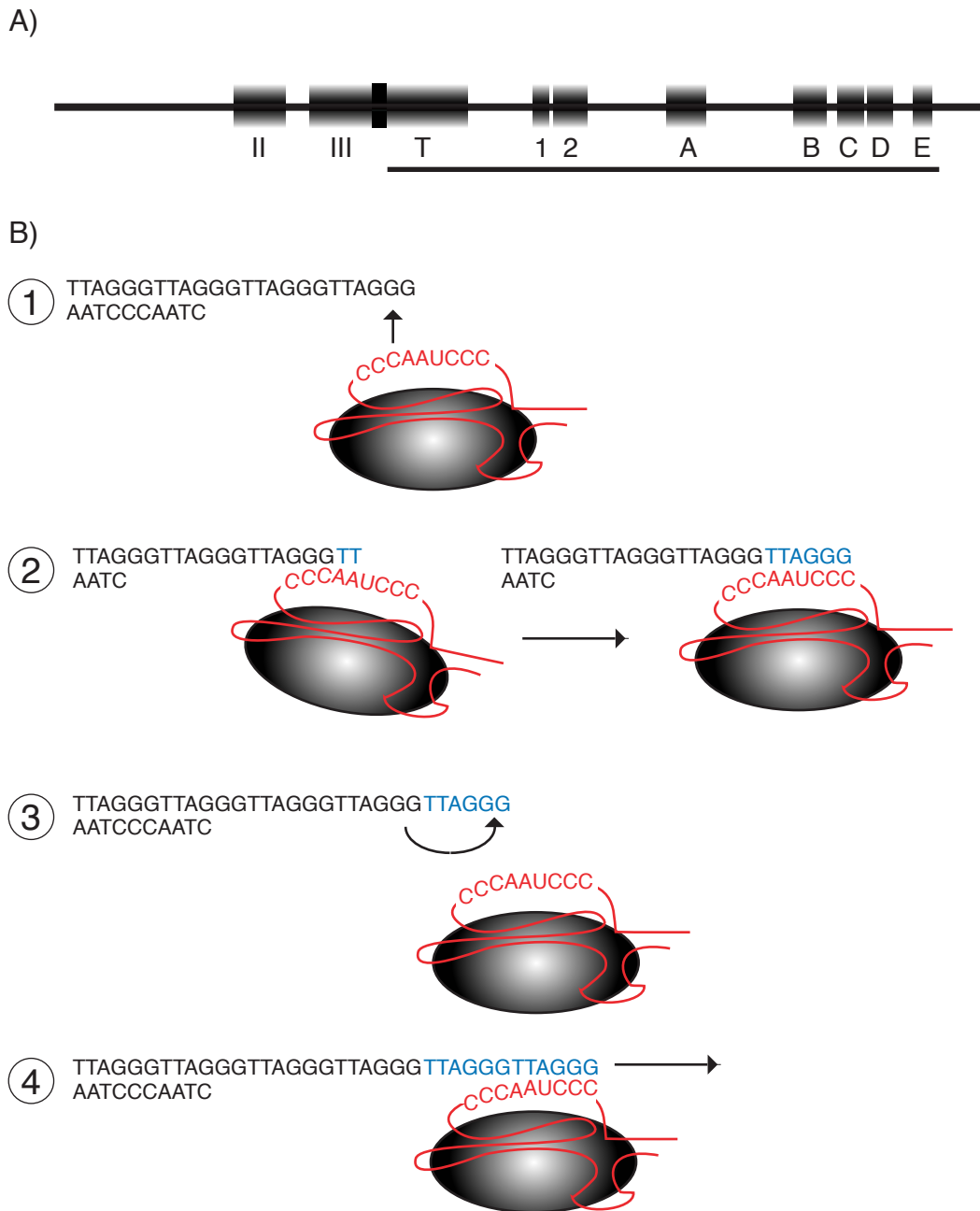
Figure 5

Telomerase Reverse Transcriptase (TERT)

A) Human TERT contains several motifs implicated in processivity, dimerization
and activity. Most conserved among different organism are the T-motif and the catalytic
reverse transcriptase motifs 1,2, A, B, C, D and E (underlined).

B) Schematic representation of the telomerase catalytic cycle at a telomere end. Represented
is the predicted telomerase RNA sequence of *T. brucei*.
Dissociation from the DNA substrate and reannealing ensure processivity. (1) Telomerase
RNA primes up with the 3' end of the telomeric G-overhang. (2) The reverse transcriptase
copies nucleotides onto the telomere. (3) Upon reaching the 5' end of the template,
telomerase dissociates and (4) realigns the 3' telomere end into the catalytic center.

repeat, yeast telomerase remains tightly associated with its substrate, indicating that the lack of processivity is not due to a high rate of substrate dissociation (131).

Although many questions about the precise molecular mechanism of telomerase action remain unanswered, the cellular consequences of telomerase deficiency have been intensively studied. In the last decade, a link between telomerase, telomere shortening and cellular senescence has been established. In contrast to somatic human cells, whose telomeres shorten during each replicative cycle, telomerase maintains telomere length in the human germline and a majority of tumors (152,154,155). Normal human cells transfected with telomerase maintained telomere length, bypassed cellular senescence, and were rendered immortal (156). These and the works of others established that telomerase activation is an essential step during tumorigenesis (157,158). Telomerase inhibition, by expression of a dominant negative allele, or through chemical compounds, led to telomere shortening and proliferation arrest (159,160). As a consequence, telomerase inhibition has become an attractive target for anti-neoplastic therapeutics (161).

In conclusion, telomerase action is essential for telomere length regulation and long-term survival of cells. Numerous factors ensure telomere homeostasis by regulating recruitment of telomerase to the telomere.

A protein-counting model that mediates telomere homeostasis in yeast

In telomerase positive cells, such as human HeLa or unicellular organisms, telomere length is maintained within a distinct size range. Telomere shortening is compensated for by repeat addition through telomerase. Short telomeres are preferentially elongated, while the length of long ones is maintained. Such telomere homeostasis can only be achieved if information about telomere length is properly relayed to the telomere terminus and consequently facilitates or inhibits telomerase action.

The machinery facilitating this was elucidated in yeast by seeding a short 80 bp telomere into strains containing various amounts of telomeric repeats in the subtelomeric region (40 bp from the "real telomere") (162). The seeded telomere was extended by telomerase but the extent of elongation decreased with increasing

24

amounts of subtelomeric telomere repeats, always adding up to a total of ~300 bp (80 bp subtelomeric + 220 telomeric; 270 bp subtelomeric + very few repeats telomeric). Proper transmission of this information depended on the telomere-repeat binding factor Rap1. Thus, telomere length is controlled by a "protein-counting model" that regulates telomerase at the telomere terminus. Consequently, the rate of telomere elongation is inversely proportional to the initial telomere length (162,163).

However, it remained unclear whether telomerase was regulated by manipulation of its catalytic activity (or processivity) or by regulation of its access to the termini of telomeres. A recent report showed that the amount of telomeric repeats added onto a telomere during a single round of replication varied from ~20 to 100 bp, irrespective of telomere length. But short telomeres were more frequently visited by telomerase and therefore elongated. Thus, telomerase' access to the telomere termini was denied at long telomeres whereas short telomeres granted it. A model was suggested where a structural change could render the telomere terminus at long telomeres inaccessible to telomerase. In contrast, short telomeres could not assemble into such a conformation and remain accessible to telomerase (164).

These and other studies established that telomere associated factors can regulate telomere elongation by telomerase (165). Similarly to the situation in yeast, a short telomere seeded onto a human chromosome end by transfection is rapidly elongated by telomerase until it reaches the size range of the other telomeres in the cell (166). This result suggested that similar telomere binding proteins could regulate telomere elongation in human cells.

Telomere length regulation in human cells

The first human telomere binding protein TRF1 was identified in 1995 (167). In the last 10 years, the components of the human telomere complex have been identified and their function intensively studied. Figure 6 lists the core factors of this complex and illustrates their interaction with one another. TRF1 and TRF2 bind to duplex telomeric DNA as homodimers, using a c-terminal myb DNA-binding domain (168). TIN2 interacts with both, TRF1 and TRF2, as well as Tankyrase and TPP1 (Figure

6B) (169,170). TPP1 connects POT1 with the TRF1 complex but POT1 can also interact with single-stranded telomeric DNA (Figure 6C) (171). TRF2 recruits hRAP1 to telomeres; and exclusively during S-phase, it also interacts with the MRE11 complex (172). The involvement of these factors in telomere length regulation and end protection is discussed below.

Overexpression of TRF1 in a telomerase positive cell line led to a gradual decrease in telomere length without altering telomerase expression levels (173). This experiment proved that TRF1 is a negative regulator of telomere length. Expression of a dominant negative allele, which displaced endogenous TRF1 from the telomeres, resulted in telomere elongation. Chromatin immunoprecipitation of telomeric DNA in cell lines with long and short telomeres indicated that longer telomeres bind more TRF1 (171). Similar to yeast, the cell employs a "protein counting model": more TRF1 on long telomeres prevents telomerase extension. Another layer of regulation is added by the fact that TRF1 binding to telomeres is controlled by at least two other factors: Tankyrase and TIN2. Tankyrase is a poly(ADP-ribose) polymerase (PARP) that uses NAD+ as a substrate to catalyze the formation of ADP-ribose polymers onto proteins (174). Overexpression of Tankyrase dissociates TRF1 from the telomeres and leads to telomere elongation. TRF1 dissociation depends on the PARP activity of tankyrase and leads to rapid degradation of TRF1 (175,176). Conclusively, Tankyrase can regulate telomere length by modulating the amount of telomere bound TRF1. A second modulator is TIN2 (177). TIN2 forms a ternary complex with Tankyrase and TRF1 (178). Downregulating TIN2 in wild-type or PARP-deficient Tankyrase backgrounds demonstrated that TIN2 modulates Tankyrase-dependent ribosylation of TRF1. In conclusion, this complex consists of three negative regulators, TIN2 inhibits Tankyrase activity, Tankyrase inhibits TRF1's capability to bind to telomeres, and TRF1 negatively regulates telomere length. Yet, the question remains, how do double-stranded DNA binding proteins like Rap1 or TRF1 affect telomerase action at single-stranded telomere termini?

A) Telomere associated factors

TRF2

hRAP1

MRE11 complex

TRF1

Tankyrase

TIN2

POT1

TPP1
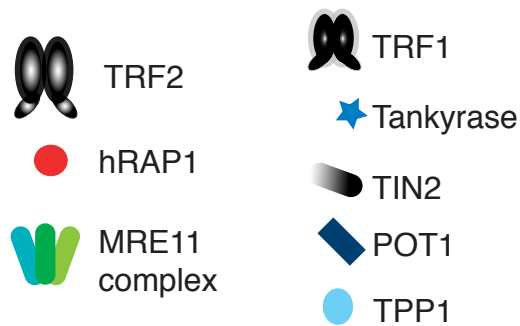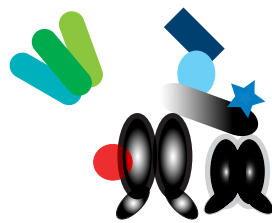
B) Telomere complex

C)
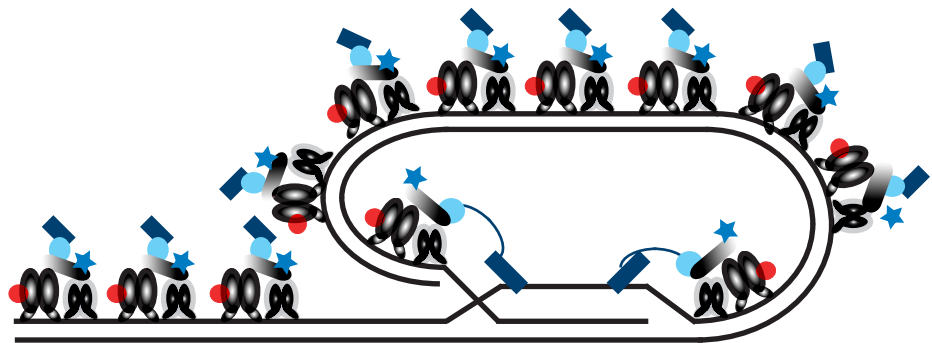
Figure 6
Telomere associated factors in human

A) Telomere binding factors: TRF1 and TRF2 homodimers bind directly to telomeric DNA through conserved myb-domains. Both recruit various other proteins to form the telomere complex shown in panel B.

B) TRF1 and TRF2 are connected by TIN2. TIN2 interacts with Tankyrase and TPP1. TPP1 connects POT1 to TIN2. hRAP1 interacts with TRF2. The MRE11 complex interacts with TRF2 exclusively during S-phase.

C) Telomere associated factors could facilitate t-loop formation. POT1 can associate with telomeres through its interaction with TPP or by directly binding to single stranded telomeric DNA.

A key to these questions was provided by the identification of proteins that specifically bind the telomere terminal G-strand overhang in *Oxytricha nova*: single-stranded telomere binding proteins alpha and beta (179). The alpha subunit binds ssDNA through four oligonucleotide / oligosaccharide-binding (OB) folds. Through structural similarity, human and fission yeast homologues of the alpha subunit were identified and called POT1 (Protection of Telomeres 1) (180). In humans, POT1 localizes to telomeres through its interaction with components of the TRF1/TRF2 complex. POT1 binds to single-stranded telomeric oligonucleotides *in vitro* and this preloading inhibits elongation by telomerase (Figure 6C) (171,181). It was suggested that long telomeres with more TRF1 could enhance binding of POT1 to the overhang and restrict telomerase from elongating the 3′ terminus (171,181). Consistent with this notion, a POT1 mutant, deficient in binding single-stranded DNA led to a dramatic increase in telomere length (171).

Similarly to human POT1, the single-stranded DNA binding protein Cdc13 plays an important role in telomerase action at *S. cerevisiae* telomeres. A temperature sensitive allele of cdc13 activated the RAD9 checkpoint and induced G2 cell cycle arrest (182). rad9 / cdc13 double mutants accumulated single-stranded DNA in telomeric and telomere proximal regions, indicating that Cdc13 might function in telomere protection or replication (182). Numerous experiments confirmed this hypothesis (183). Cdc13 recruits two major complexes to the telomere end: through its interaction with Stn1 and Ten1, Cdc13 protects telomeres and recruits DNA Polα, which is responsible for lagging strand synthesis, to the terminus (184). Secondly, through its interaction with another single strand binding protein Est1, Cdc13 recruits the telomerase complex to the telomere end (185,186). Microarray studies showed that EST1 transcription occurs in late G1 phase and subsequent experimental evidence demonstrated that this restricted expression pattern is highly relevant for telomerase recruitment (187,188). By Chromatin Immunoprecipitation (ChIP) it was shown that Cdc13 association with telomeres peaks during late S-phase, which is

consistent with the increased overhang length observed in late S-phase (109). However, the catalytic subunit of telomerase Est2 was already present at telomeres during the G1 phase of the cell cycle. This result came as a big surprise since *in vivo* telomerase activity has been observed exclusively in S-phase (189). An elegant model was proposed in which telomerase is recruited to telomeres through the interaction of its RNA component TLC with the KU70/80 heterodimer (137,190). During late S-phase, EST1 becomes expressed and serves as a linker between Cdc13 and telomerase, thus mediating telomerase access to the telomere termini (191).

Telomere protection

H.J. Mueller in 1938 and Barbara McClintock in 1941 proposed that genomic integrity can only be achieved if chromosome ends are protected from activities that normally repair double-stranded breaks. Telomere-binding factors play an important role in maintaining genomic integrity. TRF2 binds double-stranded telomeric DNA in similar fashion as TRF1, through a conserved myb-DNA binding domain (106). TRF2's function in telomere protection was elucidated by overexpression of a dominant negative allele that displaced endogenous TRF2 from the telomere. As a consequence, telomeres lost their 3´ terminal G-overhang, creating a double-stranded break and a substrate for non-homologous end joining (NHEJ). Consistent with this observation, roughly 15% of chromosomes fused with each other. These fusions depended on the DNA Ligase IV, the main ligase involved in NHEJ (106,192). Depending on the cell type, TRF2 mediated telomere deprotection initiated p53-dependent apoptosis or cellular senescence (193).

Factors that bind the single-stranded portion of telomeres are also involved in telomere protection. For instance, deletion of *S. pombe* Pot1 led to dramatic loss of telomeric sequences and frequent chromosome circularization (180). A mutant allele of *S. cerevisae* Cdc13 led to dramatic accumulation of single-stranded DNA in telomeric and telomere-proximal regions. This suggested that telomeres were not properly protected and nucleolytic degradation of one strand took place (182).

In conclusion, telomeres are bound by a number of proteins that regulate telomere length and protect them from being recognized as double-stranded breaks.

Life without telomerase – alternative lengthening of telomeres

In telomerase-deficient or human somatic cells, telomeres shorten through each replicative cycle (114,121,122). This molecular clock limits the proliferation capacity of cells, after which they enter a non-reversible growth arrest called senescence. Telomerase-deficient cells occasionally escape senescence or apoptosis. Yeast and human survivor cells acquire the ability to maintain chromosome ends through an alternative lengthening mechanism (ALT) (194,195). In the absence of telomerase, *Saccharomyces cerevisiae* can survive by amplifying subtelomeric repeats (Type I), or by recombination among telomeres (Type II). Both of these processes depend on the function of Rad52. In rad52 / exoI-deficient yeast, Type III survivors appear, which maintain their chromosome ends through palindrome-based amplification of subtelomeric regions (195,196). In addition to telomere-telomere recombination-based lengthening, *Schizosaccharomyces pombe* can overcome the loss of telomeric DNA by chromosome circularization (197).

Five to twenty percent of human cancers lack telomerase activity and use ALT to dramatically increase their telomere length (198). Telomere-telomere recombination appears to be the major mechanism underlying ALT. Nevertheless, fluorescent in-situ hybridization (FISH) of metaphase spreads of human ALT cells revealed that telomeric repeats are undetectable at many chromosome ends (198,199). It remains unclear whether signal-free ends represent short telomeres, how much telomeric DNA they carry, and whether these ends might be temporarily stabilized until they are able to undergo recombination. The majority of these human ALT cell lines contain extrachromosomal circular telomeric DNA, which could serve as a template to dramatically elongate short telomeres (200,201).

In the early 1980's, telomeres of *T. brucei* received considerable attention from the scientific community. As an example, the sequence of *T. brucei* telomeric repeats TTAGGG was determined several years prior to their elucidation in human cells (98,99).

In contrast to any known organism, telomeres of *in vitro* cultured or mouse passaged *T. brucei* grow at a constant rate of 6-8 bp/PD (202-204). It remains unknown how telomere homeostasis is achieved in wild-type African parasites. Telomere length changes can easily be detected by digesting genomic DNA with frequently cutting restriction enzymes such as AluI, MboI, RsaI or HinfI. These enzymes do not cut in telomeric repeats, which leaves them intact for length analysis (Figure 7A, left panel). Terminal restriction fragments, separated on agarose gels and blotted against a nylon membrane, can then be visualized by hybridization with a radiolabeled telomere repeat probe (Figure 7A, right panel).

Due to the abundance of unique *VSG* genes at individual subtelomeric loci, *T. brucei* offers an opportunity to study telomere length dynamics at single chromosome end resolution. Chromosome-internal copies of these *VSG*s serve as an internal control (Figure 7B). By hybridization of terminal restriction fragments with *VSG* 121 and *VSG* bR2 probes, for example, we confirmed the previously reported constitutive growth of *T. brucei* telomeres. The terminal restriction fragments grow at a rate of ~6–8 bp/PD, whereas the chromosome-internal copies do not change in size over time (Figure 7B, arrowhead). It was also shown that the active ES telomere is subject to frequent truncations, but it is unclear whether these truncations are comparable with the Telomere Rapid Deletions (TRD) observed in yeast and human cells (201,205). Attempts to establish a link between telomere length at silent and active ES, or the order of *VSG* expression remained inconclusive (206,207).

Telomere length and telomere end sequence

Numerous studies have measured telomere length in several kinetoplastid protozoa. Telomeres of laboratory-adapted *T. brucei* range in size from 3–20 kB with an average size of ~15 kB (101). The telomere terminal sequence (TTAGGG-3´) has been elucidated by adapter-based cloning (208). This result was also confirmed by biochemical studies of *T. brucei* telomerase and suggests that the telomerase RNA component ends in AAUCCC-5´ (209).

By comparison, *L. amazonensis* have short telomeres that range in size from 200 bp –1000 bp, and speculative evidence suggests that they have short (~12 nt) G-overhangs that terminate in GTTAGG-3´ (210,211). *L. major* and *L. donovani* telomeres range in size from 3–20 kB and end in TTAGGGT-3´, indicating that, in contrast to *T. brucei* and *T. cruzi,* the *Leishmania* telomerase RNA templating region ends in a different nucleotide (212-214). *T. cruzi* telomere length varies among different strain isolates and can be classified into two groups: group I has short 450–1500 bp telomeres, and group II has long 1–10 kB telomeres (215). Like *T. brucei*, *T. cruzi* telomeres terminate in TTAGGG-3´ (216). Telomere length variation has also been observed in different isolates of *S. cerevisiae* and wild-type inbred and laboratory mouse strains (217,218).

Telomere binding activities in T. brucei

Several groups identified factors that, based on their biochemical properties, had the ability to interact with double-stranded or single-stranded telomeric or telomere-like sequences in *T. brucei*. The first to be identified were ST-1 and ST-2; ST-1 is a 39 kDa protein whereas ST-2 appears to be a complex made of five polypeptides, ranging between 35-55 kDa. ST-1 and ST-2 preferentially bind to telomeric single stranded $(CCCTAA)_3$ and $(TTAGGG)_3$ oligonucleotides, respectively, yet both exhibit 5-10-fold higher affinity for single-stranded 29-bp motifs (219-221). This 29-bp degenerate T_2AG_3-repeat element is associated with MC but it remains unclear whether it is present on all megabase chromosomes as well (17,204,219).

Another 40 kDa activity that binds to 7 tandem CCCTAA repeats, as well as PolI promoter motifs was identified independently in another set of experiments (222). This activity had very similar biochemical properties like ST-1 and all attempts to further purify this activity and determine its coding sequence failed. Similarly, C1–3 and *La*GT1–3, activities, which interact with the telomeric G-rich overhang of *T. brucei* and *Leishmania amazonensis,* respectively, have been identified, partially purified and analyzed by mass spectrometry (223,224). The molecular masses of *T. brucei* C1–3, did not match with any known proteins in the database. In *L. amazonensis La*GT1, a 18-20 kDa protein is the most abundant and specific activity; *La*GT2, a 35 kDa protein has higher affinity to RNA and similarity to Rbp38p, an unknown protein found in mitochondria and the nucleus of *L. tarentolae* and *T. brucei*; *La*GT3, is a 52 kDa homologue of RPA-1 and probably the most interesting candidate (224). Nevertheless, verification, co-localization, overexpression or deletion studies have not been performed on any of these proteins, rendering their involvement in telomere affairs rather speculative.

tbKu70/80

The KU heterodimer, consisting of 70 and 80 kDa subunits, is conserved from higher eukaryotes to bacteria and archaea, and is best known for its role in repairing double-stranded breaks using Rad52 dependent NHEJ (225). KU has been found in cytosolic and nuclear fractions of peripheral B-cells. Upon stimulation, KU shuttles to the nucleus where it is involved in creating a large repertoire of antibodies through V(D)J-recombination of immunoglobulin genes (226). In *S. cerevisiae*, KU-deficiency leads to short stabilized telomeres, the persistence of S-phase restricted long G-overhangs throughout the cell cycle, and inhibition of subtelomeric
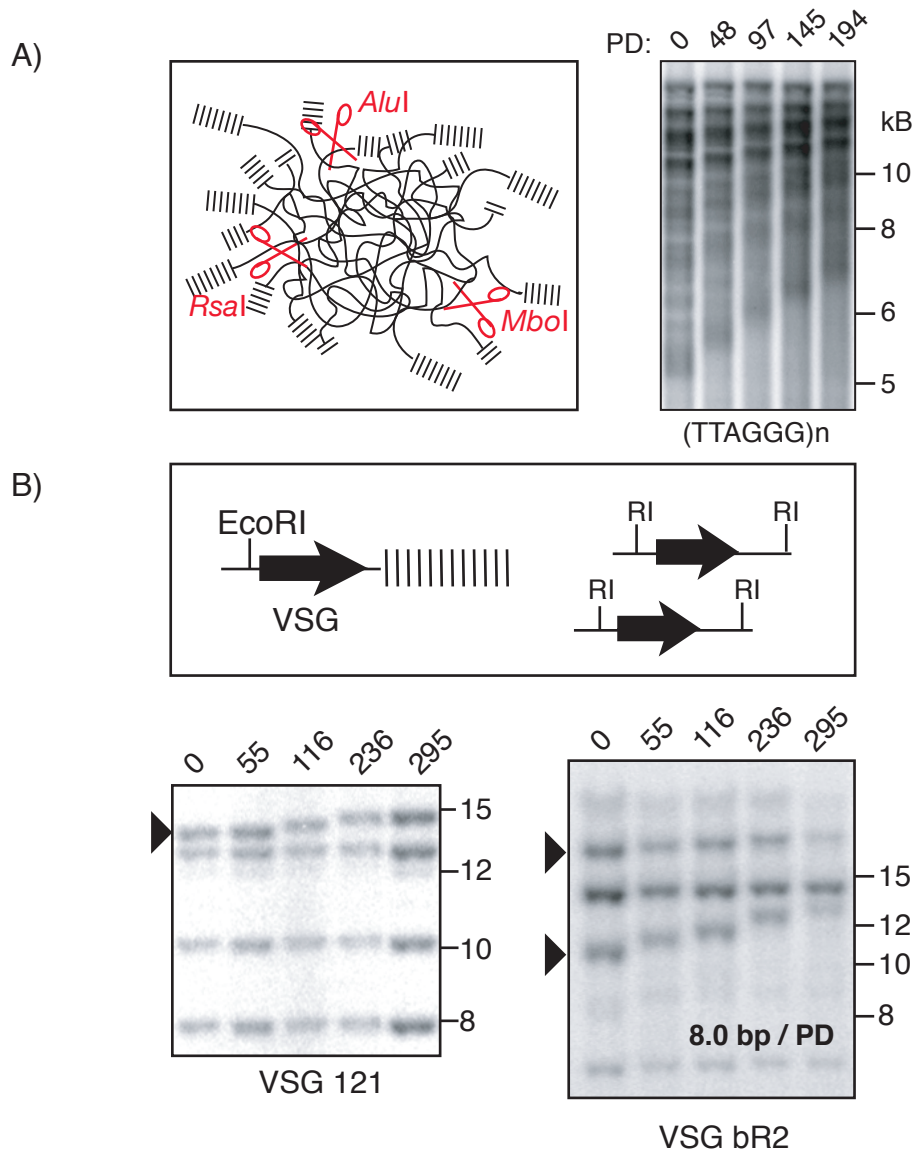
Figure 7
Growth of *T. brucei* telomeres

A) Genomic DNA is digested with frequently cutting restriction enzymes AluI, MboI, and RsaI. Digests are separated by agarose gel electrophoresis, Southern-blotted and probed with a radiolabeled telomeric (TTAGGG)n probe (right panel). Distinguishable bands represent growing telomeric fragments over a time course of 194 PD (from Janzen *et al.*, 2004).

B) Upper panel: Telomere growth at single chromosome end resolution using EcoRI that liberate a terminal restriction fragment that can be visualized by using subtelomeric *VSG* genes as hybridization probes. Chromosome-internal copies serve as loading control. Lower panel: Terminal restriction fragments containing *VSG* 121 or bR2 grow over a time course of 295 PD (arrowheads). Chromosome-internal copies do not change in size over time.

transcriptional silencing (TPE) (225,227). In conjunction with Mlp1 &2, KU tethers telomeres to the nuclear periphery (228,229).

In *T. brucei,* all but one *VSG* ES are transcriptionally repressed, and TPE may be involved in exerting this effect. Consequently, the identification of KU was of great interest to the trypanosome research community (51,85). *tb*KU-deficient *T. brucei* are viable, not impaired in double-stranded break repair nor is the repression of transcription at silent ES affected. Through co-immuno-precipitation of GFP and TY-epitope tagged KU, and co-localization by immuno-fluorescence microscopy, our group showed that *tb*KU forms a heterodimer. KU deficiency leads to progressive telomere shortening at a rate of 3–6 bp /PD (51). We showed by in-gel hybridization that, in contrast to *S. cerevisiae*, deletion of *tb*KU does not result in the acquisition of long G-overhangs throughout the cell cycle (51). Interestingly, Conway *et al*. noted that, upon dramatic shortening, critically short telomeres appeared to stabilize in length (85). At the time, we proposed a model where *tb*KU might be essential for telomerase recruitment or action at long telomeres, but might be dispensable at short telomeres (51).

TbTRF

The most characterized telomere binding protein in kinetoplasts to date is *tb*TRF, the *T. brucei* homologue of mammalian TRF2 (230). *tb*TRF was shown to localize to telomeres by immuno-fluorescence microscopy (IFM) and Chromatin Immunoprecipitation (ChIP). Purified *tb*TRF binds double stranded TTAGGG repeats, as judged by electrophoretic mobility shift assays (EMSA), and homodimerizes as shown by yeast two-hybrid analysis. RNAi of *tb*TRF leads to cell cycle arrest and a reduction of G-overhang signal in *T. brucei*. Previously, it was shown in human that expression of a dominant-negative allele of TRF2 results in cell cycle arrest, reduction of telomere terminal G-overhang, and chromosome fusions. Although no chromosome fusions were observed in TRF-deficient *T. brucei*, the results strongly suggest that *tb*TRF is a homologue of mammalian TRF2 (106,230).

Telomerase activity was detected in *T. brucei*, *L. major, L. tarentolae* and *T. cruzi* (209). The biochemical properties of partially purified *T. brucei* telomerase (*tb*TERT) were analyzed by its ability to extend different end-labeled oligonucleotides. *In vivo* experiments already suggested that *tb*TERT can elongate a variety of different telomeric substrates (231). Consistent with these results, *tb*TERT extended input primers with various telomere permutations *in vitro* by forming a ladder with a periodicity of 6 nt. After addition of 6 nt, the enzyme dissociated itself from the elongated product and repositioned at the 3´ end of the telomere terminus. For reasons that are not clear, telomerase stalling or translocation gives rise to a band of increased intensity on the acrylamide gel. Thus by testing telomerase elongation on oligonucleotides that ended in different sequences, the precise nucleotides added before translocation mapped the template boundaries of the *T. brucei* telomerase RNA template. These results suggested that *tb*TERT template RNA consists of 3´-CCCAATCCC-5´. In comparison to ciliates, processivity of *tb*TERT was relatively low (209). Telomerase in *T. cruzi* (*tc*TERT) has been characterized to a similar extent. Telomerase activity was recovered from parasites of four different life-cycle stages, yet telomerase processivity was very low (addition of 2–3 nt). *tb*TERT elongated any telomere oligonucleotide substrate, whereas *tc*TERT clearly prefers oligos that terminate in A or T. These results suggested that *T. cruzi* telomerase RNA contains a 3´-CCCAATCCC-5´ template region and, that at least *in vitro*, different 3´ ends have dramatically different elongation efficiencies. The implications of this result remain speculative, but the authors concluded that *tc*TERT might rely on itself (rather than other proteins) to establish sequence specificity with its substrate. Lastly, like many other telomerases, *T. cruzi* telomerase exists in a ~670 kDa complex. Since *T. cruzi* telomerase itself is ~133 kDa, it is presumed that this molecular weight is achieved through multimerization or interaction with other associated factors (232).

Chapter II: T. brucei telomerase, telomere shortening and G-overhang structure

Introduction

In this chapter, we describe the identification, characterization and deletion of telomerase in *Trypanosoma brucei*. We show, by comparative sequence analysis, that *tb*TERT contains the hallmark reverse transcriptase motifs and the telomerase characteristic T-motif. We monitored telomere length after deletion of *tbTERT* and show that the rate of telomere shortening correlated precisely with the amount of DNA predicted to be lost due to the end replication problem: 3–6bp/generation.

Identification and characterization of T.brucei TERT

We searched the emerging *T. brucei* genome data for sequences that could encode the characteristic motifs of telomerase reverse transcriptase (143). Our original search yielded a short DNA fragment containing motifs 1, 2, A and B of the reverse transcriptase domains. The complete *TERT* sequence was obtained by sequencing BAC and plasmid clones that covered the telomerase coding region. From these additional sequence data, we were able to assemble a 3,579 bp ORF, which encodes a 132 kDa protein that contains all the domains that are known to be required for catalytic activity (Figure 8A). TERT orthologues can also be identified in the recently completed genome sequences of *Trypanosoma cruzi* (49.1% identity to *tb*TERT) and *Leishmania major* (33.6% identity), the causative agents of Chagas' disease and cutaneous Leishmaniasis, respectively. In contrast, *tb*TERT shows weak sequence identity with human TERT (15.6%), reflecting the early divergence of *T. brucei* in the evolutionary tree (Figure 8B) (233). Within the T-motif, these three kinetoplastid protozoa contain a highly conserved insertion, of unknown function, that is not present in other organisms (Figure 8B and Figure 9). We used RT-PCR to verify that this insertion was present in the mRNA and did not represent an intron in the genomic sequence. Figure 9A shows a schematic representation of the telomerase open frame, the location of the putative intron and the positions of three primers used in PCR

Figure 8

Alignment of telomerase reverse transcriptase motifs

A) Schematic representation of the telomerase-specific T-motif and the conserved reverse transcriptase motifs 1, 2, A through E in *T. brucei TERT*.

B) Alignment of telomerase specific motifs of *T. brucei* (*tb*TERT), *T. cruzi* (*tc*TERT), *L. major* (*lm*TERT), *human* (*h*TRT), *S. cerevisiae* (*sc*Est2), *S. pombe* (*sp*Trt1) and *E. aediculatus* TERT (*ea*P123). Sequences of each motif are aligned from top to bottom according to their degree of conservation. Highly conserved residues are marked with an asterisk. Sequence similarities are shaded.

Figure 9

A TERT N-terminal region present in kinetoplastid *TERT*

A) Schematic representation of the telomerase open frame, the location of the putative intron and the position of three primers used in PCR reaction to amplify the "intron – like" region on genomic DNA and cDNA.

B) PCR reactions on cDNA and gDNA.
Forward primer C together with primer sets (labeled A and B) was used to amplify the region of interest on genomic DNA. In parallel, the same primers were used on cDNA. (-) PCR reactions on "cDNA" that lacked reverse transcriptase during cDNA synthesis. If the region of interest is indeed an intron, the cDNA amplification product should be ~80 bp smaller. This size change should be resolvable on the 1.8% agarose gel we used.

reactions. Both primer sets (labeled A and B) were used to amplify the putative intron region on genomic DNA and cDNA. If this region were an intron, hence not present in the mRNA, a size change of ~80 bp in the PCR product would be expected. To exclude the possibility that the cDNA is contaminated with remaining DNA, we performed the PCR reaction on "cDNA" that lacked reverse transcriptase during the synthesis step, and as expected, no band was amplified (Figure 9B). No size difference between cDNA and gDNA derived PCR products was detected, indicating that the region in the T-motif is not an intron and a specific feature of kinetoplastid protozoan telomerase. We do not know anything about the function of this region.

Telomerase deletion

To determine whether *tb*TERT was a single-copy gene, we digested the genome of *T. brucei* with nine infrequently cutting restriction enzymes and hybridized the southern blot with a probe that covered the entire TERT ORF (Figure 10A). In each digest only one band hybridized with the probe, indicating that *tb*TERT is a single-copy gene. This result was confirmed by the subsequent sequencing of the *T. brucei* genome, which showed that *tb*TERT is located on chromosome 11.

*tb*TERT was deleted by replacing both alleles with Hygromycin and Puromycin resistance genes flanked by Actin Un-Translated Regions (UTR). Regions flanking *tb*TERT served as targeting sequences to facilitate proper integration (Figure 10B). Southern blotting, using the *tb*TERT ORF as a hybridization probe confirmed that TERT signal is absent from the three homozygous clones (Figure 10C, upper panel). Subsequent reprobing of the membrane with Hygromycin and Puromycin ORFs confirmed integration of the marker genes into the *tb*TERT locus (Figure 10C, middle and lower panel). Next, we assessed the growth of TERT-deficient clones. In comparison to wild-type single marker (SM) and heterozygous mutants (+/-), TERT-deficient clones showed no growth impairment (Figure 10D). This allowed us to monitor changes in telomere length over long periods.

Telomerase deficiency results in progressive telomere shortening

During a 2.5 months time course (~267 PD), genomic DNA of TERT-deficient mutants was isolated on a weekly basis and digested with frequently cutting restriction endonucleases (MboI and AluI), liberating the uncut repetitive telomere tracts for length analysis on agarose gels. We first visualized the size distribution of all telomeres, by hybridizing the gel with a radiolabelled $(TTAGGG)_4$ probe (Figure 11). Telomere length initially ranged from 3–20 kbp, and some telomeres were resolved as discrete bands. Each band displayed moderate progressive shortening. The lengths of specific telomere bands, of differing size ranges and from different gels, were measured. The shortening rate, determined by linear regression analysis on independent chromosome arms, varied from 3–6 bp/PD. The range of 3–6 bp/PD reflected the resolution limit of accurate size separation on agarose gels.

Telomere shortening at silent expression sites

The presence of unique *VSG* genes in several subtelomeric regions allowed us to measure the shortening rate of individual telomeres. PFGE and Southern hybridization of three clones using *VSG* 1.8 or bR2 probes, indicated that these cells contain four copies of *VSG* 1.8 and three copies of *VSG* bR2 (Figure 12A): two copies of *VSG* 1.8 and one copy of *VSG* bR2 are located at chromosome-internal sites and two are subtelomeric (Figure 12B, right panel). DNA samples from a 220 PD time course were digested with enzymes that cut either upstream (EcoRI for *VSG* bR2) or inside (BglI for *VSG* 1.8) a *VSG* open reading frame, releasing a terminal restriction fragment that was visualized on a Southern blot using a *VSG* 5´ region as the hybridization probe (Figure 12B).

Restriction fragments containing chromosome-internal copies of *VSG* 1.8 do not change in size, whereas the subtelomeric fragments gradually shorten (arrowheads in Figure 12B, upper panel). During 220 PD, the terminal restriction fragment shortened
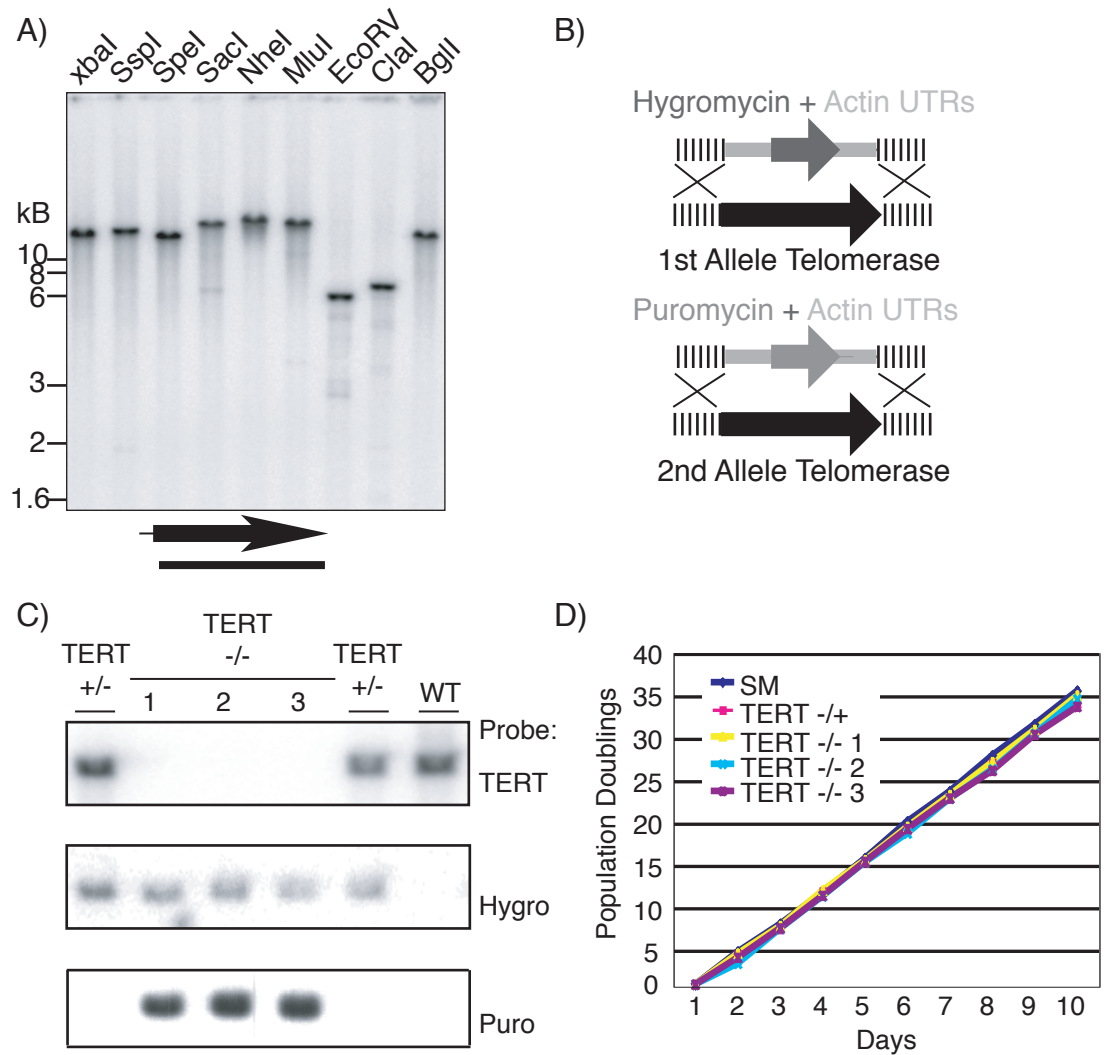
Figure 10
Deletion of telomerase and growth curve of telomerase-deficient mutants

A) *T. brucei* telomerase is a single copy gene. Restriction digest with various enzymes that do not cut within the *TERT* orf. Southern blotting and subsequent hybridization using the *TERT* orf as a probe.

B) Schematic representation of the strategy used to replace *TERT* with drug resistance confering marker genes. Both alleles were replaced by the hygromycin phosphotransferase gene (flanked by actin Untranslated Regions) andthe Puromycin acetyl-transferase gene, respectively.

C) Southern Blot confirming deletion of both *TERT* alleles. Upper panel: Membrane was probed with the *TERT* ORF. Middle and lower panel: the same blot reprobed with Hygromycin and Puromycin ORFs.

D) Deletion of *tb*TERT does not affect growth of *Trypanosoma brucei*. Growth curve of three independent *tb*TERT-deficient clones in comparison to wild-type single marker (SM).
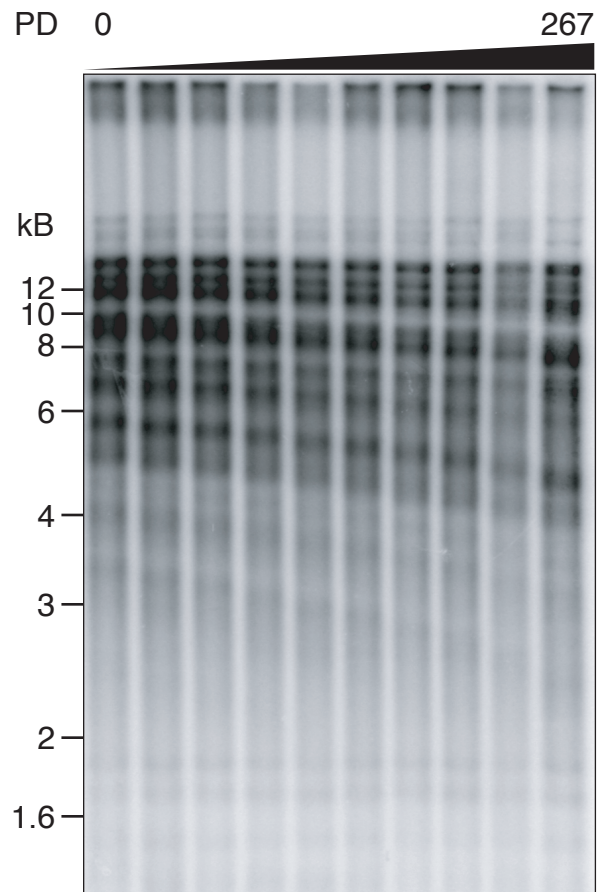
Figure 11

Overall telomere shortening in telomerase-deficient mutants

Over the course of 267 population doublings (PD), genomic DNA
was isolated at intervals of ~26 PD and digested with MboI and AluI.
Terminal restriction fragments were visualized, using a radiolabelled
(TTAGGG)$_4$ probe. ImageQuant software (Molecular Dynamics) was
used to distinguish individual bands and determine their shortening rate.

by about 1,000 bp, corresponding to an average telomere shortening rate of ~4.5 bp/PD. Telomere shortening was also observed at *VSG* bR2 ES (Figure 12B, lower panel). The two subtelomeric copies are subject to progressive shortening (marked by arrowheads) and the chromosome-internal copies remain at the same length. Again, telomerase deficiency resulted in a loss of ~950 bp during 220 PD, confirming the shortening rate of 4–5 bp/PD. The results of several independent experiments are summarized in Table 1.

TABLE 1:

Shortening rates at different telomeres in independent experiments	
Bulk telomeres	bp/PD
	4.4
	5.6
	5.4
Silent ES telomeres	bp/PD
VSG bR2	3.5
VSG bR2	4.8
VSG bR2	3.1
VSG 121	3.2
VSG 1.8	4.9
VSG 1.8	4.5
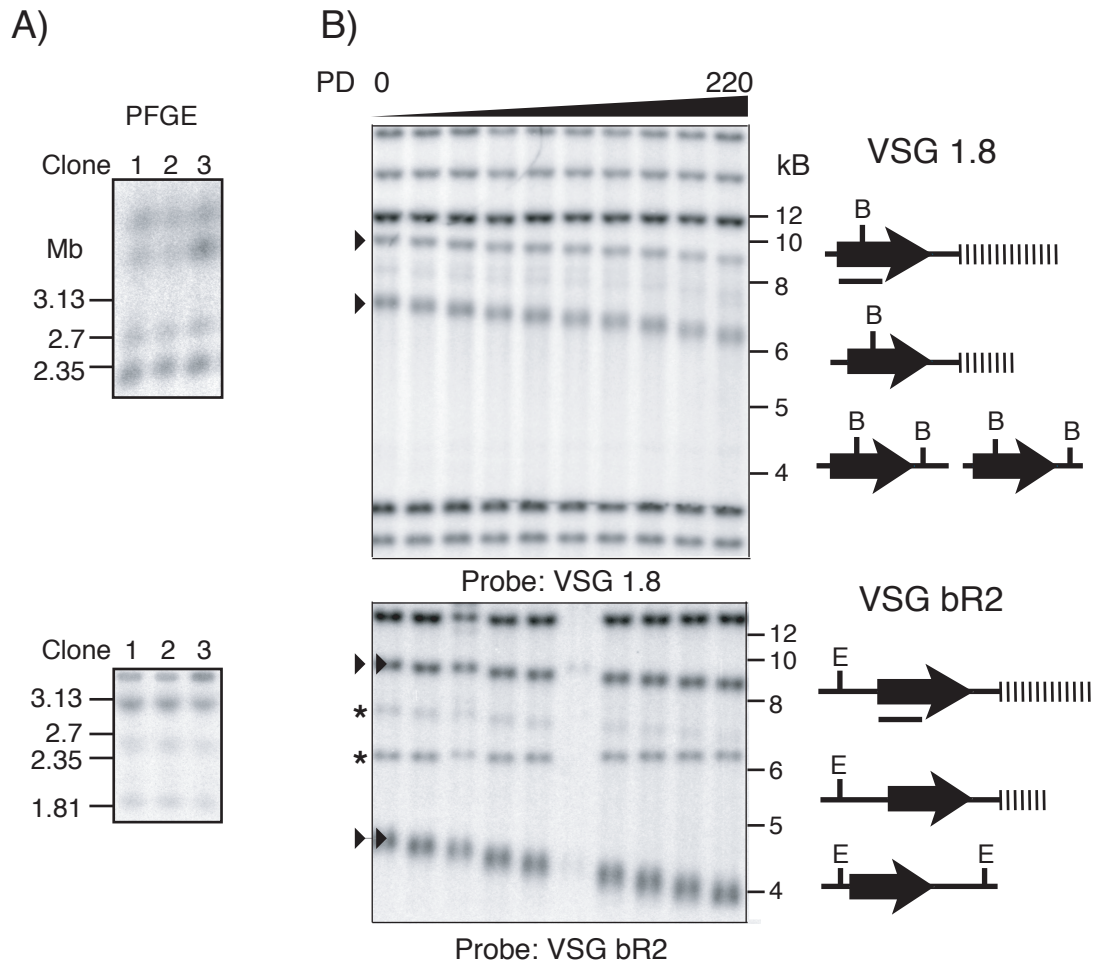
Figure 12
Progressive telomere shortening at silent expression sites

A) By separation of individual chromosomes by PFGE and southern blotting using
VSG 1.8 (upper panel) and bR2 (lower panel) probes, we identified the copy numbers
of these *VSG*. The signal on top of the lower panel is derived from chromosomes that
remained trapped in the slot.

B) Terminal restriction fragment analysis of silent ES telomeres harboring *VSG* 1.8
(upper panel) and *VSG* bR2 (lower panel) in the telomerase-deficient mutant. Time
of culturing is indicated in population doublings (PD). Telomeric fragments containing
VSG 1.8 and *VSG* bR2 (arrowheads) gradually shorten. Right panel: schematic
representation of *VSG* 1.8 and bR2 genes and positions of BglI and EcoRI sites used in
the respective DNA digests. Bars indicate the probes used for hybridization.
Bands labeled * are due to cross hybridization of the probe with other *VSG*s.

To verify that the observed phenotype can be attributed to telomerase deletion, we complemented TERT-deficient clones with a tetracycline inducible vector, containing the *tb*TERT ORF. Re-introduction of *tb*TERT resulted in telomere elongation and reversed the telomere shortening phenotype and these results will be discussed in more detail in chapter IV. Furthermore, the actively transcribed ES telomere is subject to frequent terminal deletions, and it is therefore not suitable to accurately determine the rate of progressive shortening in the absence of telomerase (202-204). The consequences of telomere shortening at the active ES will be discussed in Chapter V.

T. brucei G-strand overhangs are undetectable by conventional in gel hybridization

In all studied organism, the rate of telomere shortening in the absence of telomerase correlates with the length of the G-overhang (111,116). In *S. cerevisiae*, telomerase deficiency leads to a telomere decline that correlates precisely with the predicted shortening due to the end replication problem, and with the length of G-overhangs found outside of S-phase (120-122). The moderate telomere shortening rate observed at bulk telomeres and at several silent ES telomeres in telomerase deficient *T. brucei,* led us to investigate the length of the G-overhangs using a conventional in-gel hybridization assay. This assay permits the detection of single-stranded regions larger than ~30 nt on digested genomic DNA fragments (109).

DNA was digested with frequently cutting restriction enzymes and run in parallel on two agarose gels, which were then dried at room temperature. To detect G-overhangs, one gel was hybridized with a radiolabelled oligonucleotide probe complementary to the G-rich strand (Figure 13, $(CCCTAA)_4$ probe). As a negative control, and to test whether the DNA denatured during isolation and handling, the duplicate gel was probed with a non-complementary probe (Figure 13, $(TTAGGG)_4$ probe). To verify equal loading, both gels were denatured and re-probed (Figure 13, lower panels). Due to the large number of MC, the *T. brucei* samples contain 10–100-fold more telomeric
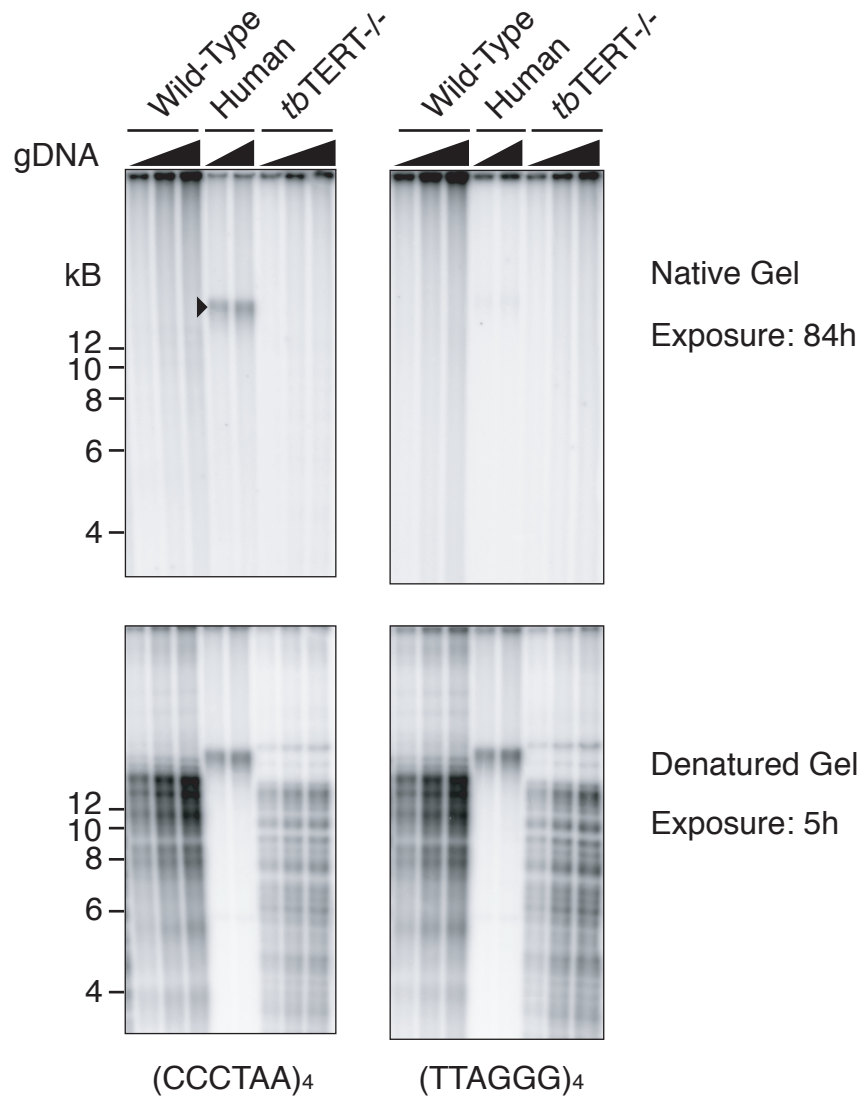
Figure 13

G-overhang Assay in telomerase-deficient *T. brucei*

T. brucei G-overhangs are undetectable using a conventional in-gel hybridization overhang assay. Overhang assay in wild-type bloodstream *T. brucei*, telomerase-deficient *T. brucei* and *human* HeLa cells (positive control). Arrows on the top of the gel indicate the increasing amounts of digested DNA loaded onto the gel (wild-type and *tb*TERT-/-, 0.5, 1.0 and 1.5 μg; *human* HeLa DNA, 5.0 and 7.0 μg).
Upper panels: native gels were hybridized with (TTAGGG)$_4$ or (CCCTAA)$_4$ probes. The arrowhead indicates the G-overhang detected on human HeLa DNA. Exposure time: 84 h.
Lower panels: equal loading of samples was confirmed by denaturation and re-hybridization of the gels. Exposure time: 5 h.

DNA than does the same quantity of human DNA. Despite this abundance of chromosome ends, no G-overhang-specific signal was detected by in-gel hybridization. G-overhangs were readily detected on the positive control, human HeLa DNA, as indicated by the arrowhead in Figure 13. Whereas TERT-deficiency did not lead to detectable changes in G-overhang length, a slight decline in telomere length and signal intensity were visible (Figure 13, right lanes) as a consequence of telomere shortening during continuous culture. We also tested whether G-overhang length varies between *T. brucei* isolated from different life cycle stages. As expected, no significant change was observed between procyclic and bloodstream trypanosomes (Figure 14). These experiments were repeated extensively, using hybridization and washing temperatures that varied from 20°C to 50°C and using different *T. brucei* clones, including wild-type isolates, and the results were indistinguishable.

G-overhang structure in tbKU80-deficient trypanosomes

S. cerevisae telomeres acquire a long single stranded G-overhang during S-phase (109). During the rest of the cell cycle, overhangs are short (12–14 nt) and undetectable by conventional in-gel hybridization (109,120). In yeast, deletion of the KU70/80 complex, involved in non-homologous end joining, leads to detectable long G-overhangs throughout the cell cycle (227). To further test the sensitivity of our assay and to examine whether the loss of *tb*KU80 would alter G-overhang structure, G-overhang assays were performed on KU-deficient *T. brucei* (Figure 15). DNA was isolated, digested with MboI and AluI and separated on agarose gels. On dried native gels hybridized with a radiolabeled $(CCCTAA)_4$ oligonucleotide probe, human G-overhangs were clearly detectable in this sample (Figure 15, upper left panel, arrowhead). A $(TTAGGG)_4$ probe was used to confirm that the DNA was still in its native condition (Figure 15, upper right panel). No overhang signal was detectable in DNA derived from either wild-type or *tb*KU80-deficient trypanosomes with the $(CCCTAA)_4$ probe, despite loading at least 10-fold more trypanosome telomeric
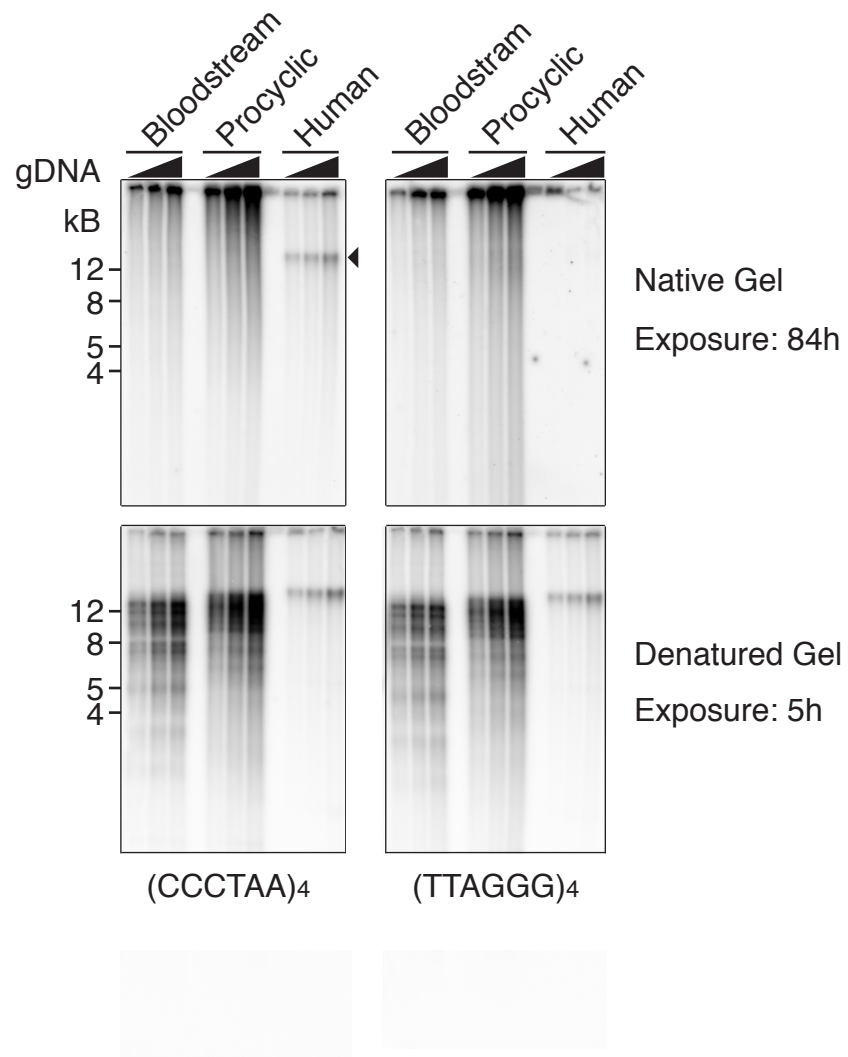
Figure 14

G-overhang: procyclic form compared to bloodstream form *T. brucei*

Upper panel: native in-gel hybridization using C- and G-strand specific probes. Arrowhead indicates G-overhangs on human HeLa DNA.

Lower panel: same gels upon denaturation and rehybridization with the same probes ensure equal loading. Increasing amounts of each DNA sample were loaded: *T. brucei* DNA: 0.5, 1.0 and 1.5 μg; *human* HeLa DNA, 5.0 and 7.0 μg
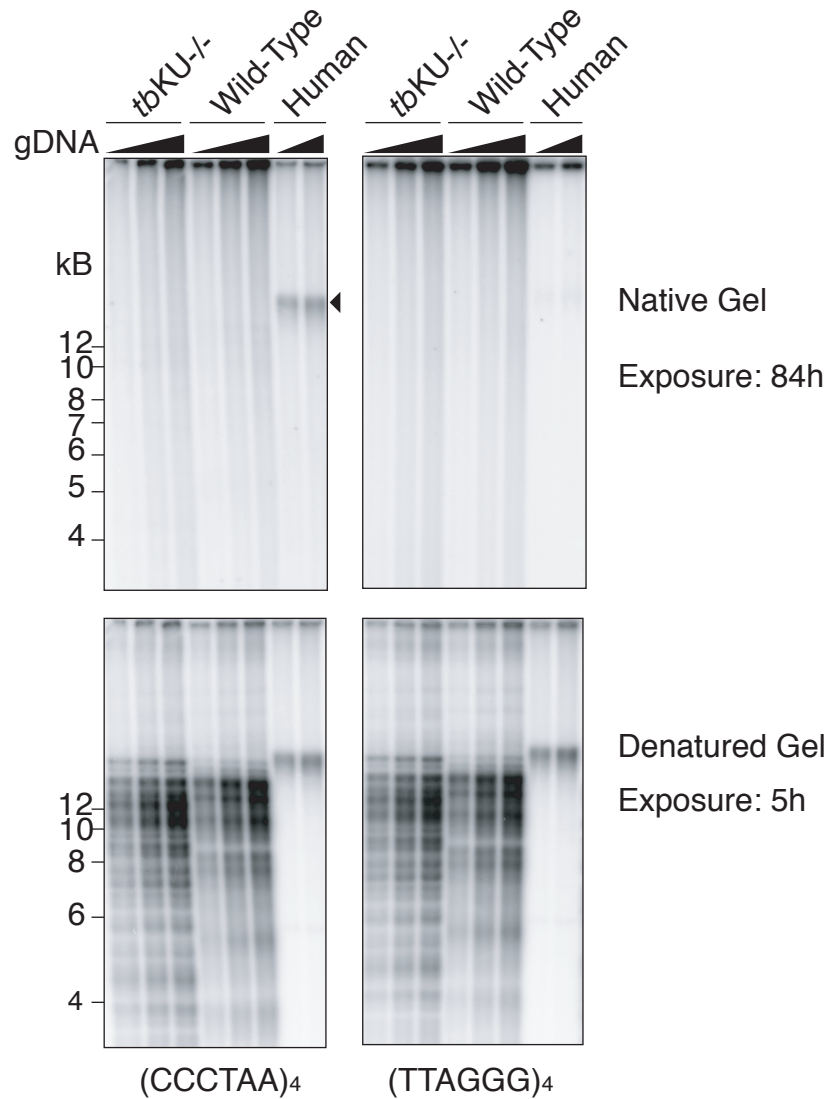
Figure 15

G-overhang structure in KU80-deficient *T. brucei*

DNA was extracted from *tb*KU80-deficient cells (*tb*KU80-/-), wild-type cells (wild-type), and HeLa cells (*human*) and digested with MboI and AluI restriction enzymes. Different amounts of DNA (0.5, 1.5 and 5.0 µg for *T. brucei* and 5 and 7 µg for *human*) were separated by gel electrophoresis and analyzed with radio-labeled probes (left panels and right panels). Equal loading was verified by denaturation and re-hybridization (lower panels).

DNA compared to the HeLa cell sample as is evident after denaturation and re-hybridized with the same probes (Figure 15, lower panels).

Nevertheless, *tb*KU plays an important role at the telomeres; its deletion leads to telomere erosion at precisely the rate of TERT-deficient *T. brucei*: 3–6 bp/PD. Thus *tb*KU is likely to be involved in either telomerase recruitment or activation. However, in contrast to yeast, *tb*KU does not play a role in establishing proper telomere terminal structure (51). As the detection limit of this assay is ~30 nt, we conclude that trypanosomes have short overhangs and that, unlike yeast, *tb*KU80 has no apparent influence on overhang structure in *T. brucei*.

T. brucei G-overhangs are not degraded during DNA isolation

To test whether G-overhangs might have been degraded by a hypothetical nuclease activity in the *T. brucei* lysate during DNA isolation, we mixed HeLa-cell DNA and *T. brucei* cells, then re-isolated DNA from the mixtures, reasoning that the HeLa cell G-overhangs would also be degraded in the mixture (unless the putative nuclease was tightly tethered to trypanosome telomeres, and only acted in *cis*). After DNA isolation, the telomeric tracts were separated on agarose gels and overhang assays were performed (Figure 16, lanes 7–18). The HeLa G-overhang signal (arrowhead) was undiminished after re-isolation in the presence of *T. brucei* cells. Lanes 4–6 confirm that G-overhangs cannot be detected on much larger amounts of *T. brucei* telomeric DNA. The gel was then denatured and re-probed to verify the ratios, as determined by the telomere signal (quantified using a phosphorimager), of *T. brucei* in the mixed samples (Figure 16, lower panel, lanes 7–18). Furthermore, the 100-fold higher relative abundance of telomeric repeats in *T. brucei* DNA is readily apparent when equal amounts of *T. brucei* and HeLa DNA are loaded (Figure 16, lower panel lanes 1–6).
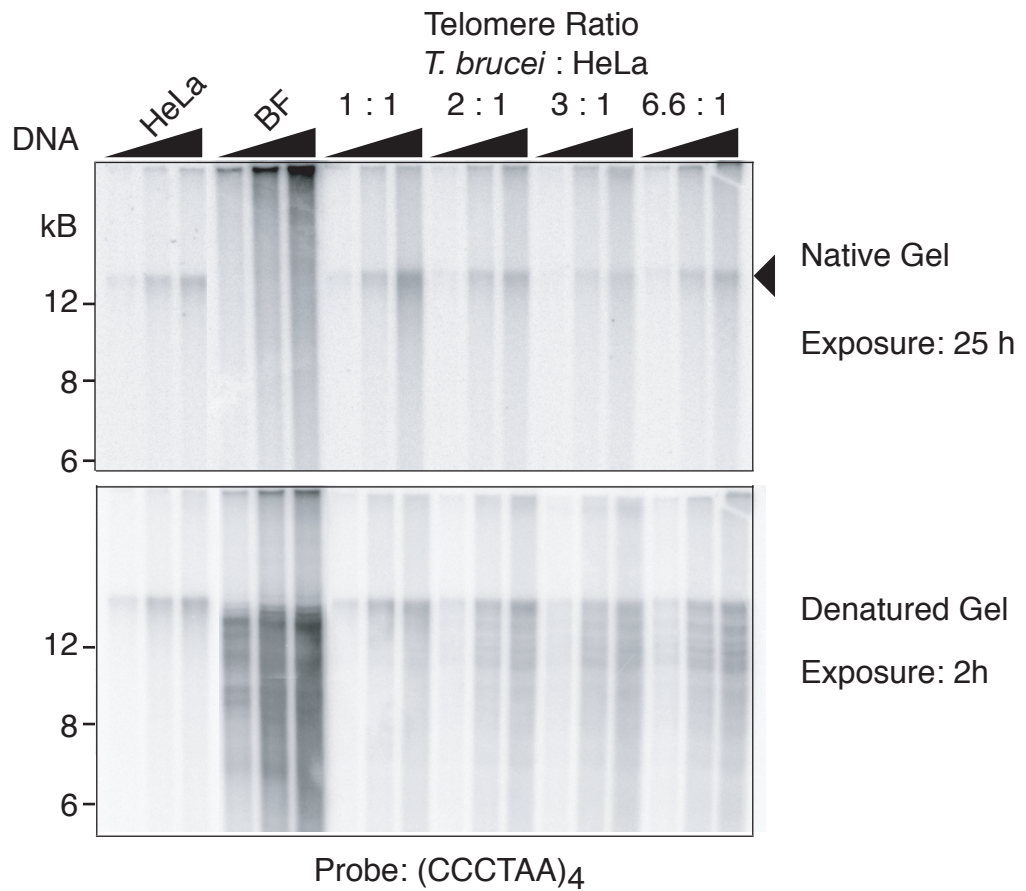
Figure 16

HeLa cell G-overhangs are not degraded during DNA isolation in the presence of *T. brucei* cell extracts

Upper Panel lanes 1–6: the proportion of telomeric DNA in *T. brucei* is 100-fold higher than in HeLa cells. The samples contained 0.5, 2.5 or 5.0 µg of MboI- and AluI-digested DNA of HeLa cells (HeLa: lanes 1–3) or wild-type *T. brucei* (BF: lanes 4–6). Upper Panel lanes 7–18: the HeLa G-overhang signal is not diminished when telomeres are isolated from mixtures of HeLa DNA and *T. brucei* cells. Increasing numbers of *T. brucei* cells were mixed with 0.5, 2.5 or 5.0 µg HeLa DNA. The amounts of *T. brucei* cells are such that they contributed to the mixtures 1.9-, 2.5-, 3- or 3.6- fold as much telomeric DNA as the HeLa cells.

Lower Panel: the same gel after denaturation and re-probing.
Increasing amounts of *T. brucei* DNA are evidenced by the characteristic banding pattern of *T. brucei* telomeric DNA.

Enzymatic modification of T. brucei telomeres

As an additional control, because we could not detect any G-overhang signal on *T. brucei* telomeres, we created artificial G-overhangs and detected them by in gel hybridization (Figure 17). Artificial G-overhangs can be created by treating *T. brucei* DNA with bacteriophage T7 (Gene 6) exonuclease, as previously described (100,234). T7 (Gene 6) exonuclease specifically creates 3´ G-overhangs by degradation of the 5´ C-rich strand (Figure 17A). After enzymatic modification, *T. brucei* DNA was digested to liberate telomeric tracts and a G-overhang-specific signal could be detected by in-gel hybridization using a $(CCCTAA)_4$ probe (Figure 17, upper left panel). The gel distribution of the created overhang signal was similar to the distribution of *T. brucei* telomeres (compare upper and lower panels of Figure 17), indicating that G-overhangs were created at telomere termini. To verify that T7 (Gene 6) exonuclease exclusively degraded the C-rich strand and to test whether the DNA was still in its native condition, a duplicate gel was probed with a non-complementary $(TTAGGG)_4$ probe (Figure 17, upper right panel), We also tested whether Exonuclease I, a 3´ single-strand-specific exonuclease (Figure 17A), would have any effect on *T. brucei* DNA. As expected, Exonuclease I had no effect on hybridization of probes to either the G or C-rich strands (Figure 17). This experiment shows that artificial G-overhangs could be created on *T. brucei* telomeres *in vitro* and detected by in gel hybridization, although the exact size of these overhangs was not determined.

G-strand overhangs are detectable on concentrated minichromosomes by PFGE

The genome of *T. brucei* consists of 11 large MBC, 5–7 IC and ~100 MC, that can be separated by PFGE (14,15). Under the used conditions, the 11 MBC migrate in the middle of the gel and are well separated (Figure 18, right panels). IC can be partially resolved but MC are focused at the bottom of the gel. To investigate whether G-
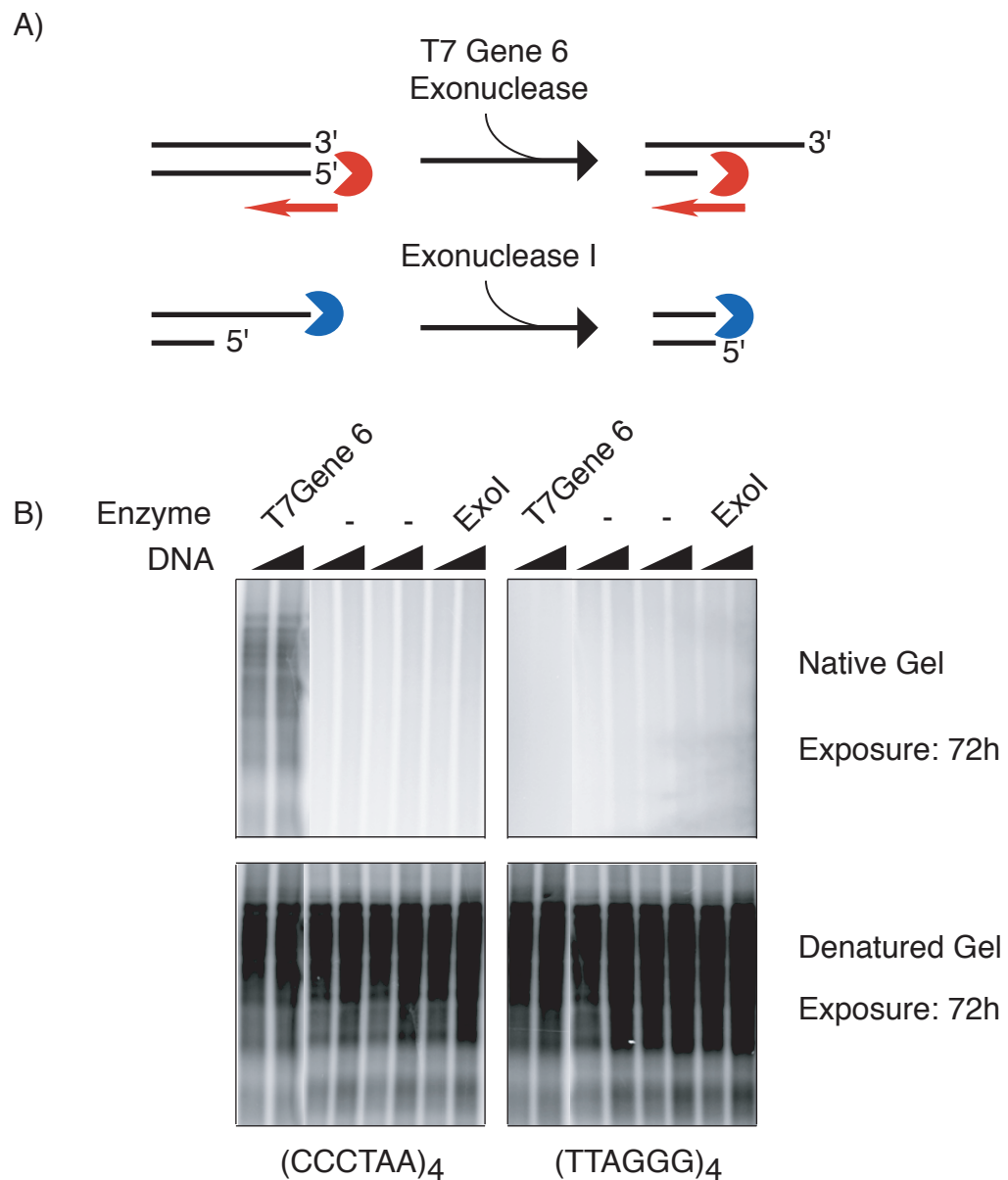
Figure 17
Creation of artificial G-overhangs by enzymatic modification of *T. brucei* DNA

A) T7 Gene 6 exonuclease specifically degrades the 5´ DNA terminus to create 3´ overhang. Exonuclease I attacks 3´ overhangs.

B) Upper panels: native gels, increasing amounts of DNA (0.5 μg and 0.75 μg) were used. DNA was modified as indicated on top of each lane: T7 (Gene 6) exonuclease (far left), exonuclease I (far right lanes) or unmodified (-). Duplicate gels were hybridized with (CCCTAA)$_4$ (left panel) or (TTAGGG)$_4$ (right panel). A G-overhang specific signal can be detected by hybridization with (CCCTAA)$_4$ probe (left panel). Lower panels show the same gels after denaturation and re-hybridization with the same probes.
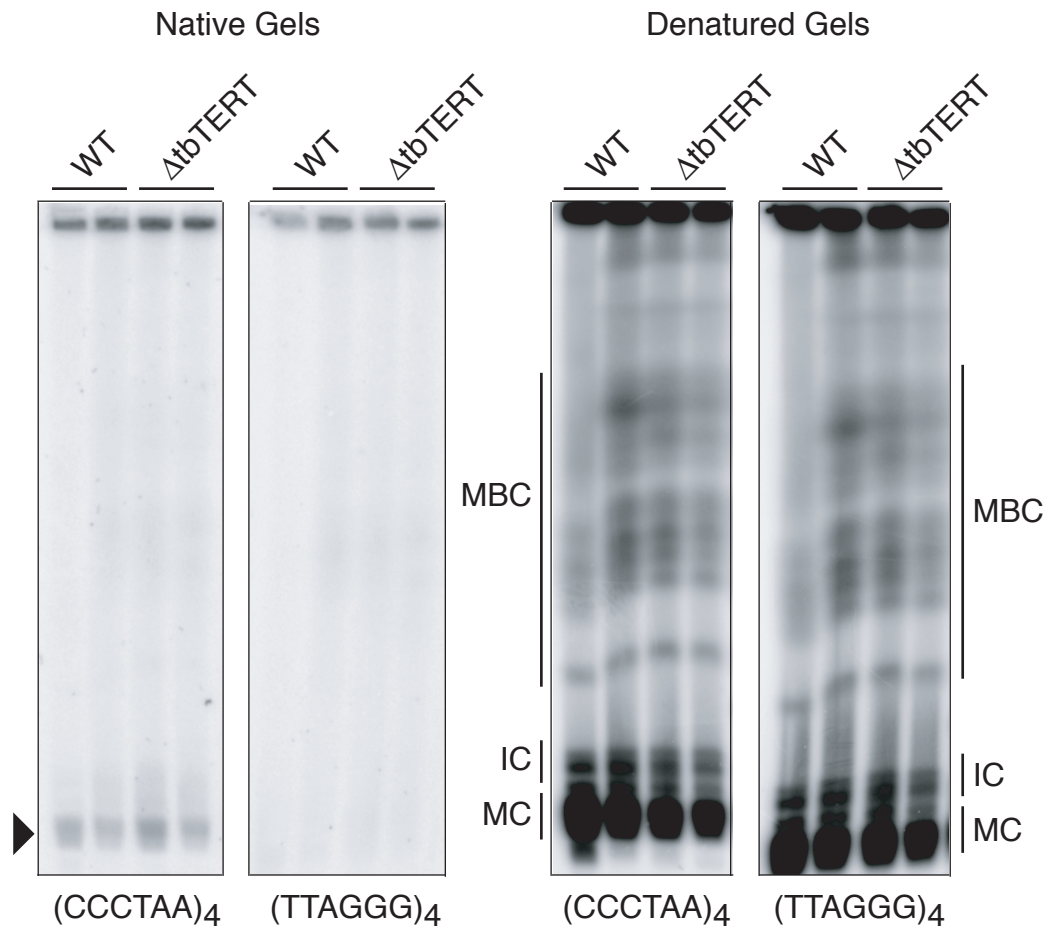
Figure 18

T. brucei G-overhangs are detectable by PFGE-overhang assay

Left panels: Native gels were run in parallel, dried and hybridized with $(TTAGGG)_4$ and $(CCCTAA)_4$–probes. Weak G-strand overhangs signal can be detected on abundant MC (arrowhead). Right panels: Gels upon denaturation and re-hybridization serve as a loading control. MBC and IC can be partially resolved whereas MC migrate at the bottom of the gel.

overhangs are detectable on highly concentrated MC, two gels were run in parallel, dried and hybridized with $(TTAGGG)_4$ and $(CCCTAA)_4$ probes as described before. Using this technique, a very weak G-overhang signal can be detected on MBC and IC. A robust G-overhang signal can be detected on MC (Figure 18, left panel, arrowhead). To verify the amount of DNA loaded in each lane, the gels were denatured, neutralized and re-hybridized with the same probes.

About 80% of telomeric signal on denatured conventional overhang assays is derived from MC (Figure 13). Since this signal cannot be detected by conventional overhang assay, we conclude that it is a consequence of the high concentration of telomere ends in a small area of the gel. Similarly, short (12–14 nt) yeast G-overhangs were recently detected by concentrating telomeres at one position in the gel (120).

Discussion

In this chapter, we presented the identification and characterization of *T. brucei* TERT and demonstrated that its deletion results in progressive telomere shortening at a rate of 3–6 bp/PD.

The shortening rate of 3–6 bp/PD is comparable to that observed in telomerase-deficient *S. cerevisiae*, and reflects the amount of telomeric DNA predicted to be lost as a consequence of the end replication problem (121,122). In other organisms, the rate of telomere shortening correlates with the length of the G-strand overhang (116,118). A previous study suggested that *T. brucei* telomeres terminate in single-stranded regions that range in size from 75–225 nt (101). Therefore, the moderate rate of telomere shortening that we observed in the absence of telomerase was unprecedented and led us to investigate G-overhang length, using a conventional in-gel hybridization technique (109). We were unable to detect any G-overhang signal on wild-type, TERT- or KU-deficient mutants. We then demonstrated that any putative *T. brucei* G-overhangs were not being degraded during DNA isolation, and we were easily able to detect artificially created G-overhangs. Furthermore, we were also able to detect G-strand specific signal on MC by PFGE-overhang assays. Taking into consideration the moderate rate of telomere shortening in the absence of

telomerase, our results strongly suggest that G-overhangs in *T. brucei* are short (<30 nt) and therefore undetectable by conventional in-gel hybridization, and that *T. brucei* might maintain their chromosome ends in a similar fashion to *S. cerevisiae*. While about 50% of plant chromosome ends harbor overhangs longer than 20–30 nt, the remaining telomeres have overhangs smaller than 12 nt or might be blunt ended and this could also be the case in *T. brucei* (235). We also cannot exclude the possibility that *T. brucei* telomeres might transiently acquire longer G-overhangs during a particular stage of the cell cycle. However, considering the sensitivity of our assays and the excessive amounts of telomeric fragments loaded onto the gels, we think this is unlikely.

Our data suggest that *T. brucei* G-overhangs are short, yet *T. brucei* telomeres assemble into a t-loop structure (101). This supports the notion that t-loops can be formed with short overhangs *in vivo* (105). Others have proposed telomerase as a potential drug target for *T. brucei*. Considering the low rate of telomere shortening, our results do not encourage this possibility.

Chapter III: Consequences of telomere shortening at the silent ES

Introduction

Telomeres of somatic human cells gradually shorten during each replication cycle. Although the eventual consequences of telomere shortening are manifested by cellular senescence and apoptosis, telomerase-deficient cells infrequently escape senescence or apoptosis and become survivors (114,236). Yeast and human survivors can maintain chromosome ends through Alternative Lengthening of Telomeres (ALT) (194,195). Telomerase-deficient *S. cerevisiae* can survive by replenishing chromosome ends through RAD51-dependent amplification of subtelomeric Y′ repeat elements or RAD50-dependent recombination among telomeres (237,238). Both types of survivors depend on the function of Rad52 and presumably involve break-induced replication (195,239). Cells lacking telomerase, Rad52 and ExoI can survive by palindrome-based amplification of subtelomeric regions. Furthermore, *S. pombe* can overcome the loss of telomeric DNA by circularization of its chromosomes (196,197). A small percentage of human cancers lack telomerase and utilize ALT to increase their telomere length (198).

In this chapter we describe the consequences of telomere shortening in the context of the three different chromosome types in *T. brucei:* MBC, IC and MC. In particular we focus on silent *VSG* ES located on MBC.

Results

Appearance of slow migrating, telomere repeat-containing DNA in long-term cultured T. brucei

The average telomere of the Lister 427 laboratory strain used in these studies measures ~15 kb (101). To monitor long-term telomere shortening and its consequences, several independent *TERT*-/- clones were continuously cultured without

any selection regime for ~2.5 years. After ~1 year in culture, telomeres of a TERT-deficient clone shortened significantly, and a dramatic reduction of telomere signal was evident after ~2.5 years of continuous propagation (Figure 19). A slowly migrating band also appeared in extensively propagated TERT-deficient strains, which could represent circular telomeric DNA (Figure 19, asterisk). To investigate whether the slow migrating band represented telomeric circles, we separated genomic DNA by 2-D gel electrophoresis (Figure 20) (201). Wild-type single marker, long-term cultured TERT-deficient *T. brucei* and human ALT cell line Saos-2 (positive control) were separated in the first dimension, each lane was cut out of the gel, perpendicularly embedded and separated in the second dimension. To visualize telomeric repeats, we performed in-gel hybridization using a $(TTAGGG)_4$ probe. Extrachromosomal circles in DNA from human ALT cells are readily detectable by 2-D gel electrophoresis. No circles were detected in DNA from long-term cultured TERT-deficient *T. brucei,* despite loading double the amount of DNA (Figure 20A, compare right and left panels). To test whether telomeric circles could be detected in *T. brucei*, we separated equal amounts of wild-type and TERT-deficient DNA on 2-D gels and failed to detect circular DNA in *T. brucei* (Figure 20B). Furthermore, we cannot exclude the possibility that the band observed in Figure 19 is too large to be separated even on a 2-D gel and remains stuck in the slot. To further characterize the nature of this band, we performed several experiments (Figure 21). First, we tested whether the band is susceptible to Bal31 digestion (Figure 21A). Exonuclease Bal31 attacks DNA ends and nicked DNA. We incubated DNA and enzyme for 60 minutes; at frequent intervals (15, 30 and 60 minutes) we took a sample, phenol-chloroform extracted the DNA and digested it with MboI and AluI. As shown in Figure 21A, the slow migrating band is susceptible to Bal31 digestion suggesting that it represents linear or nicked circles. The extent of Bal31-dependent telomere erosion is graphically represented in the right panel of Figure 21A. Thus, this experiment does not reveal much about the nature of the band.
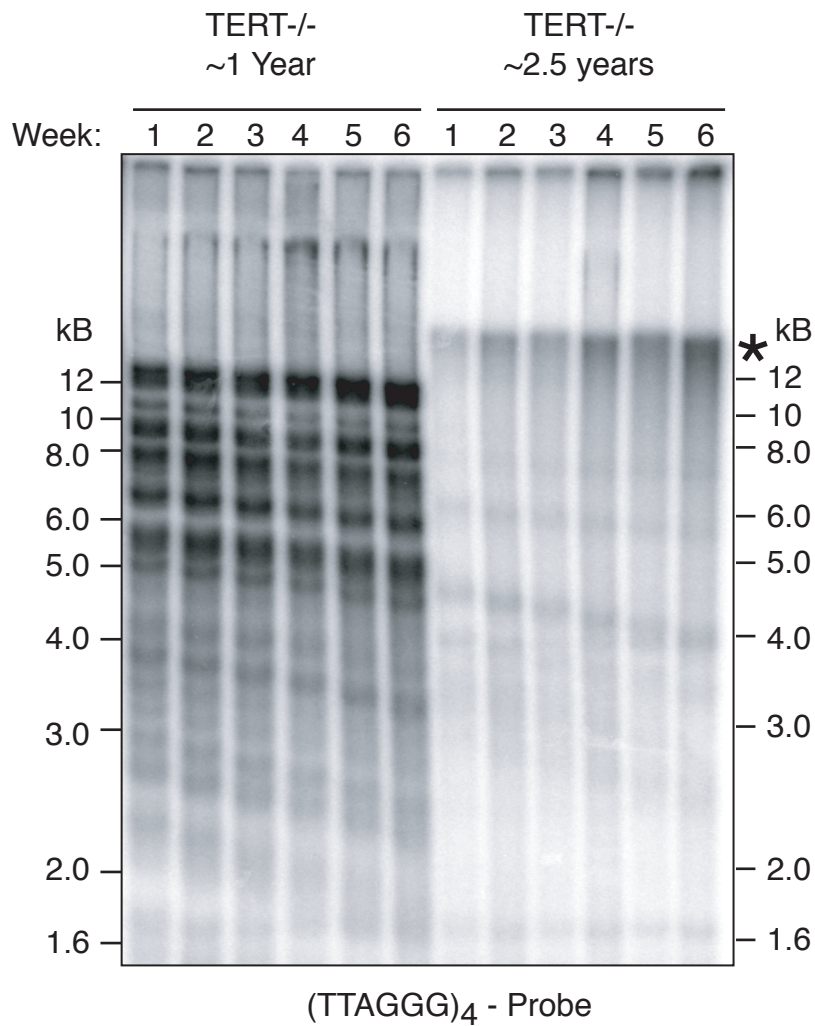
Figure 19

Telomere loss in long-term-cultured telomerase-deficient *T. brucei*.

Telomerase-deficient cells exhibit gradual telomere shortening at a rate of 3–6 bp / PD during 6 week time courses after 1 or 2.5 years in continuous culture. DNA was digested with MboI / AluI and hybridized using a $(TTAGGG)_4$ probe. Equal loading was ensured by quantification of digested DNA prior to loading using a fluorometer. Loss of telomeric DNA is reflected in the decrease in telomeric signal. (*) indicates the appearance of a high molecular band in long-term cultured telomerase-deficient cells.

1st Dimension

A)

*tb*TERT-/- (2.5 years)   Saos-2 (human ALT)

kB 23 12 8 6 4 2   23 12 8 6 4 2

2nd Dimension

circular DNA
supercoiled
circular

single-stranded DNA   single-stranded DNA

B)

*tb*TERT-/- (2.5 years)   *T. brucei* wild-type

kB 23 12 8 6 4 3 2   23 12 8 6 4 3 2
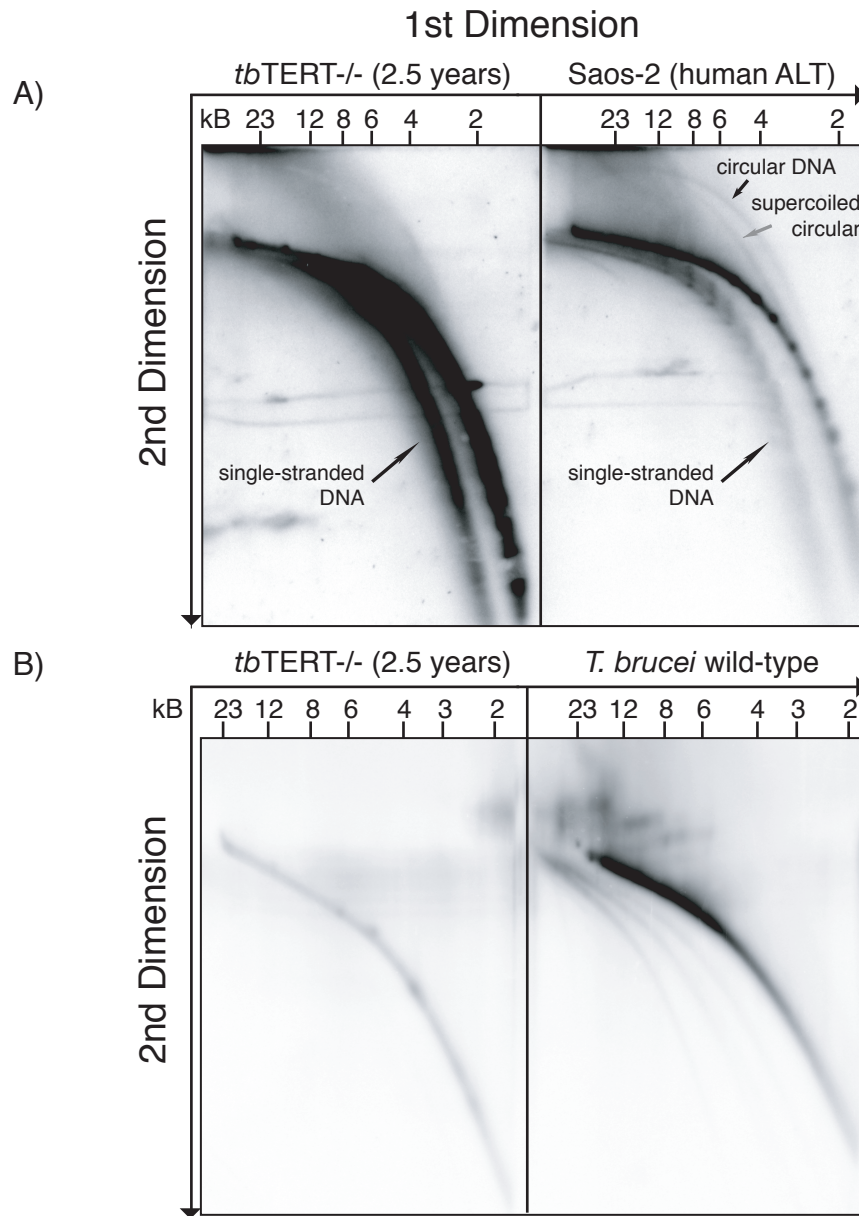
2nd Dimension

Figure 20

Failure to detect extrachromosomal telomeric circles in *T. brucei* by 2-dimensional gel electrophoresis

A) MboI / AluI digested DNA of *T. brucei* TERT-/- mutant and human ALT cell line Saos-2 (positive control) separated as described by Fangman and Breyer. To visualize telomeric fragments, gels were dried and in-gel hybridized, using a radiolabeled $(CCCTAA)_4$ probe. 8 μg Saos-2 DNA and 16 μg of *T. brucei* TERT-/- DNA was loaded.

B) Comparison between telomerase-deficient cell line (left) and wild-type *T. brucei* (right). Equal amounts of DNA were loaded for both samples (~8 μg). Note the dramatic reduction of telomere signal in the long-term cultured TERT-/- cell line.

Next we tested whether the band could represent previously identified extrachromosomal circles (240). These circles consist of highly repetitive NR-elements (digested by NlaIII) which contain imperfect telomere repeat sequences and are found in Lister 427 and other isolates yet, curiously, are absent from the genome sequencing strain TREU 927 (240). Nothing is known about the relevance or function of these extrachromosomal circles. We tested whether these circles could be amplified in long-term cultured TERT-deficient *T. brucei* (Figure 21B). Digestion of DNA with NlaIII gives rise to a smeared ladder, representing the repetitive NR-element. Southern blotting using an NR-hybridization probe, in comparison with DNA loading (as judged by Ethidium bromide staining of the gel) revealed no difference in signal intensity between wild-type or long-term cultured *T. brucei* (Figure 21B, upper and lower panel). We addressed by native in-gel hybridization using strand-specific $(CCCTAA)_4$ and $(TTAGGG)_4$ probes, whether the slow migrating band could represent single-stranded DNA (Figure 21C). The band could not be detected on the native gels, indicating that it is not single-stranded (Figure 21C, left two panels). Subsequent denaturing and rehybridization of the gels confirmed the presence of the band and equal loading between lanes (Figure 21C, right two panels, arrowhead). Note also the dramatic difference in telomere signal between parental and long-term cultured TERT-deficient cell lines. To test whether the band represents individual telomeres that have undergone dramatic elongation, we separated chromosomes by PFGE (Figure 21D). Although preliminary, we did not detect a dramatic increase of telomeric signal on any chromosome (Figure 21D, lanes 2.5 years in culture). Note the increase of telomere signal in long-term cultured cells complemented with telomerase (lane: +TERT). The nature, origin and significance of the slow migrating band remains completely unknown.
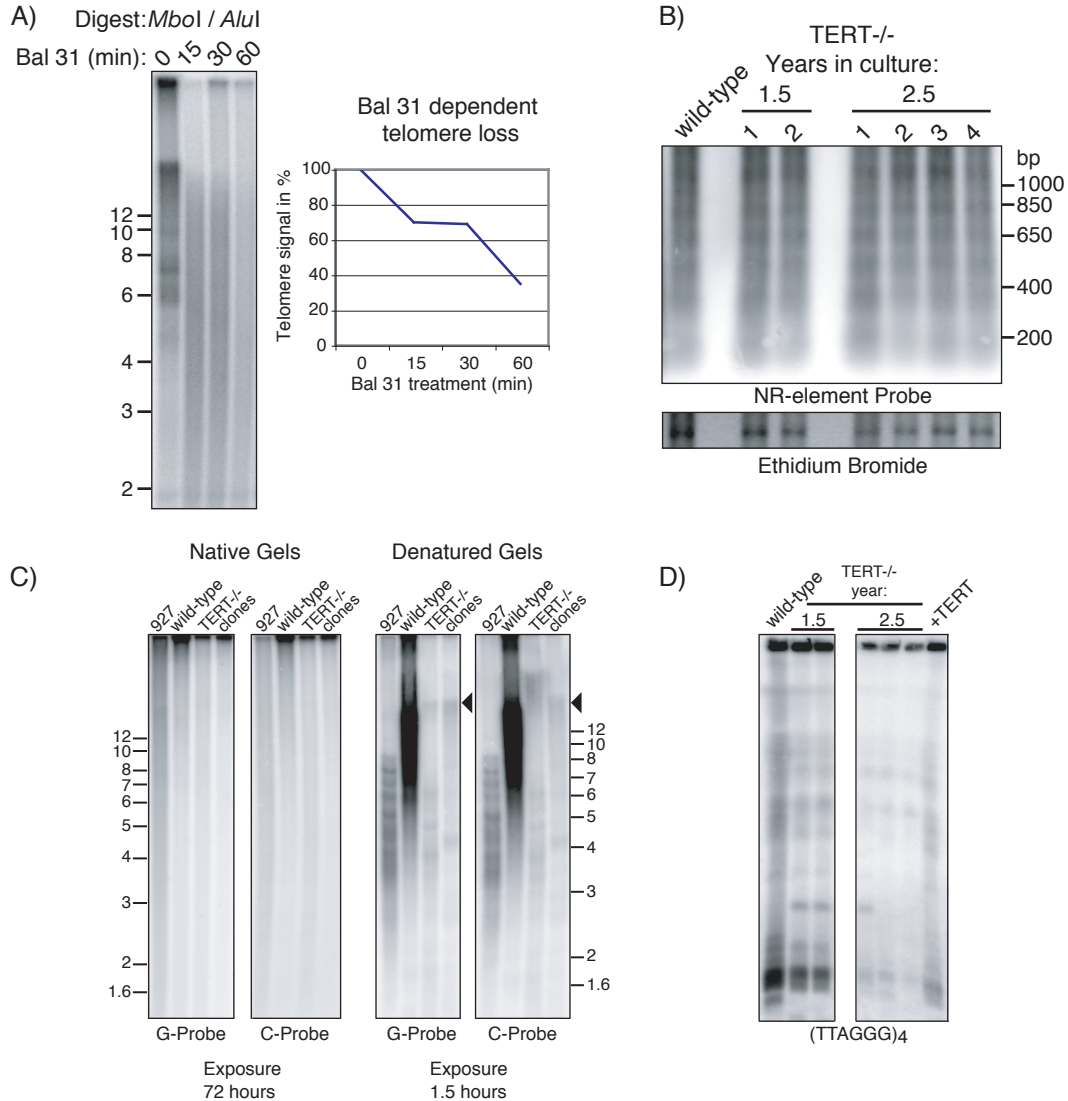
Figure 21
Characterization of the slow migrating band
A) The band is susceptible to Bal 31 digestion. Right panel:
quantified telomere signal decreases over time of Bal 31 treatment.

B) Long term cultured telomerase-deficient mutants do not accumulate
extrachromosomal NR- circles.

C) Overhang assay: the slow migrating band is double stranded.
Left two panels: no signal is detectable on native gels. Right two panels:
The slow migrating band is visible on denatured gels in long-term cultured
telomerase-deficient clones (TERT-/- clones, arrowhead). 927 is the strain used for
the genome sequencing project.

D) PFGE of long term (1.5 and 2.5 years) telomerase-deficient mutants.
No dramatic amplification of telomeric DNA occurs on individual chromo-
somes.

To measure the decline in telomere signal in different chromosome classes, gels were dried and probed with a radiolabeled $(TTAGGG)_4$ probe (Figure 22A). To ensure equal loading, the telomeric signal was normalized to a 50-bp repeat signal, which is uniquely present in long arrays upstream of ES promoters (Figure 22A, right panel). Comparable results of telomere decline were obtained when a single copy gene, the Puromycin ORF located on chromosome 11, was used as a loading control (Figure 22B, upper and lower panel). Quantitative analysis of these blots revealed that the telomere signal on MBC declined to ~12% of its initial intensity after ~2.5 years in culture. Surprisingly, the telomere signal on MC reproducibly decreased to ~6% (Figure 22A, middle panel). We also observed aberrant migration of IC, which will be discussed later (Figure 22A, right panel, arrowhead).

To investigate what could account for this difference of telomere loss between MBC and MC, and to study the effects of telomere loss on MC stability, we analyzed the karyotype of TERT-deficient cell lines in more detail by hybridization to a 177-bp repeat motif that is unique to MC (Figure 23A, lower panel). The 177-bp repeat signal decreased to approximately half of its initial intensity, relative to 50-bp and MBC-internal loading controls, over the course of ~2.5 years, as graphically represented in figure 23B. These results were reproducible for all independently propagated clones.

If MC had fused to each other, the 177-bp signal could have been redistributed over the gel and thereby reduced in the designated MC region. Although we did not observe any obvious chromosome fusions, we also quantified MC in unfractionated DNA by 'slot blot' (Figure 23C). Quantitative phosphorimager analysis of four independent experiments confirmed that the 177-bp MC signal was reduced to ~50% of its initial intensity (Figure 23D). We attribute the decline of 177-bp signal to loss of MC. This interpretation is consistent with the 50% reduction in TTAGGG signal on MC compared to MBC (Figure 22).
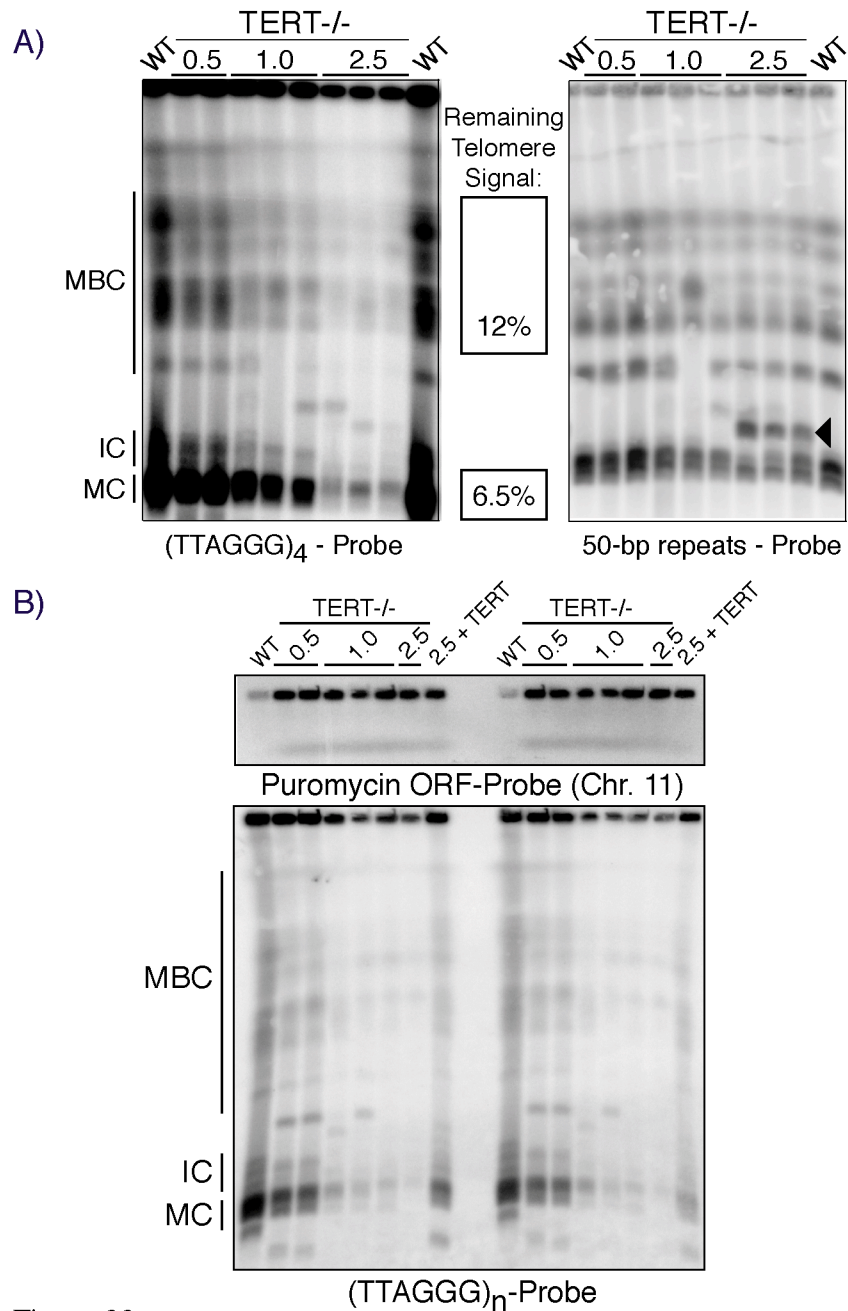
Figure 22

Telomere loss in telomerase-deficient *T. brucei* by PFGE

A) Telomere loss on different chromosome types. Megabase chromosomes (MBC), separated from intermediate (IC) and minichromosomes (MC) by PFGE. Left panel: telomeric signal decrease in long-term cultured clones (0.5, 1.0 and 2.5 years). Two or three individually cultured clones were analyzed for each time point. Right panel: a duplicate gel, hybridized with a 50-bp probe, served as a loading control to measure relative telomere signal decline on MBC versus MC. Arrowhead marks rearrangements among IC.

B) Comparable results were obtained when a single copy gene (Puromycin ORF) was used as loading control. Duplicate gels were run in parallel and probed with Puromycin ORF (upper panel) and telomeric probe.
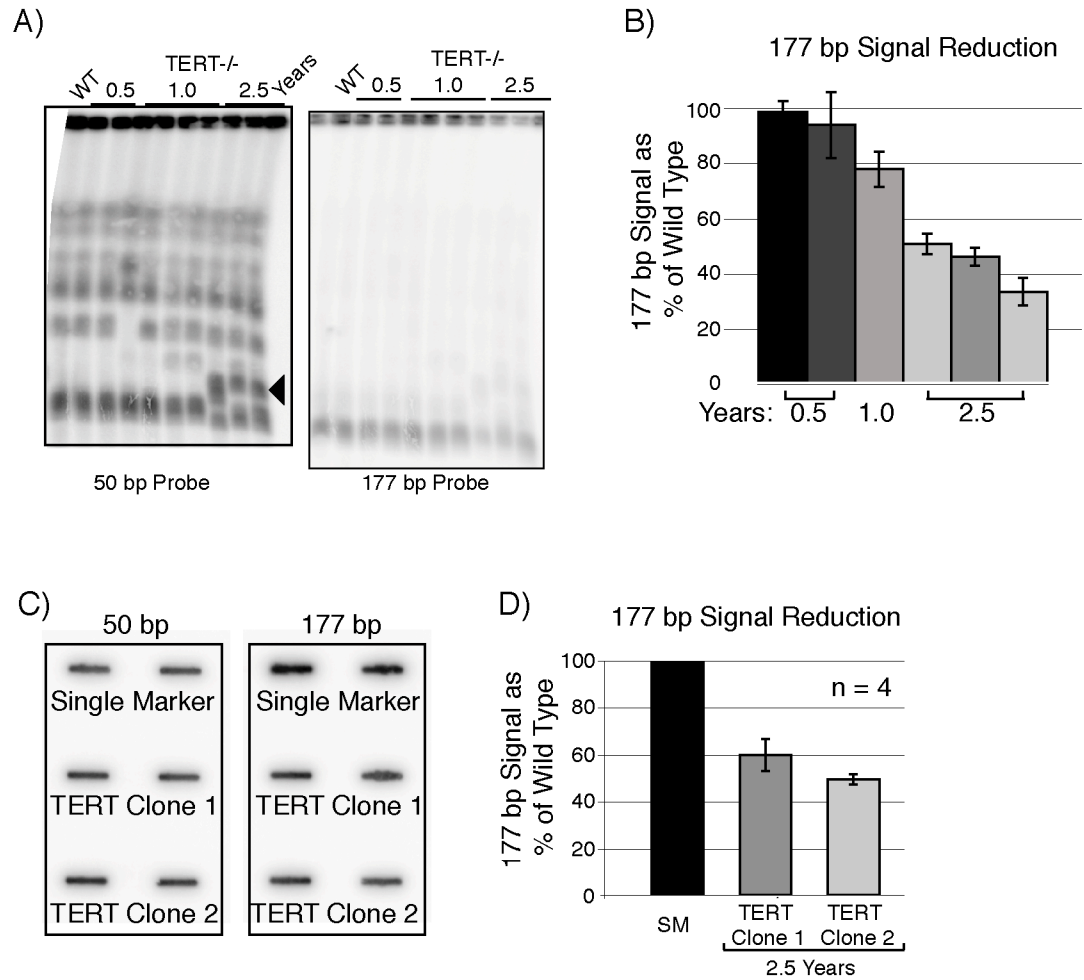
Figure 23

Minichromosome (MC) loss in long-term cultured mutant parasites

A) Whole chromosomes, separated by PFGE and analyzed by Southern blot.
Left panel: 50-bp repeat probe serves as loading control for MBC and IC
(arrowhead indicates IC rearrangements).
Right panel: the same gel upon re-hybridization with MC-specific 177-bp
repeat probe.

B) Phosphorimager quantification of MC signal in several clones at different time
points (0.5, 1, 2.5 years). 177-bp signal was normalized to 50-bp signal; bar graphs
represent average 177-bp signal of three independent gels (standard deviation indicated).

C) Slot blots using 50-bp repeat probe as loading control and 177-bp probe
to confirm MC loss in long term cultured telomerase-deficient strains (clones 1 and 2).

D) Quantified results of 4 experiments are represented graphically.

We noted new bands in the region where IC migrate. These bands hybridized with a 50-bp probe and no signal was obtained by using the MC-specific 177-bp probe (Figure 22A, arrowhead). By using PFGE conditions that specifically separate the ~5 IC, and hybridization with 50-bp probe, we confirmed that some IC in long-term culture TERT-deficient *T. brucei* migrated slower on the gel (Figure 24A, arrowheads). It is hard to judge from this gel whether the number of IC was reduced to 4 or whether two IC co-migrate. The slowest migrating band lies beneath the compression zone where resolution is limited. These changes could be the result of chromosome fusions or rearrangements. We confirmed the origin of these rearrangements to IC by using IC-specific genes *VSG* 17-21 (Fig. 24B, left panel) and *VSG* 17-13 (Figure 24B, right panel), as hybridization probes. However, since we have very little understanding of IC function or relevance, we did not investigate these events further.

We also observed one example of a rearrangement among MCB, which is consistent with the very infrequent rearrangements observed previously, and with the fact that the diploid chromosomes of *T. brucei* can differ greatly in size, due to variations in long chromosome-internal repetitive regions, transposon-like sequences and other pseudogenes that accumulate in large subtelomeric regions and possibly facilitate recombination (Figure 22A, right panel, 1 year time point) (241,242).

In conclusion, no significant rearrangements were detected in MBC using 50-bp repeat and chromosome-internal hybridization probes (Figure 22, 23). Next, we tested whether dramatic telomere shortening, loss of MC and rearrangements among IC, led to any growth defect in long-term-cultured telomerase-deficient strains. As judged by a growth curve over 11 days, telomerase-deficient clones (1–4) reproducibly grew slightly faster than the wild-type single marker strain (Figure 25A). Telomerase-deficient clones were continuously propagated for ~2.5 years, which could adapt them better to *in vitro* culture and explain their slight growth advantage. To address whether telomerase-deficient strains have impaired viability, we subcloned 50 cells into 96-well plates and counted positive wells after 4–5 days. Figure 25B represents
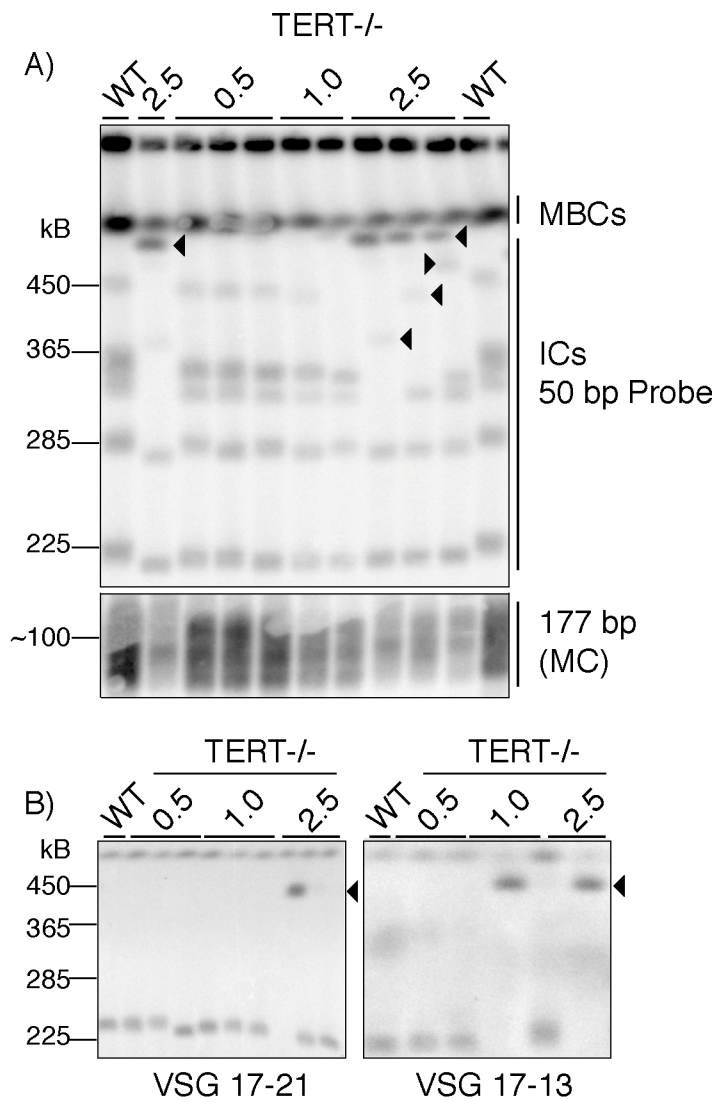
Figure 24
Genomic rearrangements at intermediate chromosomes (IC).

A) Upper panel: RAGE conditions used allow separation of individual IC.
Time of culturing is indicated on top of the gel (0.5, 1.0 and 2.5 years).
Rearrangements are visualized by hybridization with a 50-bp probe and
indicated by arrowhead. Note that megabase chromosomes (MBCs) are
not well resolved under these conditions.
Lower panel: same gel upon rehybridization with 177-bp probe confirms loss
of minichromosomes (MC).

B) Hybridization with IC-specific *VSG* probes: *VSG* 17-21 and *VSG* 17-13
reveal that high molecular bands occurring after 2.5 years of culturing are
IC-derived (see arrowhead). Note that these are two different gels.
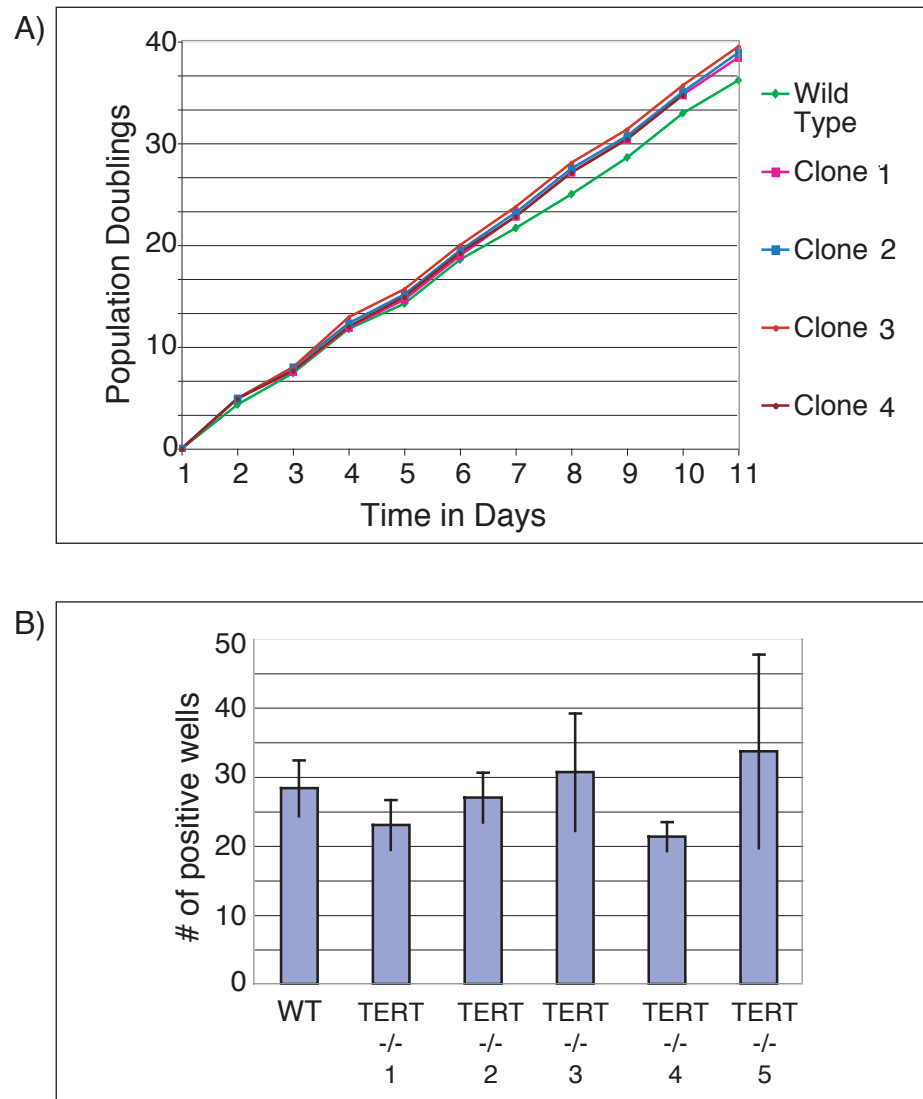
Figure 25

Long-term cultured telomerase-deficient mutants have no growth defect

A) Growth curve of long-term cultured telomerase-deficient *T. brucei* (Clone 1-4) in comparison to wild-type single marker.

B) Viability of five long-term cultured telomerase-deficient clones in comparison to wild-type, assessed by subcloning 50 cells of each strain into 96-well microtiter plates.
Standard deviation for 3 experiments per clone is shown.

results of 3 independent experiments with 5 telomerase-deficient clones and indicates that viability was not impaired in long term cultured TERT-/- mutants.

Telomere length stabilization in the absence of telomerase

To study what happens when telomeres become critically short, we monitored telomere shortening of several MBC at frequent intervals for ~2 years. After two years of continuous culture, a 21-week time course was performed with three independently cultured clones (Figure 26A). During this time course DNA was isolated in weekly intervals. Genomic blotting with numerous unique silent telomeric *VSG* probes identified ES, whose telomere had become critically short and allowed us to study the consequences of dramatic telomere loss at single-chromosome resolution. We first investigated the fate of the silent *VSG* 121 telomere. Our strain contains three copies of *VSG* 121, only one of which is telomeric. A terminal restriction fragment containing part of *VSG* 121, released by digestion with EcoRI, gradually shortened during the first two weeks of observation (Figure 26A). Between weeks 3–5, the rate of shortening decreased and the length of this restriction fragment ultimately stabilized (weeks 6-11). Thus, the length of the *VSG* 121 chromosome end remained stable during several additional months of continuous culture. We confirmed this result by analyzing the *VSG* 121 chromosome end in a second independent clone, using a different restriction enzyme to liberate the terminal fragment (Figure 26B). To exclude the possibility that stabilization is occurring exclusively at the *VSG* 121 telomere, we also analyzed a second silent ES telomere (*VSG* bR2) (Figure 26C and D). There are 4 copies of *VSG* bR2, two of which are ES-linked (arrowhead and asterisk). Non-telomeric *VSG* bR2 restriction fragments did not change in size but the ES-linked fragments gradually shortened. One ES-linked copy of *VSG* bR2 had a short telomere (asterisk) that allowed good resolution of size changes on an agarose gel. This telomere progressively shortened up to week 12 and then stabilized. At week 14, a clone was picked out of the population and kept in culture for an additional 13 weeks (Figure 26D). The *VSG* bR2 band was initially sharp (week 16).
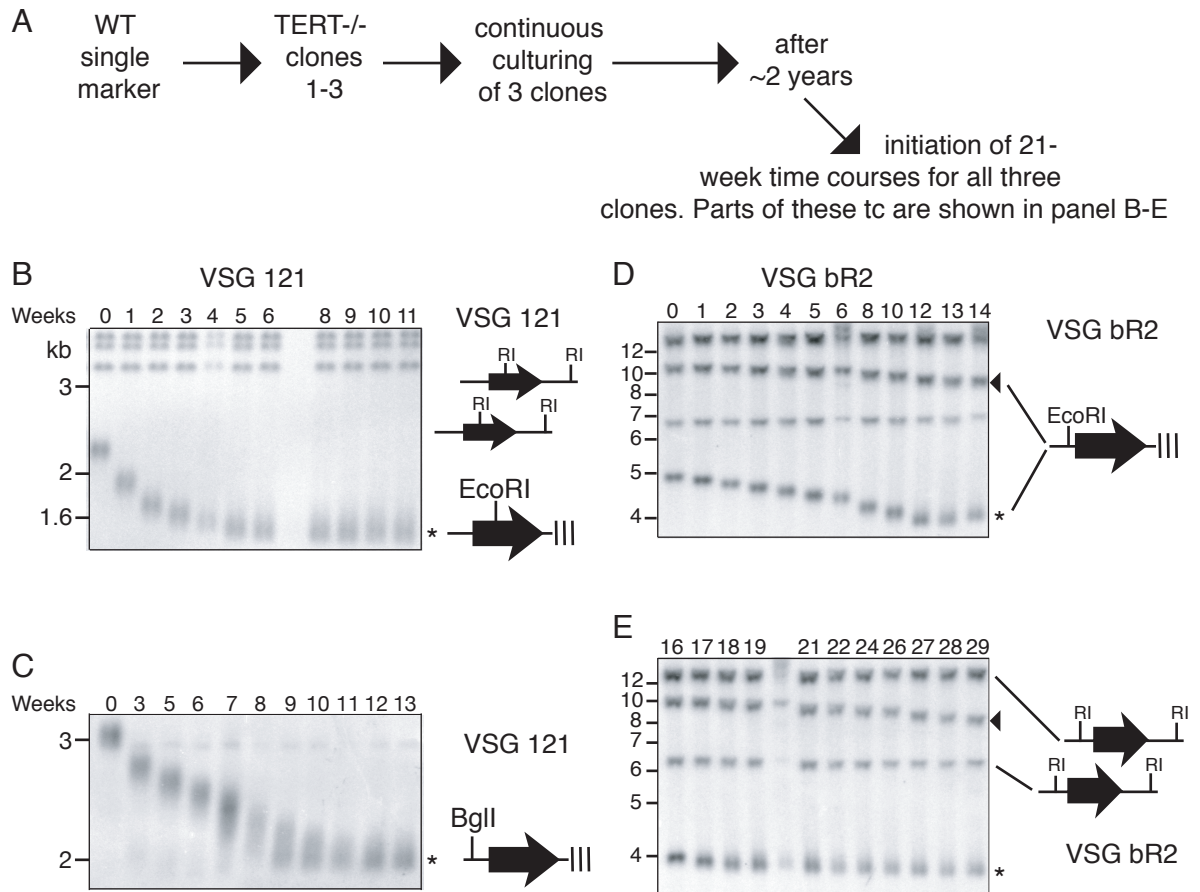
Figure 26

Telomere stabilization at short silent *VSG* 121 and *VSG* bR2 ES telomeres

Time of culture is indicated in weeks above each lane (1 week corresponds to
~24 population doublings). Bands corresponding to chromosome-internal copies
of *VSG* 221 and bR2 do not change in size.

A) 3 TERT-deficient clones were kept in continuous culture for ~2 years.
Terminal restriction fragment analysis with several probes was then performed during
a time course of 21 weeks; parts of these time courses are shown in panel B-E.
B) Stabilization of the *VSG* 121 terminal restriction fragment (*) liberated by
EcoRI occurred at week 5 of the time course.
C) *VSG* 121 telomere stabilization after 10 weeks of culture analyzed in a
second clone using BglI digestion (chromosome-internal BglI fragments
migrate higher and are not shown).
D) EcoRI liberates the two telomere-linked copies of *VSG* bR2. One copy is
located in an ES with a long telomere (arrowhead) and the second copy is
located in an ES with a shorter telomere, whose length stabilized after 12 weeks (*).
E) The population from panel C was cloned at week 14 and one clone was
propagated for an additional 13 weeks. The short telomere (*) remained stable
throughout the remaining 13 weeks, whereas the longer terminal restriction
fragment continuously shortened (arrowhead).
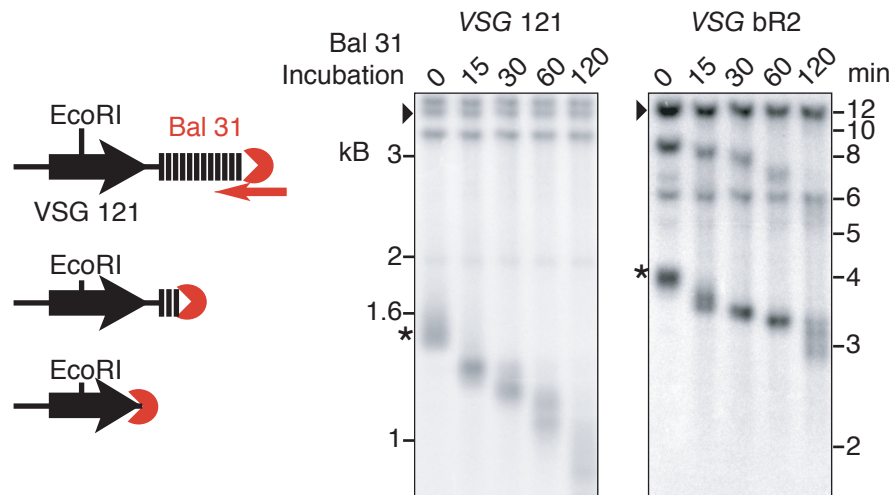
Figure 27

Bal 31 digestion of short stabilized *VSG* 121 and bR2 ES telomeres

Exonuclease Bal 31 attacks free ends. During a time course of Bal 31 incubation, stabilized terminal restriction fragments of *VSG* 121 (left panel) and *VSG* bR2 (right panel) were liberated by EcoRI digestion and are susceptible to Bal31 digestion (*) whereas chromosome-internal copies are resistant (arrowhead)

Over time, the average length of the terminal fragment did not change significantly, but the band became more heterogeneous (compare Figure 26D, week 16 and 29). Upon further culturing, telomere stabilization also occurred on chromosome arms harboring *VSG* 224 and *VSG* 1.8.

To confirm that the stabilized short chromosome ends remained terminal and did not fuse with other chromosome arms, we treated the DNA with the exonuclease Bal31, after which the DNA was cut with EcoRI to liberate terminal restriction fragments that could be visualized with *VSG* probes (Figure 27). Telomere-linked copies of *VSG* 121 and *VSG* bR2, regardless of whether they were stabilized or not, were highly susceptible to Bal31 treatment (Figure 27, asterisks), indicating that they remained terminal. Non-telomeric copies (arrowheads) were unaffected by Bal31. Telomerase-deficient *S. pombe* can survive by circularizing their chromosomes (197). Circularized chromosomes migrate slower during Rotating Agarose Gel Electrophoresis (RAGE) separation (243). Using *VSG* 121 and bR2 as hybridization probes, we verified that the chromosomes harboring these *VSG* remained linear and *VSG* 121 and bR2 did not recombine onto other chromosomes (data not shown).

Taken together, telomere length analyses of different chromosome arms over several months indicated that, upon reaching a critical length, terminal restriction fragments were stabilized by a telomerase-independent mechanism. This mechanism seems to act exclusively at critically short telomeres, since longer telomeres continued to progressively shorten. Such a distinction has not been observed in other species in the absence of telomerase.

Cloning and sequencing of short stabilized telomeres

To address whether short stabilized chromosome arms still contained telomeric repeats or whether they were maintained by amplification of subtelomeric sequences, short stabilized *VSG* 121 chromosome ends were cloned and sequenced using a telomere tailing method (244). PolyC tails were added to purified ~2kB terminal restriction fragments (previously isolated from agarose gels) using terminal
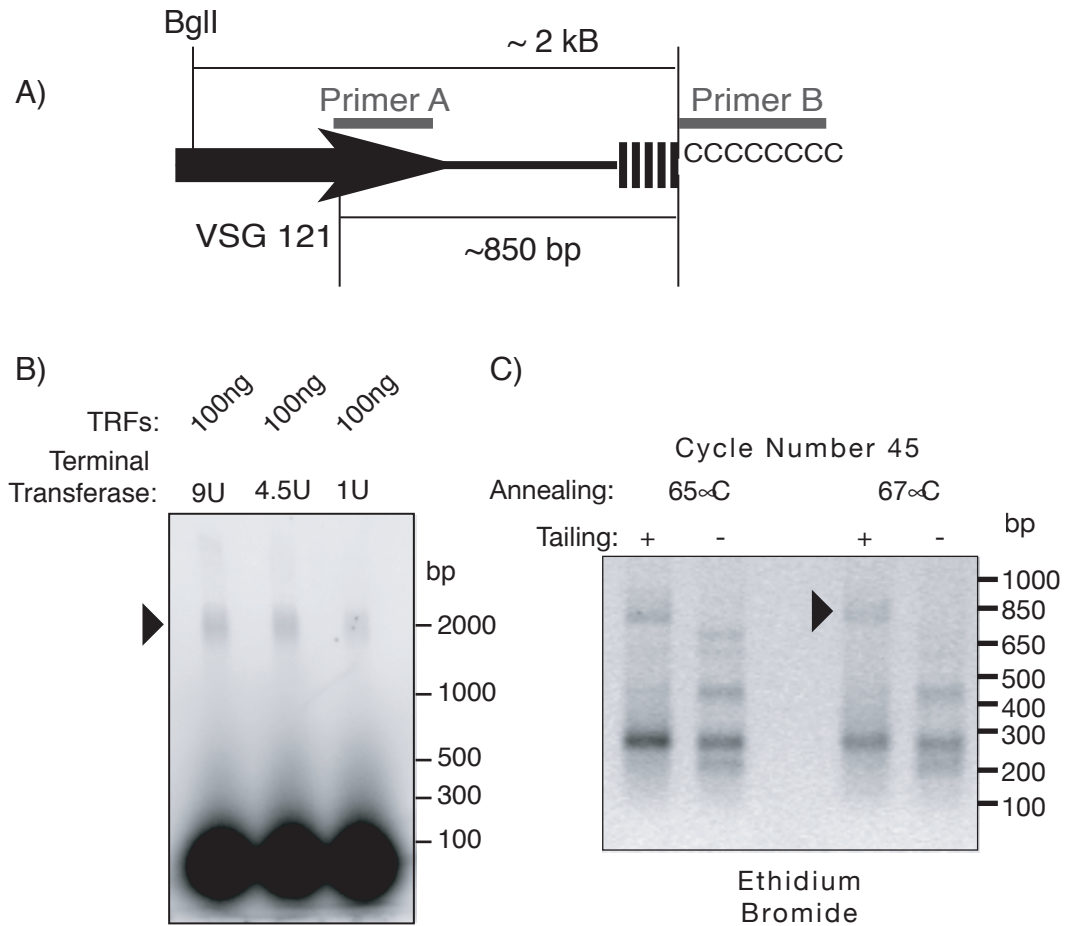
Figure 28
Tailing of short stabilized terminal restriction fragments (TRF)

A) BglI restriction fragments, representing the stabilized VSG 121 TRF were isolated
from an agarose gel and tailed using terminal transferase and dCTP.
121 chromosome termini specific fragments were PCR amplified using primers A and B.

B) Incorporation of radiolabeled dCTP into BglI TRFs verified the efficiency of the tailing
reaction. Tailed products were run on a 1.8% agarose gel, the dried gel was exposed
to a phosphoimager. Labeled TRFs are indicated by the arrowhead, excess
unincorporated nucleotides migrate on the bottom of the gel. Optimal incorporation
efficiency was obtained by using 4.5 units / reaction.

C) PCR amplified products of tailed TRFs on agarose gel (see arrowhead). High cycle
number leads to unspecific products, thus non-tailed TRFs were used as negative control.
The indicated PCR product was gel purified and subcloned into pGEM-T.

A)

Clone:	1	2	3	4	5	6	7	8	9	10

850 —
bp
650 —
500 —

B)

AGGGGG (TTAGGG)$_7$	———	CCCCCCCCCCCCCCCCCCC
AGGGGG (TTAGGG)$_6$	TTAGG_	CCCCCCCCCCCCCCCCCCC
AGGGGG (TTAGGG)$_9$	T_____	CCCCCCCCCCCCCCCCCCC
AGGGGG (TTAGGG)$_{17}$	———	CCCCCCCCCCCCCCCCCCC
AGGGGG (TTAGGG)$_{18}$	T_____	CCCCCCCCCCCCCCCCCCC
AGGGGG (TTAGGG)$_{27}$	TTA____	CCCCCCCCCCCCCCCCCCC

sub-   telomeric   partial   poly C - tail
telomeric   repeats   telomeric
region   repeats
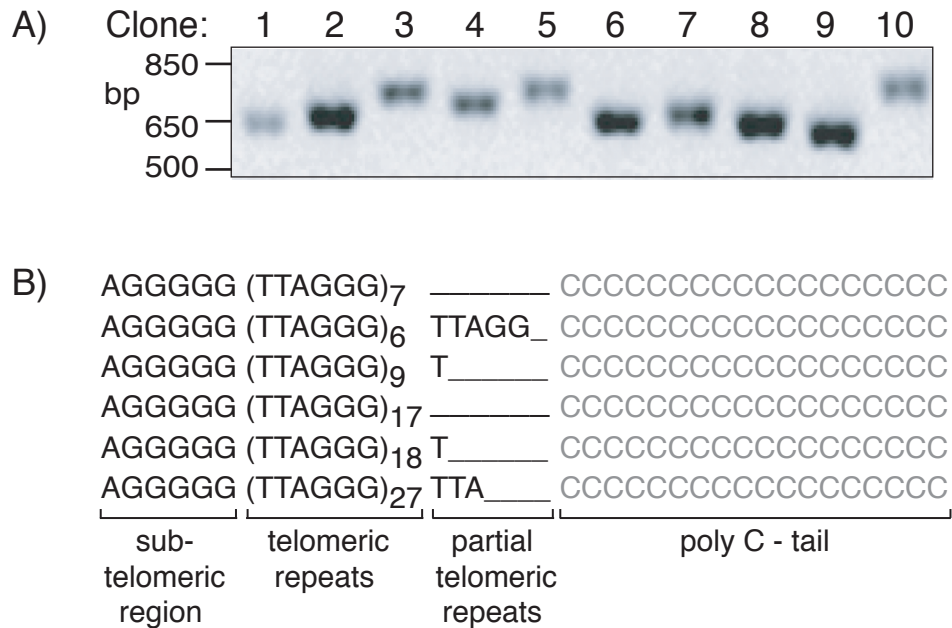
Figure 29

Cloning and sequencing of stabilized tailed terminal restriction fragments

A) Restriction analysis of individual clones showed the differently sized PCR products, confirming the size heterogeneity observed on southern blots.

B) Sequencing of individual clones revealed that chromosome termini are capped by telomeric repeats. The number of perfect hexameric repeats varied from as little as 7 up to 27. The terminal nucleotide varied between individual clones (TTAGG, T, TTA or TTAGGG). Sequences shown are representative of 17 sequenced clones. By comparison with wild-type DNA, no changes occurred in the subtelomeric region of *VSG* 121.

transferase. *VSG* 121 (primer A) and polyG primers (primer B) were used to PCR-amplify the region encompassing the 3´ end of the *VSG* 121 ORF, the subtelomeric region, and the end of the chromosome (Figure 28A). We verified tailing of purified 2kB terminal restriction fragments by measuring the incorporation of radiolabeled [32-]P-dCTP (Figure 28B). Maximum incorporation of radiolabeled dCTP was achieved by using 4.5 units of terminal transferase. Thus, we were confident that we obtained optimal conditions for the tailing reaction. Next we used primers A and B to PCR amplify the region between tail and *VSG* 121. The high cycle number led to the amplification of unspecific PCR products. To identify tailing specific products, we ran non-tailed (-) PCR reactions in parallel on the agarose gel (Figure 28C). Tailing specific PCR products were ligated into a cloning vector and analyzed by restriction digest and sequencing. The amplified products varied in size among the clones (Figure 29A). Sequencing of 17 clones (representative sequences are shown in (Figure 29B) revealed terminal TTAGGG-repeat tracts that ranged from 41–200 bp, reflecting the size heterogeneity observed by Southern blot (Figure 26). To further confirm that no changes occurred in the subtelomeric region, we PCR amplified this region in wild-type cells, using *VSG* 121 and $(CCCTAA)_5$ primers. Comparison of wild-type to mutant cells showed that no amplifications or rearrangements occurred in the ~200 bp subtelomeric region between the *VSG* and the TTAGGG repeat tract.

The very end of the sequence varied between individual clones (Figure 29B). By adapter cloning of telomere ends, it was previously shown that *T. brucei* telomeres terminate in TTAGGG (213). This and other work suggested that the templating region of telomerase RNA ends in AATCCC-5´ (209). The difference of terminal sequence that we observe at short stabilized telomeres suggests that the mechanism of telomere stabilization is independent of telomerase RNA. In conclusion, our results suggest that a potentially novel mechanism maintains 41–200 bp of terminal TTAGGG repeats in the absence of telomerase.

Does telomere length affect ES silencing?

Transcriptionally silent ES are subject to a telomere position effect (49), but it is not known whether a silent ES can become transcriptionally activated if telomeres become very short. To address this question, we measured silent ES *VSG* 121 and bR2 transcripts by northern blot as telomeres became critically short and stabilized. *VSG* 121 and bR2 transcripts remained undetectable during this time. Furthermore, these

cells continued to stably express the initial *VSG* (Figure 30). These preliminary results suggest that progressive telomere shortening and subsequent stabilization does not lead to transcriptional activation of silent ES. In a previous study, an entire ES lacking telomeric repeats, located on a circular bacterial artificial chromosome, was transfected into *T. brucei*. ES promoters of these constructs remained transcriptionally silent, suggesting that telomeres are dispensable for ES silencing (245).

Discussion

Telomere shortening led to loss of many of the apparently non-essential MC, and to rearrangements among IC. MBC remained stable. Several possibilities could account for these differences. Loss of MBC, which contain essential genes, would presumably be lethal. IC only appear to contain ES, which can be active or silent, so rearrangements or loss may be tolerated to some degree. MBC and MC exhibit notably different positional dynamics during mitosis: MC associate directly with the leading edge of the mitotic spindle whereas MBC lag behind and are partitioned by classical kinetochore microtubules (246-248). Segregation of MC normally occurs with high fidelity, as shown by their stable inheritance over 5 years of propagation, but it remains unclear how the large number of MC are faithfully replicated and segregated on one mitotic spindle (20). We suggest that MC may be attached to the mitotic spindle through their telomeres. As a consequence of dramatic telomere
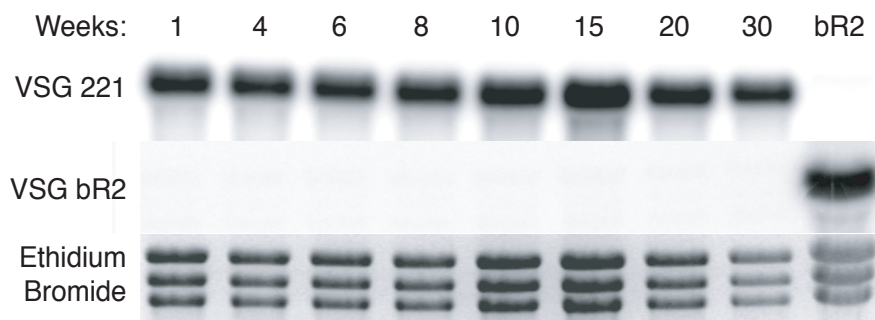
Figure 30

Northern blot: telomere stabilization does not lead to ES activation.
mRNA was isolated periodically for 30 weeks during which the *VSG* bR2 telomere stabilized.
Upper panel: Northern blot analysis demonstrates that *VSG* 221 remains actively expressed.
Middle panel: Re-hybridization of the same blot with a *VSG* bR2 probe indicates that the bR2 expression site did not become activated during telomere stabilization. A positive control for *VSG* bR2 is in the far right lane.
Lower panel: Ethidium Bromide ensures equal loading between lanes.

shortening, spindle attachment becomes unreliable, so MC can be mis-segregated and give rise to cells lacking a particular MC, or containing extra copies. During successive rounds of replication, cells harboring extra MC might require slightly more time to replicate. During 2.5 years, a minute replication disadvantage could favor the survival of cells with fewer MC. A comparable situation has been observed between different types of survivors in telomerase-deficient *S. cerevisiae*. Type I survivors, which maintain their chromosome ends by extensive amplification of subtelomeric Y´ elements have impaired viability and are usually outgrown by Type II (telomere-telomere recombination) survivors. Extensive amplifications of Y´ elements (10% increase in genome size) increases the time needed for replication and could result in the observed growth disadvantage (238).

The different segregation properties of MC and MBC might be comparable to a well-studied phenomenon in *S. pombe*, where mitotic chromosome segregation depends on centromeric sequences but, during meiotic prophase, chromosomes are aligned through an oscillatory back and forth movement called the horsetail stage (249). During meiotic prophase, the spindle pole body associates with telomeres (250). Deletion of Taz1, a telomere-binding factor, leads to deficient telomere clustering and meiotic recombination (251). Similarly, pedigree analysis of artificial minichromosomes in budding yeast demonstrated that telomeric sequences dramatically enhance faithful segregation to mother and daughter cell (252,253).

Short MBC telomeres stabilized as they reached a length of ~41–200 bp. Bal31 digestion confirmed that these short telomere tracts were indeed terminal and that stabilized chromosomes did not fuse. 41–200 bp of telomeric repeat are sufficient to stabilize a chromosome end. The size of 40 bp possibly reflects the minimal amount of sequence needed for binding of one or two TRF dimers, which are necessary for telomere protection (168,230). The terminal nucleotide varied between different clones, indicating that telomere stabilization is independent of the telomerase template RNA. Importantly, our data suggest that telomere stabilization is sufficient to ensure genomic integrity of MBC in a large majority of cells, since there was no discernable impact on long-term population growth. Nevertheless, *T. brucei* might

have an enhanced propensity to undergo homologous recombination, similarly to *sir /
tlc* deficient yeast that become survivors without going through crisis (254).

We monitored telomere loss at several MBC and IC silent ES during 2.5 years. Silent
telomere shortening occurred at a constant rate of 3–6 bp/PD, and we did not observe
any telomere-telomere recombination. We did not detect extrachromosomal telomeric
circles, which could explain why short telomeres remained stable, during several
months of continuous culture, and did not undergo the dramatic telomere elongation
observed in human ALT cells and Type II survivors of *S. cerevisiae* (194,237,238).

Immortal human ALT cells are characterized by increased telomere length and
telomere heterogeneity, and the presence of extrachromosomal telomeric circles and
ALT-associated PML bodies (198,200,201,255). There is evidence that
telomere–telomere recombination accounts for the increase in telomere length in ALT
cells (199). It has also been suggested that extrachromosomal telomeric circles could
serve as a template for rapid rolling-circle-based elongation of telomeres
(108,199,256). However, telomere FISH on metaphase nuclei of ALT cell lines
shows many chromosome arms with little or no telomeric signal (257). The lack of
subtelomeric marker genes in ALT cells has hampered efforts to follow the fate of
individual telomeres. A recent report identified a human ALT cell line that maintains
short yet stable telomeres in the absence of characteristic ALT markers (258). In this
cell line, the average telomere length was ~5 kb, as assessed by telomere blotting of
RsaI / HinfI digested genomic DNA. The precise subtelomeric location of the RsaI
and HinfI sites are unknown, but the size of individual telomeres could be shorter
than 5 kb. Could the mechanism that stabilized telomere length in this cell line be
similar to the mechanism that stabilizes *T. brucei* telomeres as short as 40 bp?
Telomere stabilization has also been suggested to occur in Type I survivors in yeast,
where the chromosome terminus is capped by roughly 50 bp of telomeric repeats,
which remain at a stable length during subsequent rounds of replication (E. Louis,
personal communication).

We propose a speculative model that would restrict the extent of telomere elongation
and lead to the telomere stabilization that we observe. During telomere stabilization,
the 3´ telomere terminus could invade another short telomere by homologous

Limited inter-chromatid break-induced replication

A)

B)

Strictly limited elongation

Lagging Strand Synthesis

Lagging Strand Synthesis
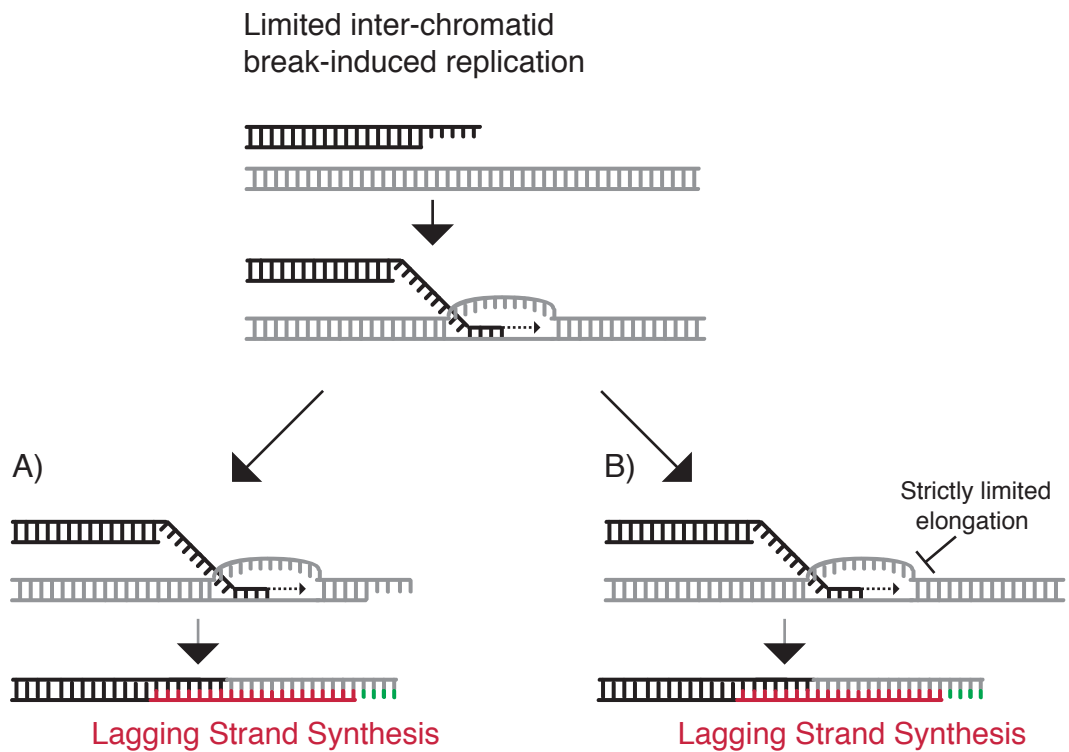
Figure 31

A speculative model for telomerase-independent telomere stabilization.

Inter-strand break-induced replication: a conventional DNA polymerase could extend the invaded 3´ end, using the C-rich strand of another telomere as template. Extension might be limited by the 5´ end of the template short telomere (1). Alternatively, *T. brucei* could have a machinery that tightly limits elongation of the 3´ terminus to 40–200 bp and give rise to telomere stabilization (2).Lagging strand synthesis (in red), could result in a limited extension of short telomeres.

recombination. A conventional DNA polymerase could extend the invading 3´ end through intra-strand break induced replication (Figure 31). Subsequent (or concomitant) lagging strand synthesis would complete replication. The extent of elongation would be limited by the size of the invaded telomere. If the majority of telomeres are short, elongation would be restricted and could lead to telomere stabilization (Figure 31A). Alternatively, inter-strand break-induced-replication in conjunction with machinery that tightly controls elongation to 40–200 bp, could facilitate telomere stabilization in the absence of telomerase (Figure 31B).

Chapter IV: Complementation of TERT-deficient T. brucei

Introduction

In human and yeast cells, telomerase activity is tightly regulated by proteins that relay information about telomere length (164,171). The ability of telomerase to extend a telomere is inversely proportional to the initial length of the telomere DNA repeats (162,163,173). This protein-counting model explains how short telomeres can be rapidly elongated whereas the length of long telomeres is restricted (162). Having short telomeres, at silent and active ES, enabled us to study telomere elongation dynamics upon re-introduction of telomerase into *T. brucei*.

Results

We complemented telomerase-deficient mutants by introduction of wild-type *TERT* and different telomerase fusion constructs: N-terminally HA-tagged *TERT* and C-terminally GFP-tagged *TERT*. All constructs were integrated into the rDNA spacer region under a tetracycline-inducible T7-promoter (Figure 32) (259). To assess the functionality of each construct, we transformed telomerase-deficient cells, and measured the rate of telomere elongation at the active *VSG* 221 ES under full tetracycline induction. Wild-type *TERT* efficiently elongated the truncated *VSG* 221 telomere whereas HA-*TERT* did not (Figure 32A and B). A *TERT*-GFP fusion construct was functional and led to rapid elongation of a short active ES telomere (Figure 32C).

Rates of telomere elongation at transcriptionally silent and active ES

Previous studies showed that an artificially seeded short telomere at the transcriptionally active ES was rapidly elongated by telomerase (231). To determine the rate of elongation at naturally shortened stabilized telomeres, and to verify that
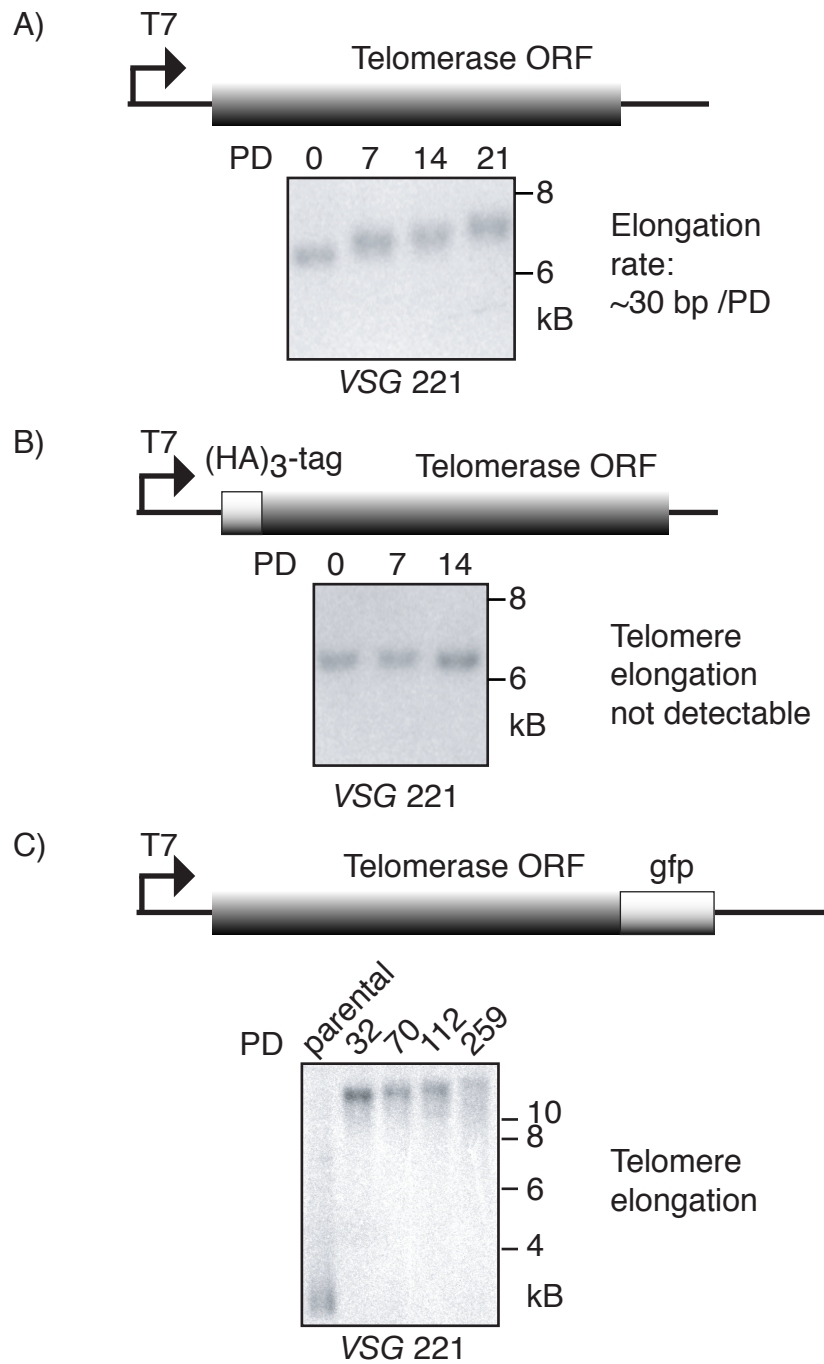
Figure 32
Complementation of telomerase-deficient mutant parasites.

A) Introduction of wild-type telomerase orf (under tetracyclin-inducable T7 promoter) results in elongation of active ES *VSG* 221 telomere.

B) Introduction of (HA)3-tagged telomerase did not result in elongation of the active ES *VSG* 221 telomere.

C) Complementation with TERT-gfp tagged telomerase leads to rapid elongation of the short active ES *VSG* 221 telomere.
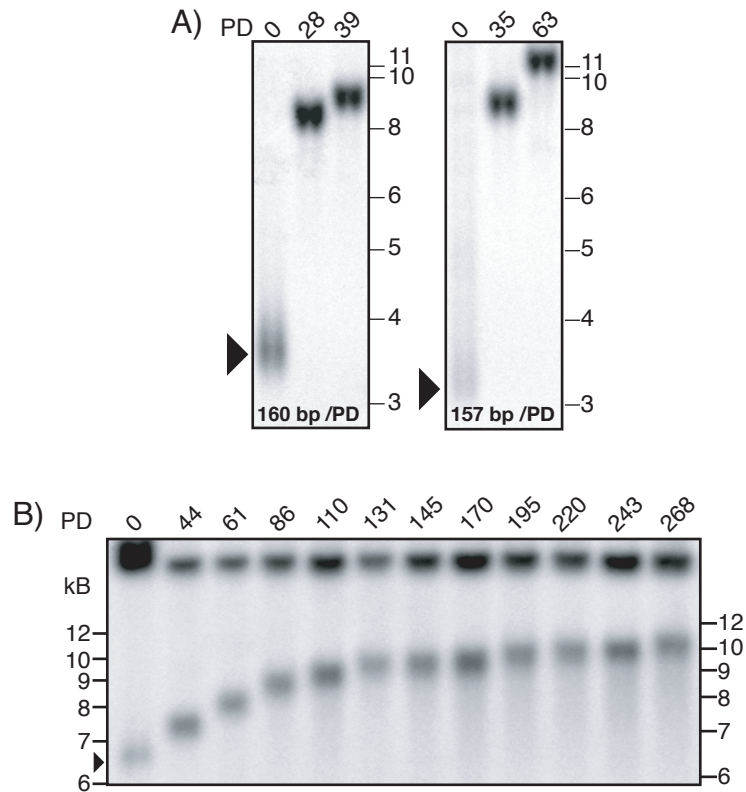
Figure 33

Telomere elongation dynamics at active ES

Telomere length prior to complementation is indicated by arrowheads. Time in continuous culture is indicated on top in PD, rates of elongation on the bottom of each panel.

A) Both panels: short active *VSG* 221 ES telomere were rapidly elongated. As the telomere reached a length of ~8.5 kB, the rate of elongation decreased.

B) Elongation of a 6.5 kB active *VSG* 224 ES telomere. During the initial 110 population doublings, the rate of telomere elongation was ~25 bp / PD. As the telomere reached a length of 9-10 kB, the elongation rate decreased to ~ 6.5 bp / PD.

Figure 34

Telomere elongation dynamics at silent ES
 The telomere elongation rate was determined at transcriptionally silent ES telomeres of varying length (arrowheads).

 A) B) and C) Elongation of three short stabilized silent ES telomeres (*VSG* 224, 121 and bR2) upon telomerase complementation. The rate of telomere elongation is constant and ranges from 5.7 bp / PD to 7.5 bp / PD.

D) The rate of telomere elongation at silent ES is constant and independent of telomere length. Upon complementation, two ES-linked copies of *VSG* 1.8, with differing telomere length, are elongated at the same rate of 6 bp / PD (see also panel C).

E) and F) Constant telomere elongation at long silent expression site telomeres in wild-type *T. brucei*. Long *VSG* bR2 and 121 telomeres continuously elongate at a constant rate.

these short telomeres could be extended by telomerase, we restored *TERT* to cells that had been in culture for ~2.5 years and studied the dynamics of telomere elongation. As shown in Figure 33A, a short 3.5-kb terminal restriction fragment containing the actively transcribed *VSG* 221 and less than 1 kb of telomeric repeats was rapidly elongated. The rate of elongation, measured from the initial day of complementation to the first possible time point at which sufficient DNA could be obtained from the cells (PD 28), was ~160 bp /PD. This experiment was repeated on six independently complemented clones with similar results, so we are confident the rapid elongation is a consequence of telomerase restoration rather than random recombination in individual clones. We then re-introduced *TERT* into a clone that had a ~5 kB telomere (terminal restriction fragment of 6.5 kB) at the active ES. Initially telomeres rapidly elongated at a rate of ~25 bp/PD. When the elongated telomere reached 8–10 kb, the rate of elongation decreased to ~6–8 bp/ PD (Figure 33B). Although the resolving power of an 0.8% agarose gel is limited as telomere restriction fragments became large, the elongation rate slowed down and remained at ~6.5 bp / PD for the last 7 weeks of the time course. Thus, when telomerase was restored to clones having different telomere lengths at the active ES, the rate of telomere elongation was inversely related to initial telomere length. Although preliminary, we noted that the extent of rapid elongation might be more pronounced at short telomeres. As an example, in the right panel of figure 33A, the long ~9kB telomere continuous to elongate at a high rate whereas the elongation rate at the ~8kB telomere in figure 33B is clearly lower. We do not know what causes this discrepancy and have not investigated this further.

In contrast, the rate of elongation at transcriptionally silent telomeres was only 6–8 bp / PD when telomerase was restored, regardless of their initial length (Figure 34). Telomeres harboring *VSG*s 224, 121 and one copy of *VSG* bR2 were short (40–200 bp) and stable, prior to reintroduction of telomerase (Figure 34A, B and C). The same extension rate was observed at the larger of the two *VSG* bR2 telomeres (Figure 34C) and at two longer telomeres of ~5.5 kb and 2.5 kb, harboring *VSG* 1.8 (Figure 34D). Over 20 years ago, it was observed that *T. brucei* telomeres of 5–9 kb grow at a constant rate (202,203). We wondered whether, in accordance with the conventional

protein-counting model of telomere length homeostasis, elongation would cease when a telomere reached a specific length. To address this question, we turned to extensively propagated wild-type *T. brucei* and found that silent ES telomeres longer than 10 or 15 kb continue to grow at a rate of 6–8 bp /PD (Figure 34E and F).

In conclusion, very short transcriptionally silent and active ES telomeres have very different elongation dynamics. Short active ES telomeres are very rapidly elongated by telomerase. As telomere length increases, the rate of elongation decreases to 6–8 bp / PD, as at silent ES.

Discussion

Short stabilized telomeres in telomerase-deficient *T. brucei* enabled us to study telomere length regulation upon re-introduction of telomerase. Telomere length regulation has been studied in numerous organisms. In human cells, telomere length homeostasis is regulated by a negative feedback loop, executed through numerous telomere-binding proteins that relay information about telomere length to the telomere terminus (260). How these proteins accomplish this task remains unclear, but recent work suggested that chromatin remodeling (or t-loop resolution) could regulate telomerase access to telomere termini (164). However, this protein-counting model apparently does not appear to apply to *T. brucei,* where transcriptionally silent telomeres were elongated at the same rate, regardless of their initial telomere length. Furthermore, during *in vitro* culture, telomere homeostasis is not achieved even at long telomeres and they appear to grow indefinitely. This result implies that the negative feedback loop that regulates telomere length in other organisms is absent from transcriptionally silent telomeres in *T. brucei*.

We subsequently studied telomere elongation dynamics at short transcriptionally active ES. In contrast to silent ES, a short active ES telomere was elongated at ~160 bp /PD. As the length of an active ES telomere increased, the rate of elongation decreased until it matched the rate at silent ES. A summary of these results is depicted in Figure 32A. The only known difference between active and silent ES is
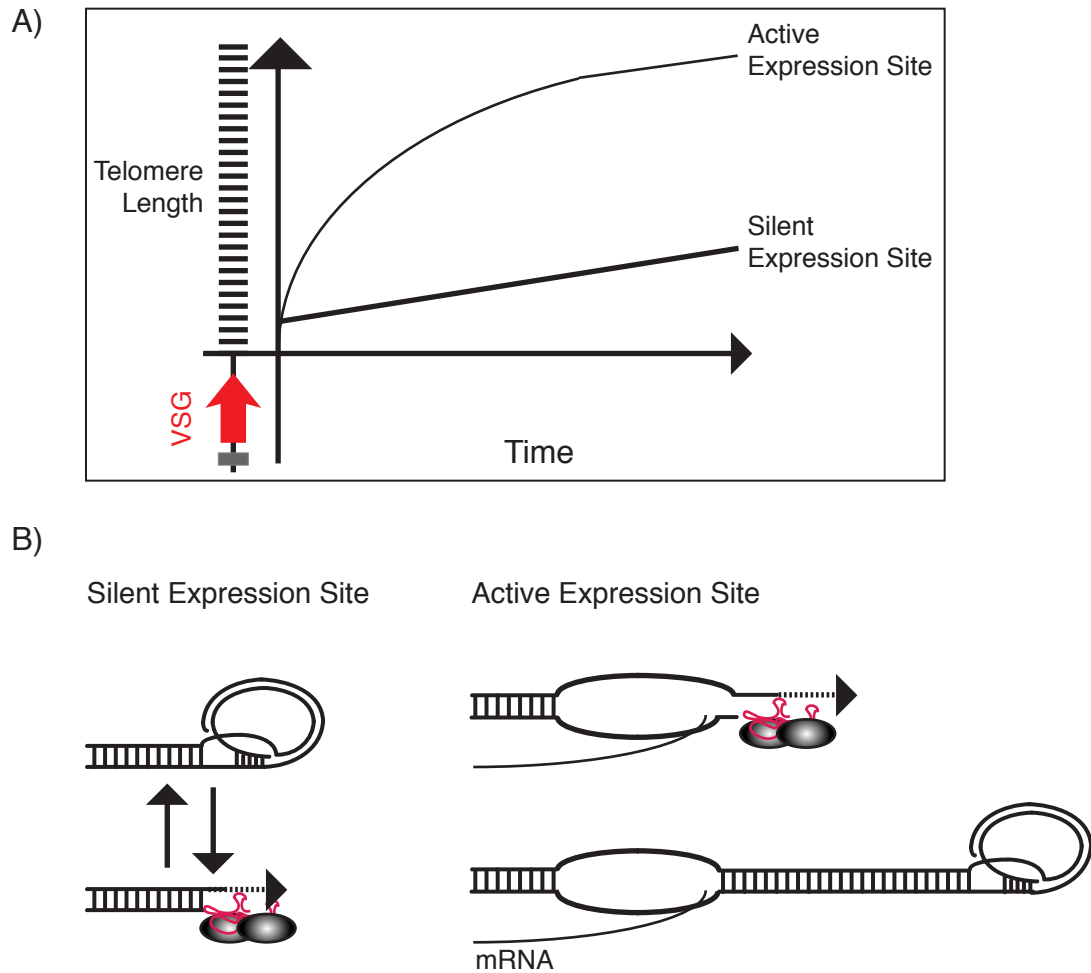
Figure 35

A) Summary of telomere elongation results. Short active ES telomeres are rapidly elongated by telomerase. Silent ES telomeres elongate at a constant rate, regardless of their initial length.

B) Model for telomere length regulation in *T. brucei*.
Left panel: silent ES telomeres: telomere termini are tucked away forming a t-loop structure. During a particular stage of the cell cycle, t-loops are resolved, telomerase accesses the short 3´ overhangs and adds 6–8 bp ending in TTAGGG. Elongation occurs at the same rate regardless of initial telomere length.
Right panel: short active ES telomere. *VSG* transcription extends into the telomere, disrupts chromatin structure (such as a t-loop) and allows telomerase unrestricted access to the 3´ terminus. At long telomeres, transcription does not reach the telomere end, allowing the telomere terminus to assemble into a telomerase-inaccessible structure. As a consequence, the rate of extension decreases to levels comparable with transcriptionally silent telomeres.

transcriptional activity, and it has been shown that transcription extends into telomeric repeats (261). Recently, a direct correlation was demonstrated between the strength of an inserted subtelomeric promoter and the rate of telomerase-dependent extension at the adjacent short seeded telomere (50). Based on all these observations, we propose a model in which transcription disrupts telomeric chromatin and enhances telomerase access and elongation (Figure 32B). After rapid elongation, transcription no longer reaches the telomere terminus, which can now reassemble into a t-loop, rendering the 3′ end inaccessible during most of the cell cycle. Its elongation dynamics now match those of transcriptionally silent ES.

Chapter V: Consequences of telomere shortening at the active expression site

Introduction

We previously demonstrated that telomerase-deficiency led to progressive telomere shortening at a rate of 3–6 bp/PD, MC loss, and genomic rearrangements among IC (Chapter II and III). At essential MBC, silent ES telomeres stabilized within a discreet size range by a potentially novel telomerase-independent mechanism.

In this chapter, we address the consequences of telomere shortening at the actively transcribed *VSG* ES. In the absence of telomerase, this telomere progressively shortens and breaks. Telomere breakage enabled us to rapidly obtain clones with very little telomeric DNA at the active ES and study the consequence of a short telomere on *VSG* transcription.

Results

Telomere breakage and shortening at the active VSG 221 expression site

Telomere length changes at the active *VSG* 221 ES can be visualized by digestion with EcoRI and hybridization with a *VSG* 221 probe (Figure 36A). The actively transcribed ES telomere is subject to frequent terminal deletions (202-204). These truncations and their subsequent repair by telomerase account for the telomere length heterogeneity we and others have observed at the active ES in wild-type cells (Figure 36B) (231). Although *VSG* 221 signal is heterogeneous, it remains within a high molecular size range (>10 kB) throughout the time course (Figure 36B).

In telomerase-deficient cells, these breaks cannot be repaired, leading to dramatic loss of telomeric DNA at the active *VSG* 221 ES (Figure 37A). In a newly cloned population, the active ES *VSG* 221 terminal restriction fragment is present as a sharp band (Figure 37A, upper panel, week 0). During subsequent culturing, and as a result of telomere breakage, the signal starts to smear towards the bottom of the gel. To verify equal loading and to confirm the progressive moderate shortening at silent ES,

the blot was re-hybridized with a probe against a silent *VSG* bR2 (Figure 37A, lower panel). We quantified the extent of telomere loss at the active ES over 8 weeks by measuring signal intensity in each lane as a function of telomere length (Figure 37B). In several independent experiments the distribution of telomere signal changed reproducibly over time, suggesting that telomere breakage occurred at a constant rate. By measuring total *VSG* 221 signal in each lane and comparing it with the intensity of time 0 signal, we observed a dramatic decline in *VSG* 221 signal during the last weeks of the time course (Figure 37C). Northern blot analysis revealed that *VSG* 221 signal loss coincided with a decrease in *VSG* 221 transcript levels (Figure 37D, upper panel). Upon reprobing of the blot with various *VSG* probes, we noted a gradual increase in *VSG* 1.8 transcript levels over time (Figure 37D, middle panel). By the end of the time course, the population expressed roughly equal amounts of *VSG* 1.8 and *VSG* 221, as judged by northern blot. We also isolated mRNA from the population and amplified *VSG*s by RT-PCR. Through subcloning and sequencing of 30 clones, we verified a *VSG* 221 : *VSG* 1.8 ratio of 1:1. No other *VSG*s were amplified during this experiment.

We investigated the events that led to *VSG* 1.8 activation, by analyzing 11 *VSG* 221-negative clones by PFGE (Figure 38). Unfortunately, under the conditions used, the silent copy of *VSG* 1.8 is not well separated from *VSG* 221 and we could not formally prove whether *VSG* 1.8 was replacing *VSG* 221 in the transcribed ES (Figure 38). This result led us to investigate further the consequences of a short telomere at an active ES.

Telomerase-deficient cell lines cannot repair telomere truncations, which allowed us to select clones that had lost large amounts of telomeric DNA from the active ES. Six telomerase-deficient clones that had undergone active ES telomere truncations are shown in Figure 39A. Clones with very short telomeres, notably clones 1, 2, 3 and 5, were only obtained after several rounds of continuous propagation and cloning, and we focused our attention on these. The sequence between the *VSG* 221 and its telomere is known, and indicates that a ~3 kb terminal restriction fragment contains ~200–400 bp of telomeric repeats (Figure 36A) (231). As judged by northern blotting,
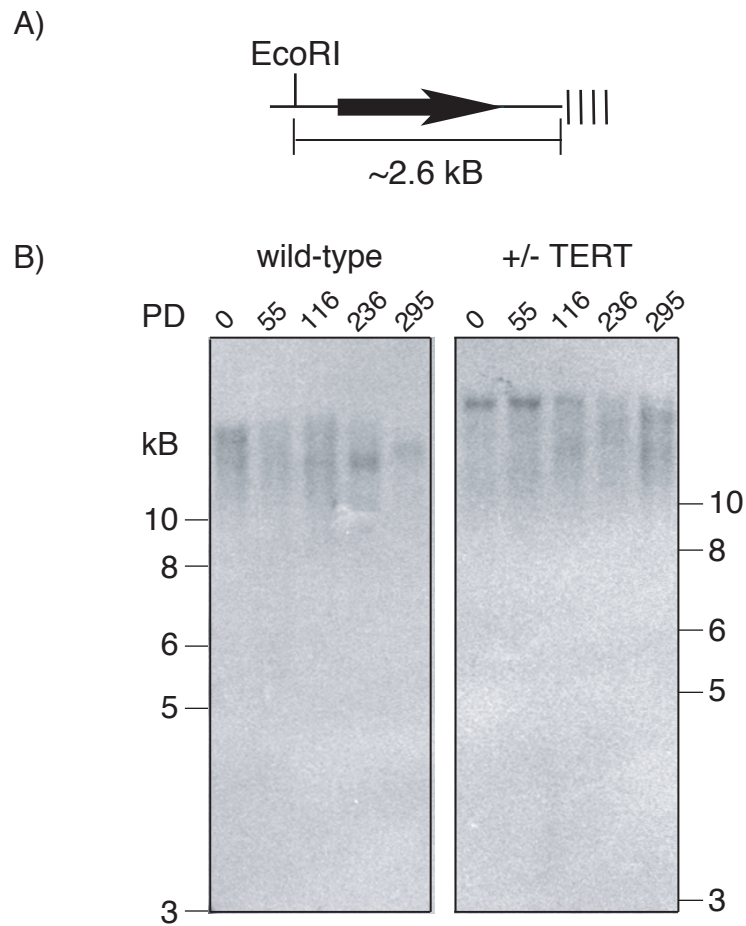
Figure 36

Telomere breakage and elongation at active ES in wild-type *T. brucei*

A) schematic representation of the *VSG* 221 ES.
EcoRI site is located between 70-bp repeats and *VSG* 221.
Black bar underneath *VSG* 221 represents the hybridization
probe used in B.

B) Active ES VSG 221 terminal restriction fragment visualized by Southern blot.
Digestion: EcoRI, hybridization probe: VSG 221.
Left panel: active ES *VSG* 221 telomere length dynamics in
wild-type over 295 PD. Right panel: same experiment in parasites
heterozygous for telomerase.
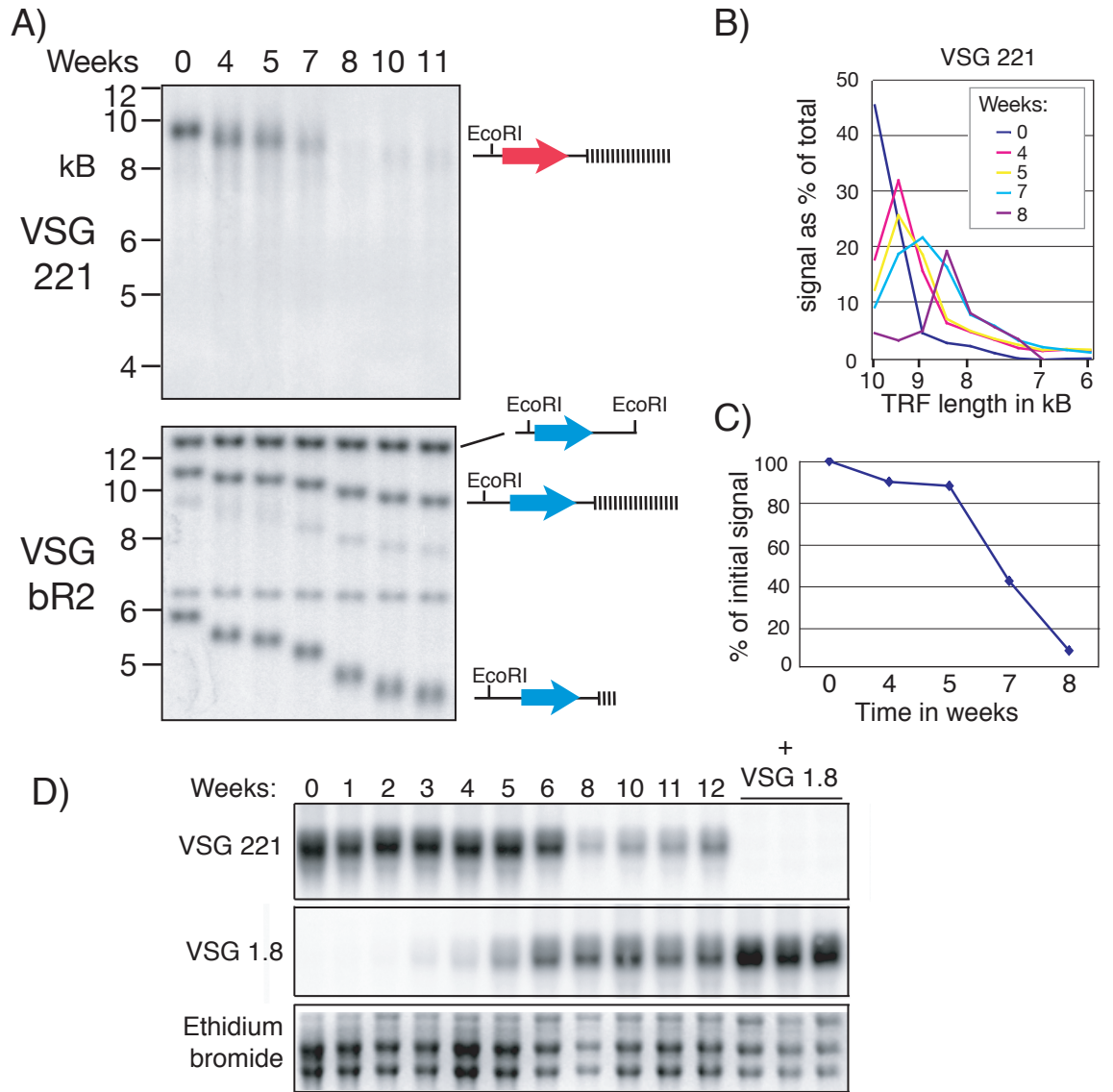
Figure 37

Telomere loss at active *VSG* 221 ES in telomerase-deficient *T. brucei*

A) Upper panel: EcoRI telomere terminal restriction fragment (TRF) hybridized with *VSG* 221. Telomere shortening and breakage leads to loss of telomeric DNA at the active ES and smearing of the 221 signal towards the bottom of the gel. Lower panel: reprobing with silent ES *VSG* bR2 verifies equal loading. Schematic representation of VSG ES are shown on the right.

B) Signal intensity distribution up to week 8 of panel A is graphically represented as a function of telomere length. Smearing of the signal is apparent as peaks become broader and move towards lower molecular mass.

C) Total VSG 221 signal in each lane over the 8 weeks time course as a percentage of initial signal (lane 1).

D) Northern blot of 13-week time course shown in panel A. *VSG* 221 (upper panel) transcripts level decreases over time and *VSG* 1.8 (middle panel) becomes activated. + controls for *VSG* 1.8 are in right 3 lanes. Equal loading verified by Ethidium bromide staining (lower panel).
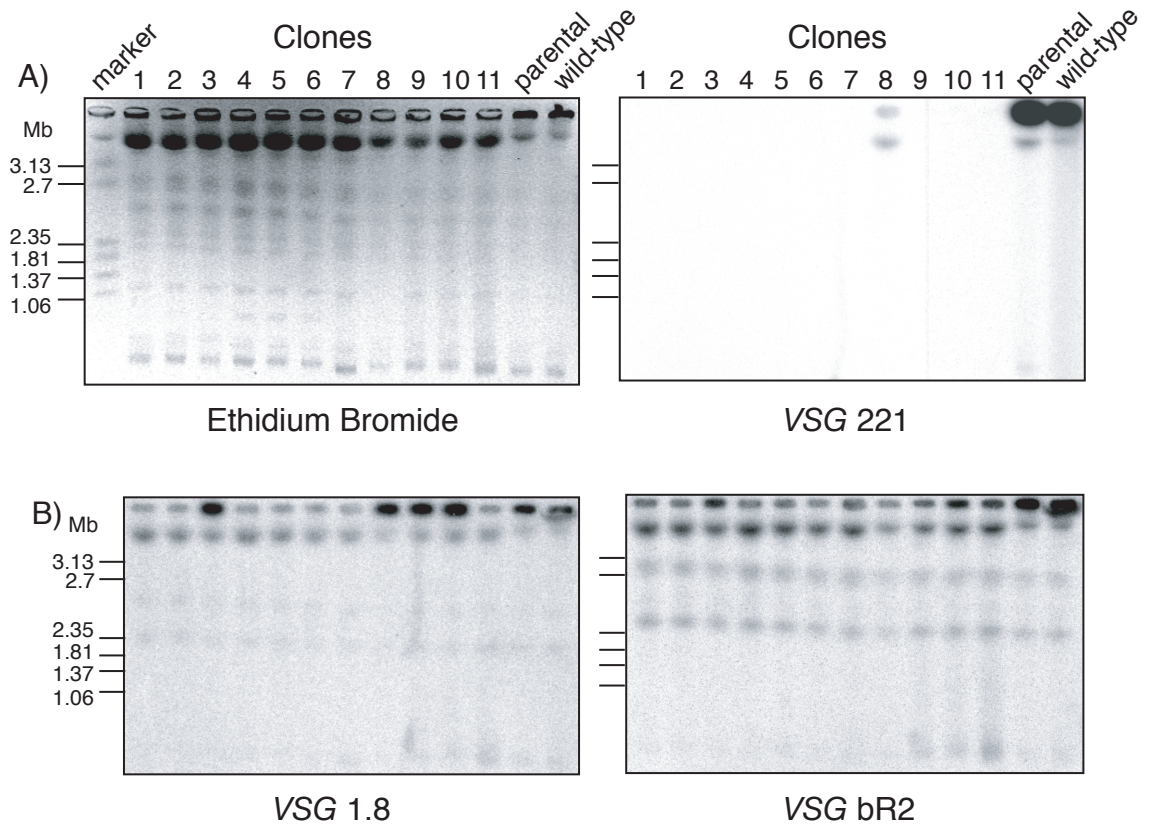
Figure 38

Characterization of VSG switchers by PFGE and Southern blotting
11 switched clones, a telomerase-negative "parental" clone and wild-type are indicated
above each lane. Size markers are shown on the left of each panel.

A) Left panel: Ethidium bromide stained RAGE gel. Right panel: Southern blot using
VSG 221 as a hybridization probe. VSG 221 is lost in 10 out of 11 clones. Since the
signal in clone 8 is weaker than in the parental cell line, we suspect it is due to cross-
hybridization.

B) Left and right panel: reprobing of the blot with *VSG* 1.8 and VSG bR2 probes,
respectively.

telomere lengths in this range did not affect *VSG* 221 mRNA levels at this time (Figure 39B).

Gradual loss of VSG 221 over time

Next we determined whether further shortening of the active ES telomere would occur, and whether it would affect the transcriptional status of *VSG* 221. We addressed these questions by keeping three independent clones in continuous culture for 15 weeks, during which we monitored population growth and isolated DNA and RNA every week. The short active *VSG* 221 ES terminal restriction fragment was slightly heterogeneous and ended in ~200–400 bp of telomeric DNA, but did not shorten further (Figure 40A, upper panel, arrowhead). In contrast to silent ES telomeres, however, the *VSG* 221 probe signal in the active ES gradually decreased during the initial 5 weeks (Figure 40A). To ensure equal loading between each lane and to confirm that longer silent ES telomeres continued to shorten, the membrane was re-probed with silent ES *VSG* bR2 and VO2 (Figure 40A, middle and lower panel). As anticipated, the two ES-linked copies of *VSG* bR2 and the single telomeric copy of VO2 (arrowheads) progressively shortened at a rate of 3–6 bp/PD. We also observed that short active ES telomeres occasionally elongated, presumably through recombination with another telomere (will be discussed later).

The loss of the *VSG* 221 gene poses two threats to the cell. First, the parasite needs a protective surface coat for survival. Secondly, loss of the *VSG* 221 gene and its telomere results in an unprotected chromosome end that probably requires repair. Since we did not detect any growth retardation, we were interested to learn how the cell addressed these problems. RNA analysis of clone B confirmed that *VSG* 224 became dominant in the population as *VSG* 221 transcript levels diminished (Figure 40B, left 4 lanes). Two other independent clones (A+C) lost *VSG* 221 over a period of ~ four to five weeks and also activated *VSG* 224 (Figure 40B, right 3 lanes).
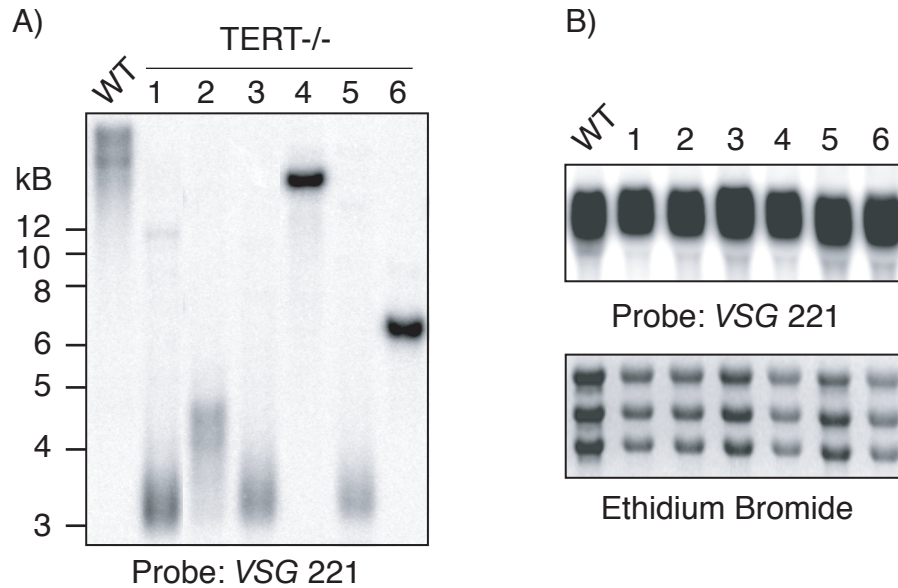
Figure 39

Selection for clones with a short active *VSG* 221 ES telomere.

A) Telomerase-deficient clones cannot repair telomere truncations and yield clones with varying active-ES terminal restriction fragments (TERT-/- lanes). In wild-type populations, telomere breakage and telomerase elongation leads to heterogeneity of the *VSG* 221 terminal restriction fragment (WT lane).

B) Northern blot of the cells from panel A confirms that they still express *VSG* 221. Bottom panel: equal loading was verified by Ethidium bromide staining.
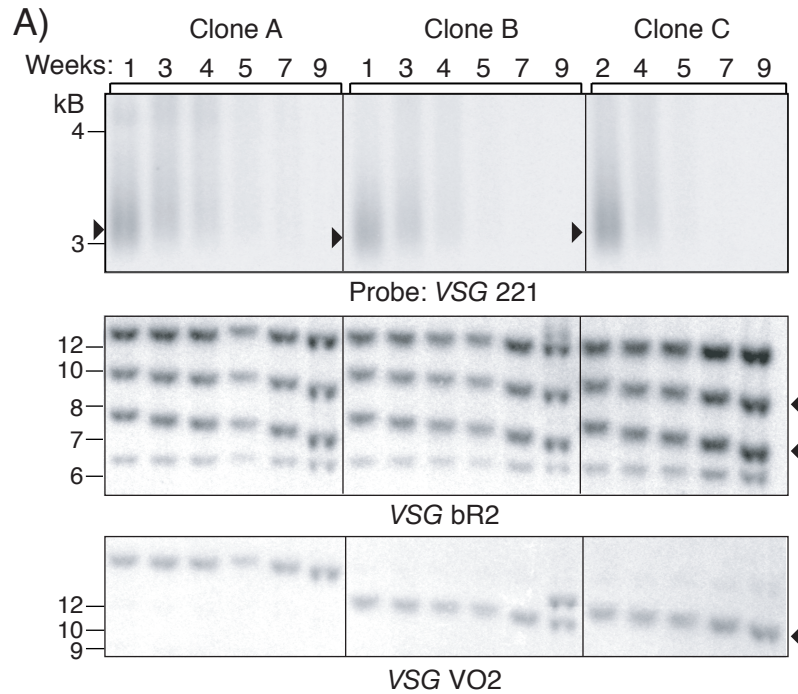
Figure 40

A short telomere at the active ES leads to loss of the transcribed *VSG*

A) *VSG* 221 loss in 3 individual telomerase-deficient short active ES telomere clones (A, B and C) during 9 weeks of continuous propagation. The size of the predominant *VSG* 221 band does not change over time, but signal intensity decreases, reflecting loss of the gene. Probes for silent ES *VSG* bR2 and V02 (arrowheads) confirmed their stability and shortening, and verified equal loading.

B) RT-PCR shows that *VSG* 224 transcripts replace *VSG* 221. Interestingly, all three clones activated the same VSG (far right 3 lanes).

To clarify the events that led to *VSG* 224 expression, we generated a ~9-kb SmaI terminal restriction fragment that hybridized with both *VSG* 221 and an upstream *VSG* pseudogene (Figure 41). At four weeks of continuous culture, *VSG* 221 was present as a smear and subsequently again lost from the population. We speculate that breaks within or downstream of *VSG* 221 could lead to partial recombination intermediates that are not properly resolved (due to lack of homology) and migrate slower on an agarose gel. By week 8, the size of the predominant restriction fragments containing the pseudogene increased to ~23 kb (Figure 41A, middle panel, asterisk) and co-localized with a new copy of *VSG* 224 (Figure 41A, right panel, asterisk), suggesting that *VSG* 224 and part or all of its associated telomere replaced *VSG* 221 at the previously transcribed ES. The silent copy of *VSG* 224 is marked with an arrowhead. In addition to the ~23 kB bands, a higher molecular band appears that does not co-localize with the pseudogene (arrow). We attribute this band to individual breaks in which the SmaI site and the pseudogene marker were deleted. Deletion of the pseudogene occurred after 8 weeks in two analyzed clones, as the duplicated copy of VSG 224 appeared (Figure 41B and C, arrow). To determine whether *VSG* 224 was activated by gene conversion or reciprocal translocation, we separated whole chromosomal DNA. In all three clones, *VSG* 221 was lost after 4 weeks and *VSG* 224, initially present as a single copy gene, was duplicated into the ES that previously carried *VSG* 221 (Figure 42A).

We independently confirmed that the ES was unchanged, using a blasticidin resistance gene that we had integrated immediately downstream of the active ES promoter, while *VSG* 221 was being expressed (23). No drug selection was applied during propagation and switching, but the cells retained the marker and were highly resistant to blasticidin, indicating that the same ES was in use (Figure 42B).
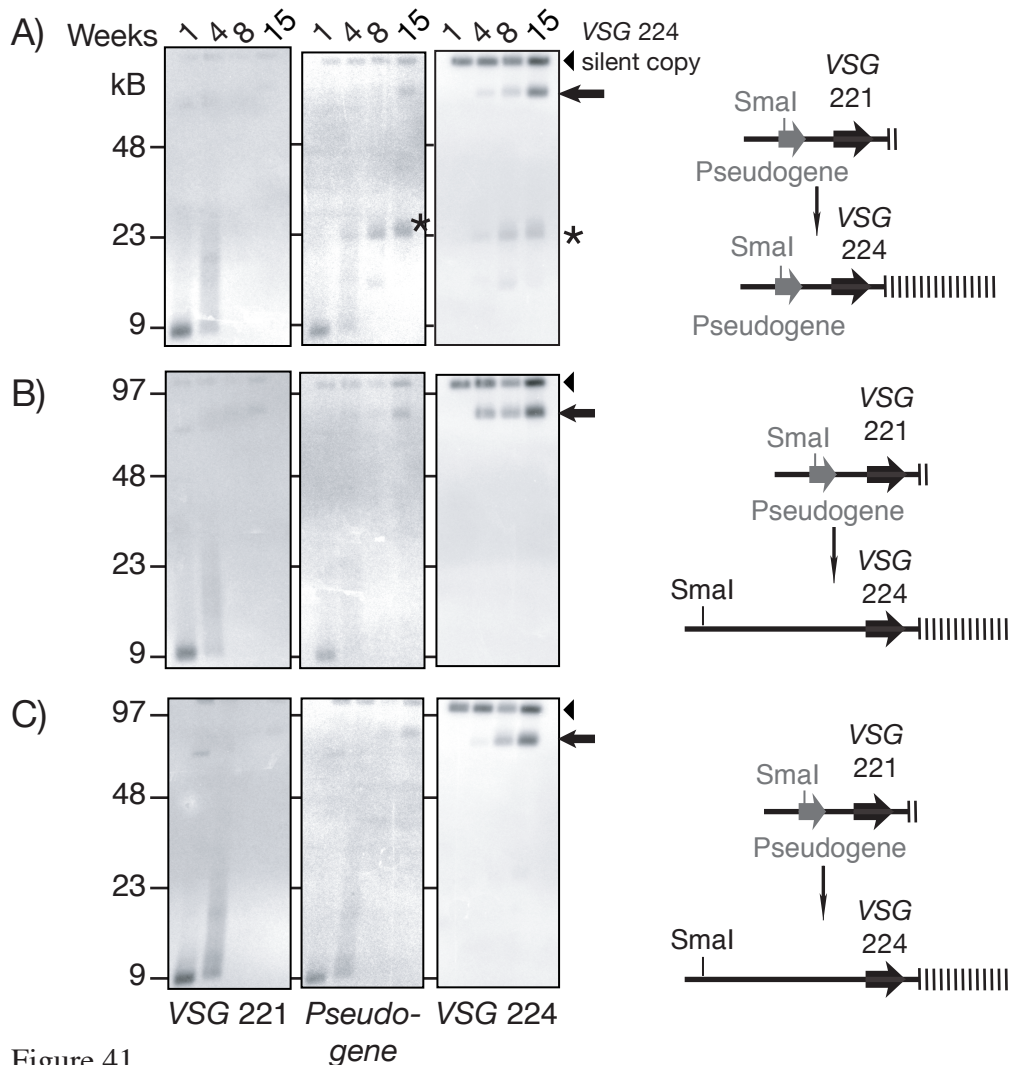
Figure 41

VSG 224 replaces *VSG* 221 at the active ES, based on restriction digest and genomic blotting.

A unique upstream *pseudogene* probe (schematic representation on the right) was used to demonstrates that *VSG* 224 replaced *VSG* 221 in the same active ES.
A) Left panels: as shown in Figure 37, the population lost *VSG* 221 by 8 weeks.
Middle panel: reprobing of the blot with an ES-specific pseudogene probe.
After *VSG* 221 loss, the size of the predominant terminal restriction fragment increases to ~23 kB (asterisk). Right panel: reprobing with the newly expressed *VSG* 224 probe. *VSG* 224 signal appeared after *VSG* 221 loss and co-localized precisely with the pseudogene signal (asterisk), indicating that *VSG* 224 translocated into the ES, previously occupied by *VSG* 221.
An arrowhead marks the silent copy of *VSG* 224. Arrow and asterisk indicate different means of *VSG* 224 activation within the population (see below).

B) and (C) In two other clones, *pseudogene*, the SmaI site and *VSG* 221 were lost (left and middle panel). Duplicated copy of *VSG* 224 is indicated by an arrow (right panel).
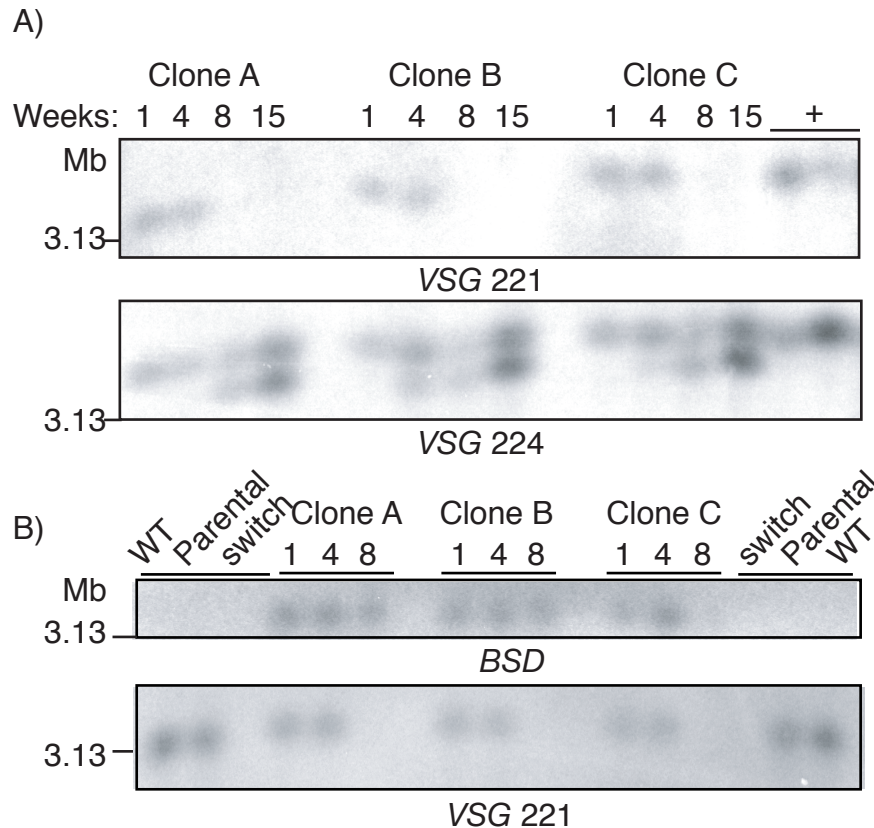
Figure 42

VSG 224 replaces *VSG* 221 at the active ES: Rotating Agarose Gel Electrophoresis

Chromosomal DNA separation by RAGE confirms that *VSG* 224 replaced *VSG* 221 at the active ES through a duplicative gene conversion event.

A) Upper panel: *VSG* 221 is lost by week 8. Lower panel: reprobing with *VSG* 224 shows that VSG 224 replaces *VSG* 221 on the same chromosome. Under the conditions used, the ~3.2 Mb chromosome VI band, harboring the 221 ES, is well separated from other chromosomes. (+) indicates *VSG* 221 positive controls.

B) Top panel: ES integrity was verified by the retention of the blasticidin resistance marker (*BSD*) that was inserted immediately downstream from the ES promoter. All three clones retained *BSD* and were highly resistant to blasticidin. Switch lane represents a switched clone from a previous experiment; Parental is the telomerase-deficient cell line without *BSD* at the active ES, WT is wild-type. Middle panel: as in the panel A, *VSG* 221 is lost after 4 weeks of continuous culture.

Could a short telomere trigger an antigenic switch?

Due to the low switching frequency and apparent growth advantage of VSG 221-expressing cells *in vitro*, our cell lines rarely lose *VSG* 221 or otherwise result in another VSG becoming dominant in the population, even after extensive propagation. Hence the appearance of a new *VSG* at the active ES locus was unexpected and could be explained in two ways. As telomere length at the active ES becomes very short, telomere breakage could lead to terminal truncations and gradual death of the VSG 221-expressing cells in the population. Switched cells, which normally arise at a low frequency, would progressively outgrow the dying cells and lead to the dominance of a new VSG in the population. Alternatively, telomere breaks could be repaired by break-induced replication (BIR) facilitated by other telomere-linked *VSG*, with a possible consequent increased rate of antigenic switching.

To address these questions, we attempted to measure switching frequency of strains with a short active ES telomere by using immune-selection in mice. However, due to extensive propagation in laboratory culture, or unforeseen consequences of short telomeres in an animal infection that were not evident in culture, these strains did not grow well in mice. Re-adaptation to mice, during three weeks of sequential transfer, appeared to select for recombination-based elongation of the active ES telomere (Figure 43).

In collaboration with Doeke Hekstra from Stanislas Leibler's laboratory, we made a mathematical model to predict the growth dynamics of a culture if a short telomere leads to gradual lethality and switchers arise at various frequencies (10^{-3}–10^{-6}). Gradual death of cells with a short active ES telomere and concomitant appearance of switchers (at a rate of 10^{-6}, but with a growth advantage), would only subtly affect population growth dynamics over 4–5 weeks. In conclusion, unless the switching frequency is dramatically higher at short telomeres, switchers must have a clear growth advantage in order to outgrow the population within 4 weeks. However, we had to assume parameters such as relative fitness of short telomere strains and growth advantage of switched parasites, for which we have no experimental data. Thus, we cannot exclude the possibility that switchers, at a frequency of 10^{-6}, could have
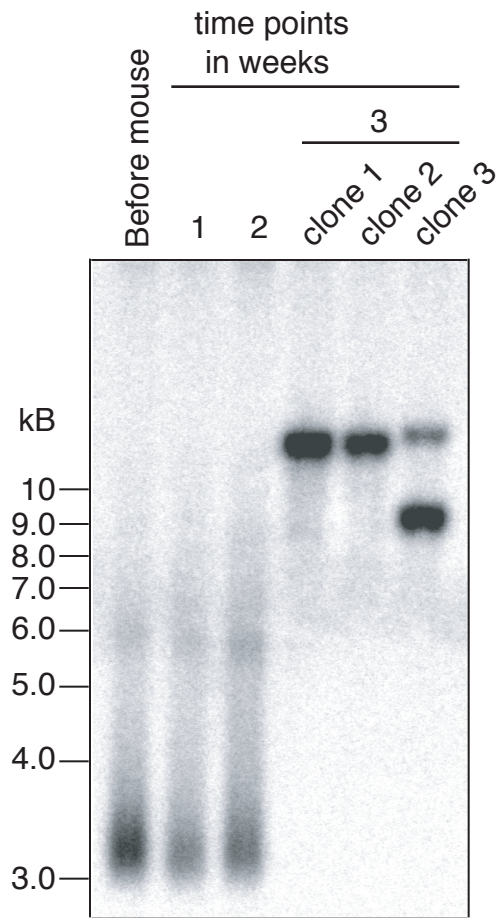
Figure 43

Recombinational elongation of active ES during mouse adaptation

VSG 221 telomere length was monitored by EcoRI digestion and hybridization with a *VSG* 221 probe. Lane "before mouse": Active ES *VSG* 221 telomere length before inoculation into mice.

Lanes 1+2: *VSG* 221 telomere length after 1 and 2 weeks of passaging in laboratory mice.

Lanes 3-6: 3 clones were picked after 3 weeks of passaging in mice. *VSG* 221 telomere length increased, presumably due to recombination.

outgrown dying parasites without giving rise to a significant decline in population fitness, which would mean that telomere break-induced repair did not necessarily increase the switching rate.

Discussion

As with silent ES telomeres, the length of a short active ES telomere could be maintained. However, in sharp contrast to stabilized silent ES telomeres, the actively transcribed *VSG* 221 was gradually lost from the population and replaced by another *VSG* through a duplicative gene conversion event. What could account for the difference between silent and active ES? One conspicuous difference is that the active ES undergoes frequent terminal truncations, which were observed many years ago (82,202,203). Although the nature of these breaks remains unclear, they could be a consequence of transcription bubble destabilization and / or nucleolytic degradation as transcription reaches a DNA terminus. It has also been shown that stalled replication forks can give rise to a double-stranded break (DSB) and subsequent repair through BIR (239). It is possible that at a heavily transcribed chromosome end, stalling occurs more frequently. At short telomeres, replication forks could stall within the subtelomeric region; thus, we hypothesize that a truncation might frequently fall within the subtelomeric region, resulting in a DSB. The DSB could be repaired through BIR (Figure 44), a mechanism that has been well studied in *S. cerevisiae* (262). During BIR, the centromere-proximal end of a break is processed into a 3´ overhang, which can invade the sister chromatid and use it as a template for repair. DNA-polymerase-mediated synthesis completes the repair (263). In *T. brucei*, the repair template could be any ES or possibly just a *VSG*-containing telomere, depending on the location of the break (Figure 44) (263), and BIR could extend into the telomere, resulting in duplicative expression of a new *VSG* and seeding of a new telomere. Depending upon the circumstances, BIR might not effectively repair every active ES break: sometimes an entire ES might be deleted, resulting in an in-situ ES switch or death (264). Although active ES deletion has been observed, the authors did

not investigate how the chromosome end remained protected. One possibility is that a telomere was seeded onto the broken chromosome end.

Thus, we speculate that telomere breakage at the active ES could accelerate *VSG* switching. Due to overwhelming technical difficulties, we were unable to measure the VSG switching rates in clones with short telomeres at the active ES, and mathematical modeling could not exclude the possibility that, when short active ES telomeres broke, *VSG* expression was compromised and these cells died. We could not determine the telomere breakage frequency in the population and, if it were low, VSG switches arising at the normal (for this strain) low frequency of ~10^{-6} /PD could dominate the population within a period of 4–5 weeks without an observable pause in population growth (74,82).

In conclusion, within a few weeks of continuous culture, the *VSG* at a short active ES telomere in telomerase-deficient *T. brucei* is replaced by a new *VSG* through duplicative gene conversion. Our observation could be explained if active ES breakage caused a DSB and its subsequent repair through BIR. The majority of antigenic switches in African wild-type isolates occur through duplicative gene conversion and it remains to be determined whether active ES-restricted telomere breakage is at least partly responsible for high rate of gene-conversion-mediated antigenic variation (73).

1. Active VSG 221 expression

EcoRI

VSG 221

2. Telomere breakage falls within subtelomeric region

3. End processing

3'

4. Strand invasion into silent ES

3'

5. 3' extension using a silent ES as template

6. Strand synthesis & dissociation results in duplicative gene conversion

VSG 224

VSG 224
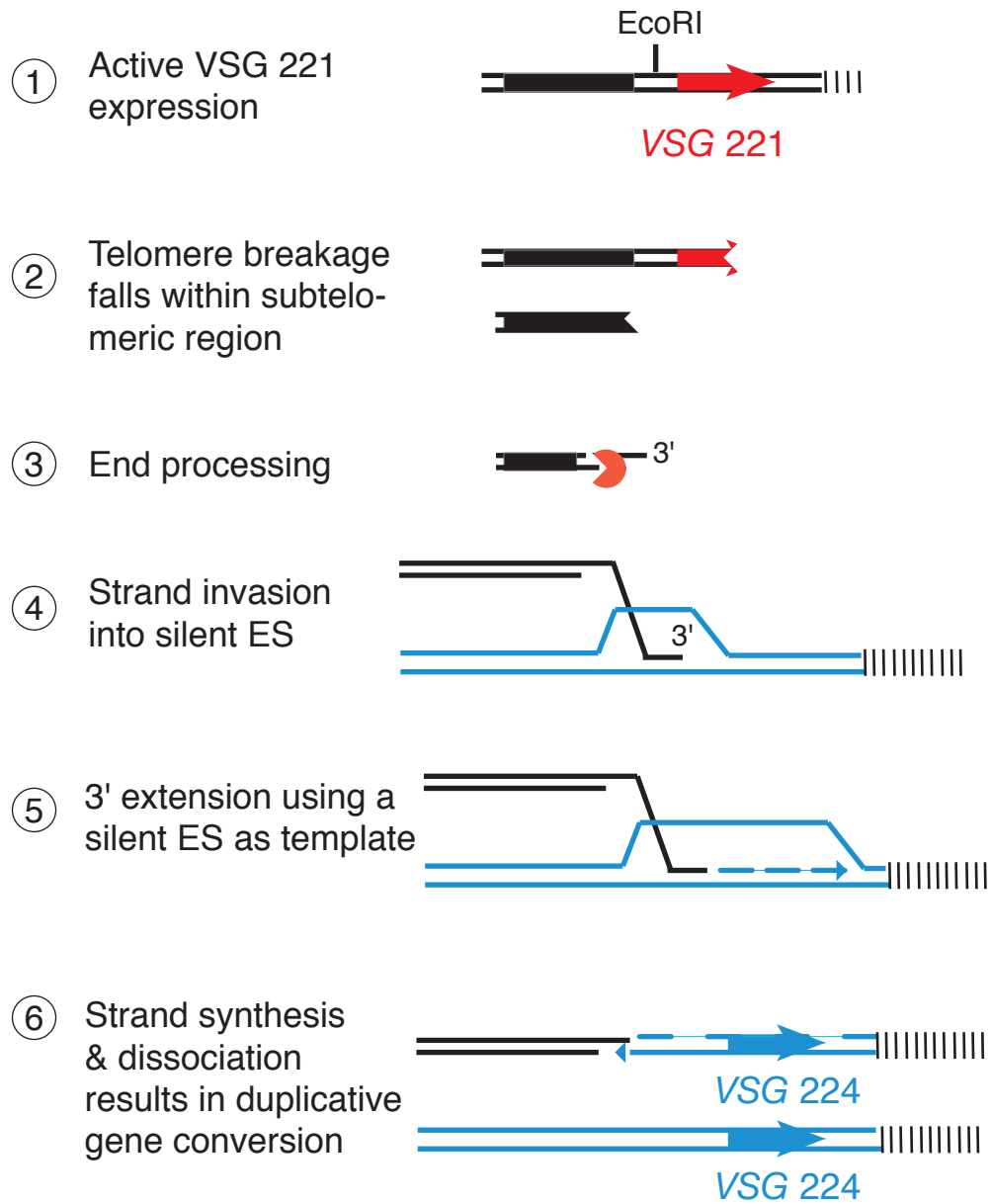
Figure 44

A model for VSG switching by Break-induced replication (BIR)

Chapter VI: Telomere length analysis in African wild-type strain isolates

Introduction

The rate of antigenic switching varies substantially among strains of *T. brucei*. African wild-type isolates have a high switching frequency of $\sim 10^{-2}$–10^{-4} /PD (73,79,90,91). The high switching frequency of wild-type isolates is not suitable for many laboratory studies. Thus, isolates were often subjected to rapid syringe passaging, a procedure during which parasites are transferred sequentially in mice in the absence of immune selection (90). After several months, such parasites become monomorphic and more virulent, with higher parasitemias and as much as a 10,000-fold reduction of switching frequency (74,75,82,90-92). Unfortunately, very little is known about the molecular changes that occur during laboratory adaptation, nor what mediates the reduction in switching frequency. Identifying these changes might improve our understanding of antigenic variation and lead to the identification of targets for therapeutic intervention.

To this point, all our results were obtained by using a telomerase-deficient cell line, and we wanted to know whether these results could be relevant to telomerase-proficient wild-type trypanosomes. In other words, if short telomeres increase the frequency of antigenic switching, rapid-switching wild-type isolates might have shorter telomeres than monomorphic laboratory-adapted strains.

In this chapter we measured telomere length in fast-switching wild-type isolates, recently laboratory-adapted strains, and extensively propagated laboratory lines. We found that wild-type African isolates and recently laboratory-adapted strains have dramatically shorter telomeres than extensively cultured strains. We also show that telomere growth at a rate of 6–8 bp/PD appears to be a unique feature of antigenic variation-proficient *T. brucei* and does not occur at such a rate in other kinetoplastid parasites. We propose a model in which telomere length and breakage affect the rate of antigenic switching, and telomere growth leads to stabilization of the active ES telomere and the well-documented switch reduction associated with laboratory adaptation.

Results

Telomere length analysis in laboratory-adapted strains and recent wild-type isolates

Based on our experiments with telomerase-deficient cell lines, we suggested that telomere shortening at the active ES might lead to an increase in the frequency of antigenic variation. This notion led us to measure telomere length in well-characterized pleomorphic and monomorphic strains, and in other available wild-type African isolates whose history was fairly clear. A summary of the lineages of the analyzed strains is provided in Materials and Methods.

The telomeres of the four Lister 427-derived cell lines (only 150 and 501 are shown in Figure 45A) are strikingly similar in length, ranging from 3–20 kB, with an average of ~15 kB, as previously shown (101,265). Telomeres of African wild-type isolates ranged in size from 3–12 kB, with an average of ~8–10 kB (Figure 45A, compare lab-strains to African isolates). To quantify telomere length differences between individual strains, we measured signal intensity within given size increments as a function of total signal in each lane and graphically represented the results of this analysis (Figure 45B, upper panel). The average signal distribution of laboratory strains versus African wild-type *T. brucei* is shown in the lower panel of Figure 45B.

In laboratory-adapted populations that stably express one particular *VSG*, constitutive elongation of all non-transcribed telomeres could account for this difference. To test this hypothesis, we measured telomere length in another recently laboratory-adapted strain, TREU927, used for the *T. brucei* genome project. As described elsewhere (92), TREU927 clone 4 was passaged 39 times in mice to increase its virulence, and predominately expresses *VSG* GUTat 10.1 (Figure 45C). Even after ~ 75 further doublings as procyclic forms, our sample of TREU927 also has dramatically shorter telomeres than the extensively *in vitro* cultured Lister 427 SM (Figure 45C). We predict that stable expression of VSG 10.1 and continuous *in vitro* growth of TREU927 would eventually lead to a strain with dramatically elongated telomeres.
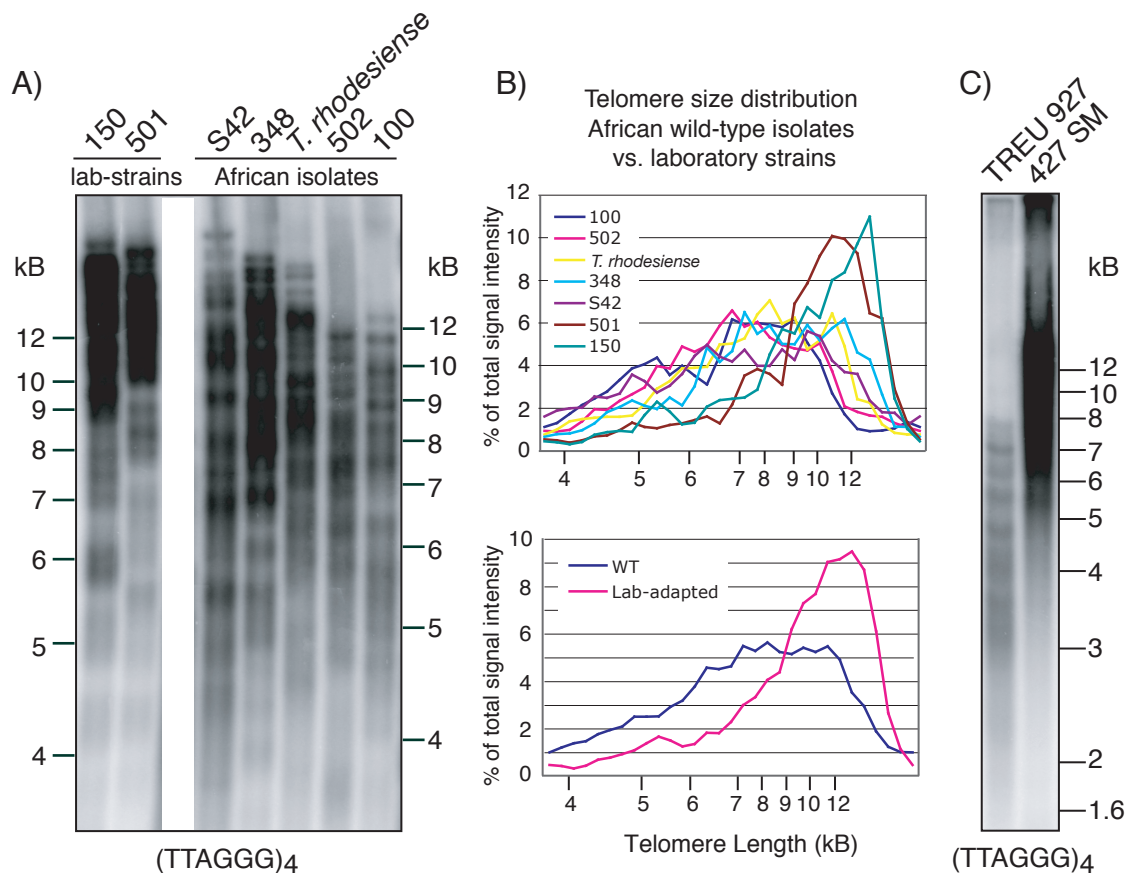
Figure 45

Analysis of telomere length in African wild-type isolates and laboratory-adapted *T. brucei*. Genomic DNA from laboratory-adapted strains and wild-type isolates was digested with AluI /MboI and separated on a 0.8% agarose gel. Telomere restriction fragments were visualized by in-gel hybridization using a radiolabelled (TTAGGG)4 probe.

A) Lanes 1 and 2: Lister 427 RUMP150 and RUMP501 have long telomeres (average ~15 kB). Lanes 3–7: wild-type African isolates (S42, 348, 151, 502 and 100) have shorter telomeres (average ~ 8–10 kB).

B) Upper panel: telomere size distribution as percentage of total signal intensity (see Materials and Methods for details). Lower panel: average telomere size distribution of two laboratory-adapted strains and five wild-type isolates.

C) Comparison of telomere length between recently laboratory-adapted TREU927 and long-term laboratory cultured Lister 427 'single marker'.
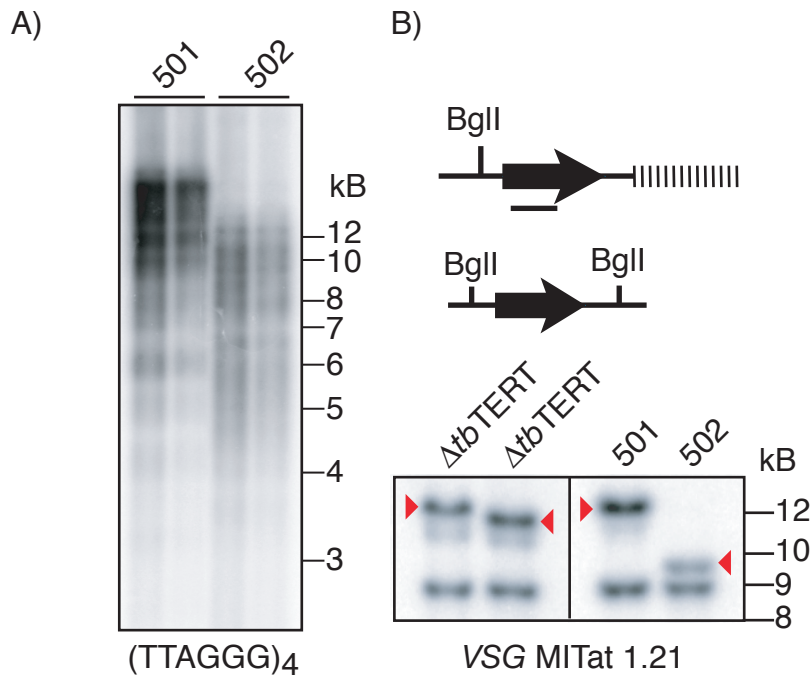
Figure 46
Telomere length difference between African isolates and laboratory-adapted strains

A) Direct comparison of telomere length between African wild-type isolate 502 and laboratory-adapted strain 501 by genomic blotting using RsaI, MboI, AluI digested DNA and (TTAGGG)$_4$ hybridization probe.

B) Telomere length comparison using BglI terminal restriction analysis of the MITat 1.21 harboring chromosome. Left two lanes show telomere shortening during a time course of telomerase-deficient cell line identifying the ES-linked copy of MITat 1.21 (arrowheads). Left two lanes: dramatic size difference between the ES-linked copy in Lab 501 vs. wild-type 502 (arrowheads). Lower band: no size changes occur at the chromosome-internal copy of MITat 1.21.

A direct comparison between the only well-characterized rapid switching strain 502 and laboratory-adapted strain 501 is shown in Figure 46A. Using a terminal restriction fragment that contains a unique subtelomeric *VSG* gene, we compared telomere length at single chromosome resolution (Figure 46B). These strains contain two copies of MITat 1.21 *VSG,* located at a telomeric ES and at a chromosome-internal locus (Figure 46B). The MITat 1.21 containing terminal restriction fragment gradually shortened in the absence of telomerase whereas the chromosome-internal copy remained stable (Figure 46B, left panel, arrowheads). The ES-linked copy of MITat 1.21 in 502 is dramatically shorter than in Lab 501 (Figure 46B, right panel, arrowheads).

Telomere length analysis before and after laboratory-adaptation

Next, we studied bulk telomere length dynamics in two strains, STIB247 and STIB386. Clones (STIB247L and STIB386AA) made soon after isolation of both wild-type strains were pleomorphic, and laboratory-adaptation during 52 mouse passages (roughly 5 months) gave rise to monomorphic lines that predominantly expressed *VSG*s GUTat 8.1 and GUTat 9.1, respectively. Although we have no information on their switching frequencies before and after lab-adaptation, the relationship between these paired samples (their DNA was kindly provided by C.M.R. Turner, Glasgow University) is not in doubt. Figure 47A shows telomere Southern blots of DNA from the two strains, before and after lab-adaptation. The only well-resolved bands are on the top of each lane and appear to elongate during propagation (arrowheads). However, we cannot be certain that they represent the same telomere pre- and post-adaptation. To address whether average telomere length increased during laboratory-adaptation, we quantified telomere signal intensity as a function of length. Telomere signal at higher molecular weight did increase somewhat in 348 during laboratory-adaptation (Figure 47B, lower panel), but not during adaptation of 247 (Figure 47B, upper panel). These results are difficult to interpret and we do not know precisely what happens, but they could be explained if ES
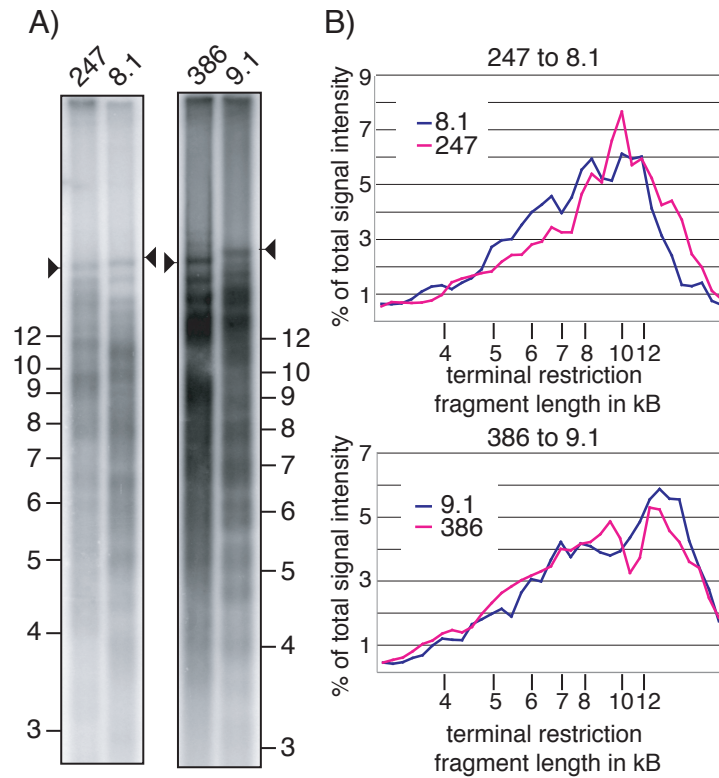
Figure 47
Telomere length changes during laboratory-adaptation of wild-type isolates
STIB247 and STIB386.

A) Southern blot of RsaI, MboI, AluI digested DNA from strains 247 and 386,
before and after 52 rapid syringe passages that led to stable expression of
*VSG*s GUTat 8.1 and 9.1 respectively. The well-resolved high molecular bands
(arrowhead) appear to elongate (although we cannot be certain that they
represent the same telomeres before and after adaptation).

B) Telomere length analysis as described for Figure 42B.
Telomere signal intensity was plotted as a function of telomere length.
Upper panel: pre- and post adaptation of strain 247.
Lower panel: pre- and post adaptation of strain 386.

rearrangements and /or *VSG* switches occurred frequently during syringe passaging, leading to continuous rearrangements of telomeric DNA and no net increase of telomere length. Furthermore, we do not know the precise doubling time of these parasites and it is possible that during the elapsed time, telomere elongated only 600-1000 bp, which may not be sufficient to cause a significant shift in overall telomere signal. Telomere elongation has never been studied in wild-type African isolates, yet there is no evidence that the elongation dynamics are different in laboratory-cultured parasites. Furthermore, as we will discuss later, elongation of a single active ES telomere could be sufficient to cause the presumed VSG switch reduction associated with rapid serial passaging.

Telomere growth at a rate of 6–8 bp/PD appears to be a unique feature of T. brucei

T. brucei belongs to a highly diverged group of kinetoplastid protozoa that includes *T. cruzi* and *L. major*, causative agents of Chagas' disease and cutaneous Leishmaniasis respectively (233). We wanted to know whether telomere growth is unique to trypanosomes that undergo antigenic variation, exemplified by *T. brucei*. To address this question, we kept *L. major*, *L. tarentolae* and *T. cruzi* in continuous culture for four weeks. We isolated DNA at weekly intervals, digested it with MboI and AluI, and determined telomere length by in-gel hybridization using a $(TTAGGG)_4$ probe. The majority of *L. major* telomeres ranged from 3–12 kB and, although minor telomere rearrangements occurred, we failed to observe any constant telomere elongation during this time course (Figure 48A, B). Next, we observed that different isolates of *L. tarentolae* have different telomere lengths, ranging from 3–9 kB to roughly 3–20 kB. Although, telomere length appears to increase slightly in strain *Lt* 77 the rate of elongation appears to be dramatically lower than in *T. brucei*. Elongation at a rate of 6–8 bp/PD should result in, at least 500 bp extension of the telomere tract (Figure 48B). To verify that the observed signal represented telomere terminal restriction fragments, we incubated DNA from strain *Lt* 95 with the exonuclease Bal31 for various times and subsequently digested the DNA with MboI

113
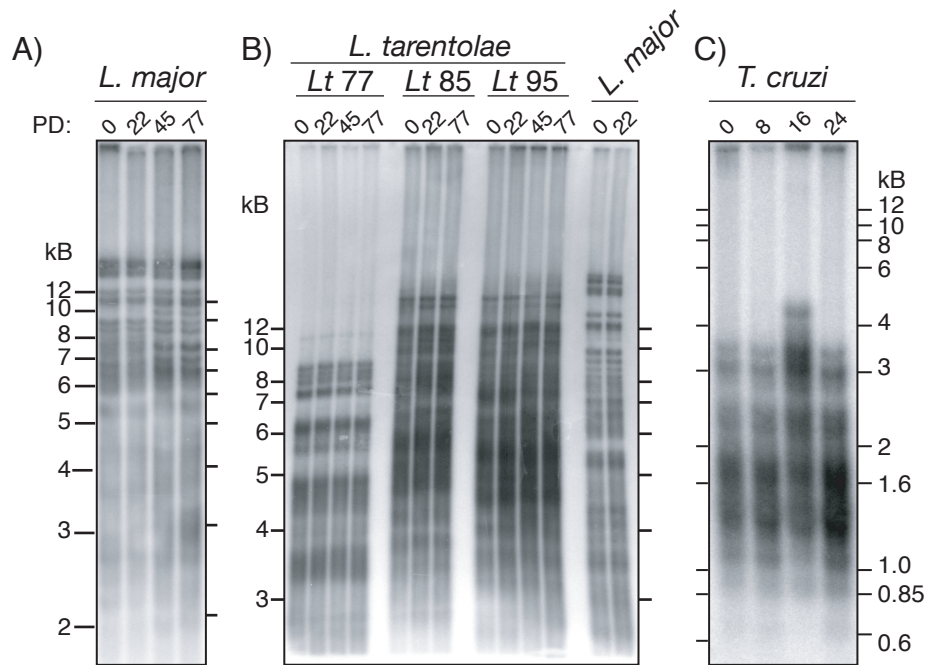
Figure 48

Telomere length analysis in three other kinetoplastid protozoa

Telomere growth at a rate of 6–8 bp/PD appears to be unique feature of *T. brucei*. Genomic DNA was isolated at weekly intervals over 4 week time courses digested with MboI and AluI; telomere restriction fragments were visualized by a (TTAGGG)4 probe. PD are indicated on the left.

A) *L. major* Friedlin strain telomeres range in size from ~2 to more than 12 kB. Minor rearrangements occur but no significant constant elongation of telomeres is visible on this blot. Yet, 77 PD of continuous culture might not be sufficient to detect.

B) Telomere length varies in three different isolates of *L. tarentolae* (from 3–9 kB to 3–20 kB) and no dramatic constant telomere elongation occurs. Right lanes show two samples of *L. major* run on the same gel.

C) Telomeres of this *T. cruzi* isolate vary in size from 500 –1500 bp and during a 24 PD time course, no significant increase in telomere length can be observed. The slower migrating band at PD 16 is due to partial digestion.
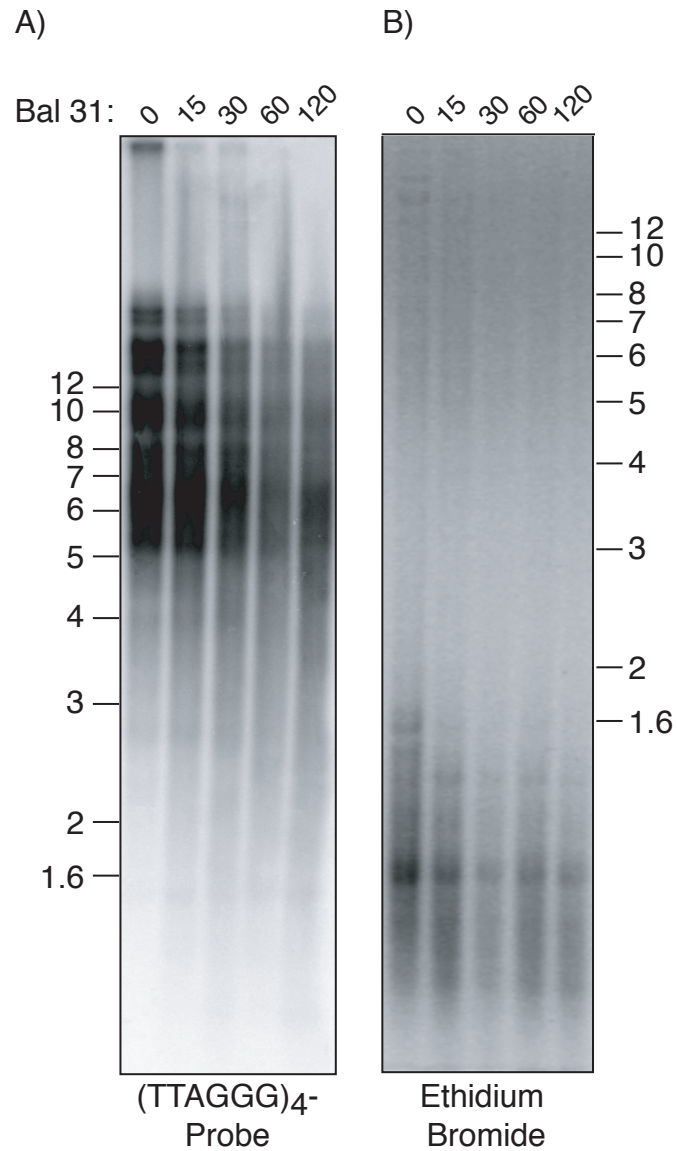
Figure 49
Bal 31 digestion of *L. tarentolae* DNA
Time of Bal 31 treatment is indicated in minutes above each lane,
after which DNA was digested with MboI and AluI.

A) A radiolabled (TTAGGG)$_4$ probe was used to visualize telomere
terminal restriction fragments by denaturing in-gel hybridization.

B) Ethidium bromide staining of the gel shown in panel A.

and AluI. As expected, Bal31 digestion diminished telomeric signal, indicating that the restriction fragments were terminal (Figure 49). As reported previously, telomeres of different *T. cruzi* isolates can vary in size from ~1–10 kB, but the question of whether they grow has not been addressed (215). Telomeres of our Y-strain clone were shorter than those of all other species and samples tested, and we could not observe any telomere length change during 24 PD (Figure 48C).

However, as this work was completed we learned that *Leishmania* telomeres do in fact elongate (P. Borst, personal communication). Yet it is unclear at what rate. This discrepancy could be explained by the fact that we cultured these strains for 4 weeks, which corresponds to only 77 and 24 PD for *Leishmania* and *T. cruzi,* respectively. We anticipated telomere growth at a rate of 6–8 bp/PD and this time frame might be too short to detect telomere elongation if it occurs at a lower rate. Furthermore, we did not measure telomere elongation dynamics at single chromosome resolution. Nevertheless, considering the limited interpretability of these results, they do suggest that robust 6–8 bp/PD constant telomere growth is a unique feature of *T. brucei*. The possible implications of these results will be discussed in chapter VIII.

Chapter VII: Preliminary results on Mre11-deficient T. brucei

Introduction

Telomerase deficiency leads to progressive telomere shortening at a rate of 3–6 bp/PD. This rate correlates with telomere decline in telomerase-deficient *S. cerevisiae* and the proposed shortening due to the end replication problem (112,113,121,122,265).

With the exception of the active ES telomere, shortening occurs at a constant rate. Silent ES telomere shortening was monitored over more than two years and, strikingly, the terminal restriction fragment remained a sharp band. This was also visualized by telomere blotting, where shortening of individual chromosome ends was measured over time. Human telomeres, in contrast, are more heterogeneous and telomere decline cannot be measured at single chromosome ends. The apparent telomere length heterogeneity in human cells could be the consequence of nucleolytic degradation and telomere rapid deletions (TRD) (201).

Invasion of upstream telomeric DNA by the terminal G-overhang can form a t-loop structure. In both human and yeast, resolution of this structure by homologous recombination can result in dramatic attrition of the telomere tract by TRD and the appearance of circular t-loop sized molecules (200,201,266). Genetic studies revealed that TRD depends on recombination pathways involving Rad52 and the tripartite Mre11/Rad50/Xrs2 or Nbs1 complex (205). Furthermore, the rate of TRD can be dramatically enhanced by overexpression of dominant-negative alleles of *sc*Rap1 or hTRF2 (201,267). Judging by appearance on southern blots, the size heterogeneity at the active ES telomere in *T. brucei*, where telomere truncations and repair by telomerase occur, looks similar to human telomeres. Are active ES truncations a result of TRD and dependent on Mre11 and / or other recombination proteins?

An Mre11-deficient cell line was previously created in our laboratory and used to investigate this question. *T. brucei* Mre11 is a non-essential gene, its deletion results in mild growth retardation, impaired double-strand break repair and gross chromosomal rearrangements (86,268). To address whether Mre11 plays any role in telomere length regulation, Mre11-deficient cells were kept in continuous culture for 280 PD and DNA was isolated at frequent intervals (Figure 50). EcoRI digestion released terminal restriction fragments that were visualized by sequential hybridization with silent *VSG* bR2 and active *VSG* 221 probe (Figure 50A). Expression-linked copies of *VSG* bR2 were not very well resolved on this blot, yet taking the slight growth retardation of this cell line into consideration, the gradual elongation rate did not appear different from wild-type cells (Figure 50, left panel). The actively transcribed *VSG* 221 terminal restriction fragment was short, very heterogeneous and elongated over time (Figure 50, right panel). After extensive *in vitro* culture, several clones were picked from the population and active ES terminal restriction fragment length was compared between Mre11- and TERT-deficient clones (Figure 50B, right panel). *VSG* 221-containing fragments appeared slightly more heterogeneous in Mre11-deficient clones than in their TERT-deficient counterparts (Figure 50B, compare left and right panel). However, telomere length varied between parental clone I and the two picked subclones II and III (Figure 50B). The length heterogeneity observed between these clones is reminiscent of the telomere breakage we observed in wild-type and TERT-deficient strains and suggest that telomere breakage still occurs in Mre11-deficient cells.
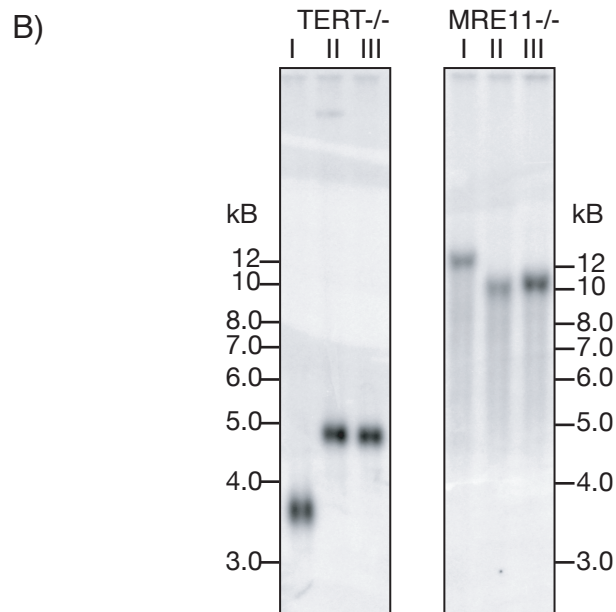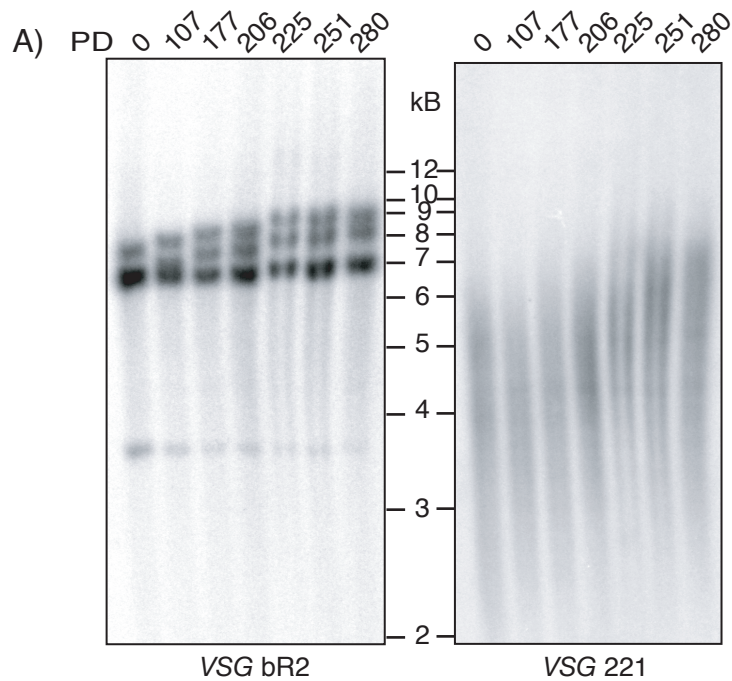
Figure 50
Telomere truncations still occur in the absence of MRE11.

A) left panel: Two ES linked copies of silent ES *VSG* bR2 gradually elongate during a 280 PD time course (arrowhead). Right panel: same blot upon reprobing with active ES *VSG* 221 probe. Length of active ES telomeres is very heterogeneous.

B) Telomere breakage at the active *VSG* 221 ES in TERT and MRE-deficient *T. brucei*. Left panel: telomere length was analyzed in three clones of TERT-deficient clones. Right panel: Lane I: parental strain and two derived clones (II and III). Note that telomere length in MRE11-deficient clones appears slightly more heterogeneous.

In *S. cerevisiae* the Mre11-complex plays a role in establishing G-overhangs throughout the cell cycle (120). To investigate whether Mre11 plays any role in G-overhang maintenance in *T. brucei*, whole chromosomes of wild-type single marker, KU-, Mre11 and TERT-deficient cell lines were analyzed by PFGE-overhang assay (Figure 51). Duplicate native gels were hybridized with $(TTAGGG)_4$ and $(CCCTAA)_4$ probes (Figure 51, upper panels). A robust G-overhang specific signal was detectable on concentrated MC and equal loading was verified by denaturation and re-hybridization with the same probes. The experiment depicted in figure 51 requires to be repeated several times and G-overhang signal intensity must be quantified by phosphoimager, in order to elucidate, whether *tb*Mre, *tb*KU or *tb*TERT are involved in G-overhang maintenance.

Discussion

In human and *S. cerevisiae*, the Mre11 complex is involved in TRD (201,205). We attempted to investigate whether *T. brucei* Mre11 is involved in the terminal truncations, we and others have observed at the actively transcribed ES telomeres (82,202,203). Our results suggest that *tb*Mre11 is not involved in telomere length regulation nor telomere terminal truncations. The observed smearing of terminal restriction fragments could be the result of cell death in the population. Mre11-deficiency results in growth retardation, yet no delay or disruption of the cell cycle (86). Viability assays have shown that cell death occurs probably in a subset of cells in a population (268). By observing telomere length dynamics over a time course, and by measuring active ES telomere length in individual clones, we show that telomere length is heterogenous at the active ES. This suggests that telomere length changes (breakage?) still occurred in the absence of Mre11. Very preliminary results suggest that Mre11 is not involved in telomere G-overhang maintenance and we speculate that Mre11 does not play a role at *T. brucei* telomeres.
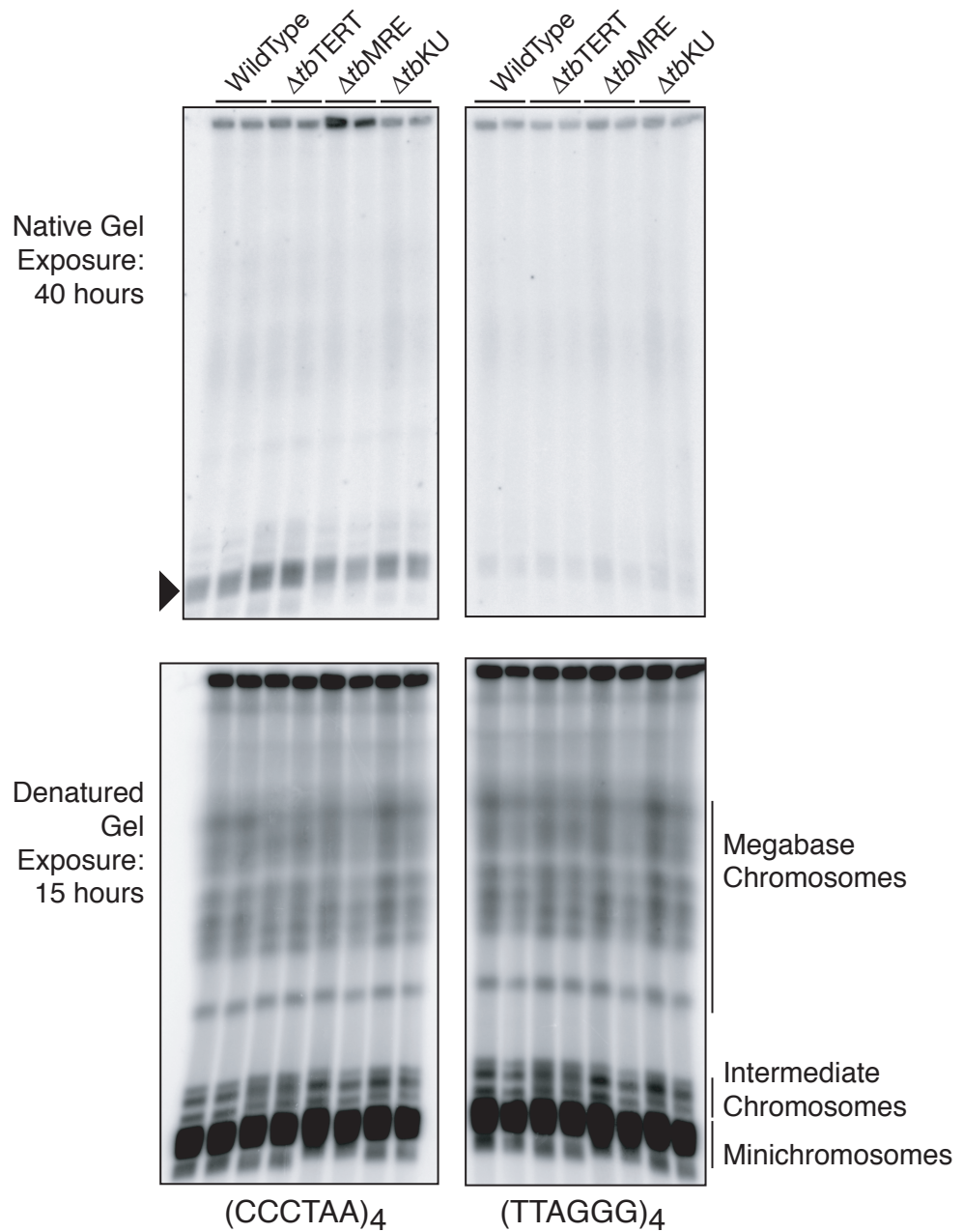
Figure 51

Pulsed-Field Gel Electrophoresis Overhang Assay (PFGE-OH) in wild-type, MRE11-, KU- and TERT-deficient *T. brucei*.

Upper panel: native PFGE were in-gel hybridized with C-rich and G-rich telomere probes. G-overhang signal can be readily detected on highly abundant minichromosomes (arrowhead).

Lower panel: Loading was verified by denturation and re-hybridization of both gels with the same probes.Chromosome types are indicated on the right, exposure times on the right.

Chapter VIII: Conclusions and perspectives

T. brucei survives in the mammalian host by sequential expression of subtelomeric *VSG* genes. Numerous other parasites express variable surface antigens from subtelomeric expression cassettes. What advantages does this location offer and do telomeres play any role in regulating VSG expression?

By creating a telomerase-deficient cell line, I aimed to address these questions.

In this chapter, I will briefly review my results and focus on questions that I find particularly fascinating and that I could not answer in the course of my thesis. Lastly, I present a speculative model of how telomere length and breakage could regulate the frequency of antigenic variation.

The length of T. brucei G-overhangs

T. brucei G-overhangs cannot be visualized by conventional in-gel hybridization, whose detection limit is ~30 nt (109). When overhang assays were performed on whole chromosomes, separated by PFGE, a G-strand specific signal was detected on MC. We propose that this signal is due to the high abundance of MC, which migrate together under the used separation condition, and does not reflect a difference in telomere end structure between these chromosome types.

The rate of telomere shortening correlates with the length of the G-overhang (118). In telomerase-deficient *T. brucei*, telomeres shorten at a rate of 3–6 bp/PD, which suggests, that overhangs are very short (6–12 nt). This issue could be resolved in detail by employing a recently established telomere-tailing and primer extension-based protocol, which permits measurement of G-overhang length at nucleotide resolution (120).

Telomere stabilization at silent ES

In chapter III, we demonstrated that critically short silent ES telomeres stabilized within a distinct size range of 40–200 bp. Unfortunately, we can only speculate how telomere stabilization is achieved. Due to the limited availability of drug selection markers it remains a challenge to sequentially knock-out two genes in *T. brucei*. The genetic requirements for telomere stabilization could be investigated by RNAi knock-down of certain candidate genes (such as Rad51, Mre11 etc.). We proposed that telomere stabilization could be relevant for telomerase-deficient human ALT cells and possibly budding yeast Type I survivors. This idea fascinates me very much, not only because it would enhance the value of *T. brucei* as a model system for telomere biologists, but also because of the implications it might have on telomerase-negative tumor cells. A collaboration between laboratories interested in human ALT and *T. brucei* could explore these possibilities in more detail.

What is the relevance of the slow migrating band in long-term cultured TERT-deficient T. brucei?

In extensively cultured telomerase deficient mutant strains, I noted the appearance of a telomere repeat containing slow migrating band. The origins or relevance of this band remains a mystery and it is unclear whether it plays a role in telomere stabilization. I cannot exclude the possibility the high molecular band is indeed circular, yet so large that it cannot be properly resolved even on a 2-D gel. On figure 19 as well as on other similar gels, the intensity of this band appeared to increase over time. Although I did not succeed in identifying the origin or relevance of this band, further propagation of the telomerase-deficient mutants might facilitate characterization of the band.

Is subtelomeric silencing impaired at short stabilized telomeres?

Telomere-associated factors are implicated in transcriptional silencing of subtelomeric reporter genes in yeast: the Telomere Position Effect (TPE) (269). TPE-like silencing occurs at silent ES in *T. brucei* (49). Does *T. brucei* TPE depend on telomere-associated factors and would short stabilized telomeres still exert this effect on subtelomeric region? Our results suggest that stabilization of a silent ES telomere does not lead to transcriptional activation of its adjacent VSG, and the strain continuous to express VSG 221. However, we do not know whether subtelomeric silencing is perturbed. This question could be addressed in detail by inserting a luciferase-reporter cassette at different positions within a silenced ES. Luciferase levels would be indicative whether partial derepression of silencing occurs during telomere stabilization.

A model for how telomere length and breakage could regulate antigenic variation

Chapters III and V covered the consequences of telomere shortening in the context of silent and active ES. In the proposed model, telomere breakage at the active ES was repaired by BIR, leading to a duplicative gene conversion event. In chapter IV, telomere elongation dynamics at silent and active ES were addressed. In chapter VI, we demonstrated that wild-type isolates have much shorter telomeres than laboratory-adapted strains. I discussed that wild-type *T. brucei* isolates have a high frequency of antigenic switching (10^{-2}–10^{-4}), which is greatly reduced (10^{-6}–10^{-7}) after long-term passaging in mice in the absence of immune selection (73,74,82,90,91).

I propose a speculative model, which is based on old data, experimental observations using telomerase-deficient *T. brucei*, and the results presented in chapter VI. This model proposes that telomere growth and breakage at the active ES could regulate the rate of antigenic variation, and explains how propagation by syringe passaging that avoids the immune response could reduce the switching frequency.

In Figure 52, the X-axis represents the duration of laboratory propagation, in mice or in culture, and the Y-axis represents the length of the active ES. The intersection between X-and Y axis marks the border between subtelomeric region (below) and telomeric repeats (above) and vertical bars represent the amount of DNA that could be lost as a consequence of breakage. These truncations lead to deletion of chromosome terminal regions and could be a consequence of having both replication and transcription bubbles approaching the end. The amount of lost DNA could reflect the distance from the chromosome end at which the replication fork stalls and gives rise to a DSB. At an active ES with a short telomere, these DSB are more likely to fall within the subtelomeric region. Breaks that fall within the telomere tract are rapidly extended by telomerase (50,231). In wild-type African isolates with short telomeres, detection of a DSB presumably triggers a cell cycle arrest and DNA repair through BIR, as it does in other organisms. During BIR, the 3´ overhang could invade another ES, where extension of the 3´ termini by DNA polymerase, and lagging strand synthesis, would repair the break and give rise to an antigenic switch through duplicative gene conversion. Both scenarios could lead to a slight growth disadvantage, favoring parasites whose ES telomere did not break but continued elongating. This rapid elongation, which is unique to short active ES telomeres, would decrease the probability of a subsequent truncation falling within the subtelomeric region, thereby reinforcing stable expression of a single VSG (Figure 52). Another consequence of stably transcribing a single ES is that all silent ES telomeres will grow constantly, without being afflicted by truncations, in contrast to what would happen if there was rapid in-situ switching among ES, which would expose multiple ES to truncations and further accelerate VSG switching.
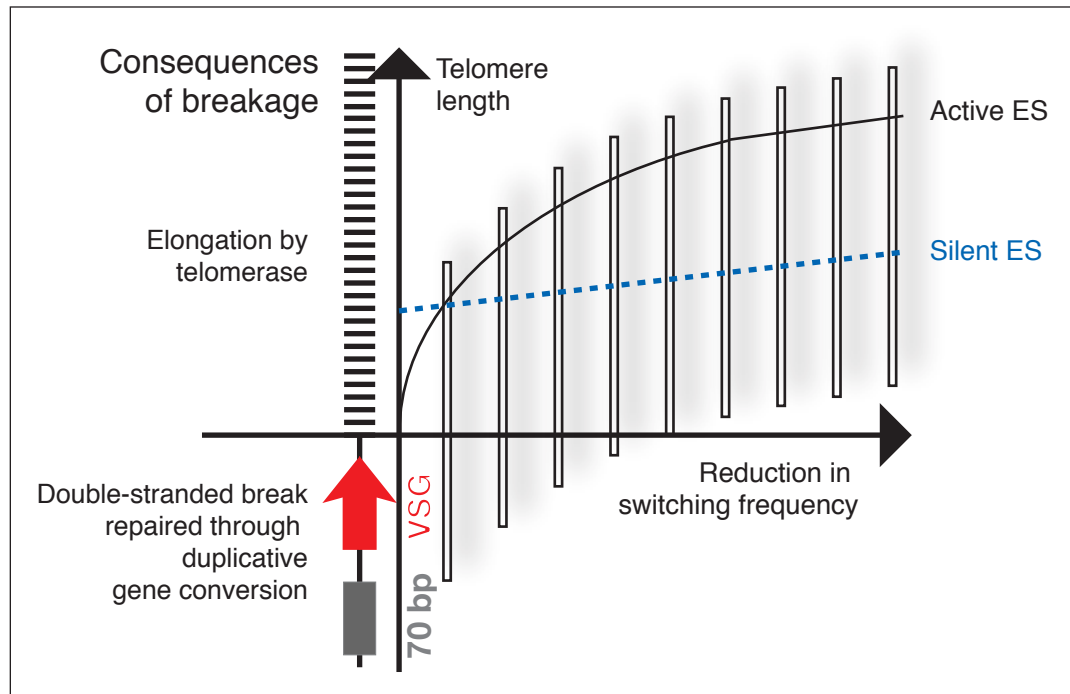
Figure 52

Model for how telomere length and telomere breakage could regulate the frequency of antigenic variation. X-axis represents time of laboratory adaptation. Y-axis represents the length of the active *VSG* 221 ES. Telomere and subtelomeric regions are separated by X-axis. Telomere truncations are represented by shadowed vertical bars. Telomere elongation dynamics at silent and active ES are indicated on the right, consequences of telomere truncations on the far left.

In conclusion my model proposes that telomere length and stalled replication fork induced DSB could regulate the frequency of antigenic switching. Consistent with this model, deletion of Rad51—a homologue of bacterial RecA implicated in homologous strand annealing during BIR—led to a ~10 fold decrease in switching frequency (88). As discussed below, this model could also be applicable to the regulation of antigenic switching in other bacterial and fungal pathogens that express variant antigens from subtelomeric loci.

Telomere length homeostasis in wild-type isolates

As pointed out above, stable *VSG* expression and consequent telomere growth could account for the telomere size differences observed between laboratory-adapted strains and wild-type isolates, so how could telomere length homeostasis be achieved in wild-type isolates? Considering the number of metacyclic and bloodstream form ES in *T. brucei*, it is likely that most MBC arm is occupied by an ES.

In a natural infection, telomere length homeostasis could be achieved through in-situ ES switches. Upon activation, these telomeres would suffer truncations that counteract their constant growth. Maybe telomeres must reach a certain length before transcriptional activation occurs, otherwise telomere truncations would eradicate the new *VSG* too rapidly, exhausting the *VSG* repertoire too quickly and jeopardizing long-term survival of the cell. Thus the dramatic truncations that occur at the active ES explain the need for silent ES telomeres to elongate at a constant rate. The telomere lengths of wild-type isolates would represent an equilibrium between constant telomere growth at silent ES, rapid elongation at the active ES, telomere truncations and antigenic switching.

Borrelia burgdorferi, the causative agent of relapsing fever and lyme disease evades the host immune response by sequentially expressing different Major Variable Antigens (VMP). VMP are encoded by genes located at telomeres of linear plasmids. *VMP* gene expression switching can occur via gene conversion at a rate of roughly 10^{-3}–10^{-4} per cell generation (94,270,271). The surface of *P. carinii,* a fungus that causes pneumonia in immune-compromised mammals, is covered with a dense coat of Major Surface Glycoproteins (MSG), which play a role in mediating adherence to alveolar epithelial cells (272). Indirect immunofluorescence studies showed that only one particular MSG protein is expressed at a given time (93,273). The *P. carinii* genome contains ~100 different *MSG* which reside at chromosome ends (93). It has been proposed that switches occur through recombination where the single ES associated *MSG* is replaced by a new *MSG* through gene conversion and that *MSG* switching occurs at a high frequency of ~10^{-2} per cell division (273). However, despite the similarity between these organisms, it remains to be determined whether the telomere adjacent to the actively transcribed *VMP* or *MSG* is subject to frequent breakage or growth.

Chapter IX: Material and Methods

Trypanosome cell lines and plasmid constructions

T. brucei bloodstream forms, strain Lister 427 antigenic type MITat 1.2 clone 221a (274,275), were cultured in HMI-9 at 37°C. This cell line, when engineered to express T7 RNA polymerase, Tet repressor and neomycinphosphotransferase, was designated the bloodstream-form 'single marker' line (259), and was cultured in HMI-9 containing 2.5 µg/ml G418 (Sigma).

Homozygous *TERT* deletion mutants were generated by sequentially replacing the two alleles with genes encoding resistance to 0.1 *µ*g/ml Puromycin and 5 *µ*g/ml Hygromycin, by a double crossover event, using the *TERT* 5´ and 3´ untranslated regions (UTR) as targeting sequences. The UTRs were amplified by PCR from genomic DNA. NotI and PmeI sites (bold) were included to facilitate subsequent cloning steps: 5´ UTR upper primer; **GCGGCCGC**AATGCTGTTTCTGTCTGCATAA: 5´ UTR lower primer; **GTTTAAAC**GTAGTCGGCTGTCCAACGTTAG: 3´ UTR upper primer; **GTTTAAAC**AATGCAAGCTTTTCTCCTTCACGCG: 3´ UTR lower primer: **GCGGCCGC**AATATAAGTAAGGGAAAGACA. PCR products were cloned into pGEM-T easy (Promega), released by a NotI / PmeI digestion and ligated together into NotI digested, alkaline phosphatase treated pBluescript II SK(+) (Stratagene) creating Vector 2-4. The puromycin *N*-acetyltransferase ORF, flanked by ~100 bp of 5´ and 220 of 3´ UTRs from the *T. brucei* actin gene, was released from pHD309-puro. The restriction fragment was blunt ended by DNA Pol I (large Klenow fragment) and ligated into PmeI digested, dephosphorylated Vector 2-4 creating Vector 2-4-Puro. The gene encoding hygromycin phosphotransferase, plus ~100 bp of 5´ and 300 bp of 3´ UTRs from the *T. brucei* actin gene, was released from pHD309-hygro and ligated into PmeI-digested Vector 2-4 creating Vector 2-4-Hygro. Vectors 2-4-Puro and 2-4-Hygro were digested overnight with NotI, prior to transfection into *T. brucei* single marker cell line as described previously (259).

Alignment of telomerase reverse transcriptase sequences

TERT sequences from *T. brucei, T. cruzi* (GeneDB ID: Tc00.10470535097456) and *L. major* (GeneDB ID: LmjF36.3930) were aligned with TERT characteristic motifs from other organisms, using the ClustalX multiple sequence alignment function of MegAlign software (DNAstar Inc.).

RNA isolation and VSG RT-PCR

T. brucei mRNA was isolated using RNAstat60 according to the protocol provided by Tel-Test Inc. The dominant VSG in the population was cloned by reverse transcriptase PCR using oligos against the conserved *T. brucei* spliced leader sequence (5´-GACTAGTTTCTGTACTATAT-3´) and a *VSG* C-terminal conserved region (5´-GACTAGTGTTAAAATATATCA-3´). Polymerase chain reaction was carried out for 30 cycles under the following conditions: 1 minute at 94°C, 1 min at 40°C, 1 min at 72°C.

TERT N-terminal RT-PCR

mRNA was isolated as described above, cDNA was generated by using ProSTAR™ First-Strand RT-PCR Kit from Stratagene.
Forward Primer C: 5´-ACGACGCTGTGTCTGGTAAT-3´, was used in conjunction with two different reverse primers: A: 5´-TTCGGAAGTCACACGCT-3´ or reverse primer B: 5´-CGGGCTTTTAGAGGTA-3´ on genomic DNA and cDNA. PCR conditions were as follows: initial denturation for 2 min at 94°C, then 28 cycles of 30 sec at 94°C, 30 sec at 50°C and 60 sec at 72°C. To detect small size changes, PCR products were separated on a 1.8% agarose gel.

Time course and telomere blots

Telomere length changes were analyzed by culturing parental cells in parallel with heterozygous and homozygous telomerase deletion mutants. Every week, genomic DNA was isolated as previously described (101). Genomic blotting and hybridization was performed as described previously (276). Size changes in silent ES telomeres were detected by digesting genomic DNA with the restriction enzymes indicated in the figures. Terminal restriction fragments containing *VSG* genes were detected as described by Horn *et al.* (82).

G-strand overhang assay

G-strand overhang assays were performed according to a published protocol (109) with minor modifications. Gels were hybridized overnight at 30°C in Church Mix (0.5 M NaPO$_4$ pH 7.2, 1 mM EDTA pH 8.0, 7% SDS, 1% BSA). After washing 3 times for 30 min with 4 x SSC (1 x SSC is 15 mM tri-sodium citrate, 150 mM NaCl) and once for 30 min with 4 x SSC + 0.1% SDS at 20°C, the gel was exposed to a phosphorimager screen for at least 72 h. The gels were then denatured, neutralized, and hybridized overnight with the same probes. After washing as described above but at 55°C, the gel was exposed to a phosphorimager screen for 3–5 h.

T. brucei cell and HeLa genomic DNA mixing experiment

To determine whether *T. brucei* cell extracts might degrade G-strand overhangs, *T. brucei* cells were centrifuged and washed twice in 1 x TDB (5 mM KCl, 80 mM NaCl, 1 mM MgSO$_4$, 20 mM Na$_2$HPO$_4$, 2 mM NaH$_2$PO$_4$, 20 mM glucose, pH 7.7) then mixed with HeLa cell DNA at different ratios and DNA was re-isolated as described above. G-overhang assay was performed as described above.

Enzymatic modification of T.brucei DNA

DNA was incubated with 30 units of T7 (Gene 6) Exonuclease (US Biochemicals) for 20 min at 37°C or with 20 units of *E.coli* Exonuclease I (US Biochemicals) for 12 h at 37°C (100,234). Overhang assay conditions were the same as above.

2-dimensional gel electrophoresis

MboI / AluI digested DNA of *T. brucei* TERT deficient mutant and human ALT cell line Saos-2, kindly provided by Sean Rooney, de Lange laboratory (positive control) were separated on 2 dimensional (2D) gel electrophoresis according to a protocol from Fangman and Breyer (201). Both DNA were separated in the first dimension on a large 400 ml 0.4% agarose in 1xTBE gel without ethidium bromide. The gel was run at 18 volts for 24 hours at room temperature. The gel was stained for 20 minutes in 1xTBE with 0.3 μg/ml Ethidium Bromide, migration was verified in the darkroom using the handheld UV light stick at long wave length. Bands of positive control and TERT deficient cell lines were excised from the gel, transferred to a second gel tray and embedded perpendicular in 400ml 1.1% agarose in 1x TBE +0.3 μg/ml.
The gel was run at 150 volts at 4°C for approximately 7 hours. The gel was photographed on the UV box, DNA was transferred to a membrane by Southern blotting for subsequent hybridization. To visualize telomeric fragments, denaturing in gel hybridization, using a radiolabeled (TTAGGG)$_4$ probe gave better results (as described for overhang assays).

Complementation of telomerase-deficient mutant strains

To complement the TERT deletion phenotype, the *tbTERT* open reading frame was amplified using primers that introduce NdeI restriction sequences at 5´ and HpaI site at the 3´ of the gene. The PCR product was cloned into pGEM-T easy (Promega) and clones from independent PCR reactions were sequenced to exclude the possibility of

PCR-derived mutations. To put the ORF under the control of an inducible T7 promoter, the 3.579 kB PCR product was released by NdeI / HpaI digestion and cloned into NdeI / HpaI digested pCO-57; this step removes a GFP cassette from pCO57, a derivative of pLew82 (259). Proper integration was verified by restriction analysis and sequencing. To introduce a GFP tag at the telomerase C-terminus, NdeI sites were introduced by PCR at both ends of the TERT orf, cloned into pGEM-T easy, released and ligated into NdeI cut and dephosphorylated pCO57. The constructs were linearized by digestion with NotI and transfected into telomerase-deficient cell lines. Selection for integration positive clones was achieved by the addition of 2.5 μg/ml Phleomycin. Upon reintroduction, TERT expressing clones were verified by Southern blot (data not shown) and maintained in continuous culture for several weeks. DNA was extracted on a weekly basis and telomere length changes at transcriptionally silent and active ES were monitored by Southern hybridization. Expression of the fusion product was induced by addition of 100 ng / ml doxycycline. To assess whether TERT-gfp is fully functional, its ability to elongate a short telomere was compared with a re-introduced wildtype allele of telomerase as well as an HA-tagged version of *tbTERT*. Wildtype and TERT-gfp constructs were fully functional whereas HA-TERT did not elongate telomeres (data not shown).

Bal31 Digestions

Bal 31 digestion was performed as described previously (101). Briefly, 100 μg of DNA in 500 μl volume were incubated at 30°C with 5 Units of Bal 31. At different timepoints (15, 30, 50 and 120 minutes), a 100 μl sample was removed, added to 2 μl 0.5 M EGTA, incubated at 65°C for 10 minutes and stored at -20°C until DNA was extracted by Phenol – Chloroform - Isoamyl-alcohol, precipitated and dissolved in $T_{10}E_{0.1}$ (10 mM Tris pH 7.4, 0.1 mM EDTA) buffer. Subsequently, DNA was EcoRI digested and loaded on a 0.8 % agarose gel. Southern blotting and hybridization procedures were performed as described (265).

Telomere tailing procedure and PCR amplification

These experiments were carried out as described before with minor modifications (244). To increase the efficiency of telomere tailing, Terminal Restriction Fragments (TRF) corresponding to the size of stabilized VSG 121 telomere (~1.6 kB), were isolated from an 0.8% agarose gel. Approximately 100 ng of TRF in 1x one-phor-all buffer (Pharmacia), 1mM dCTP and 5 U of terminal deoxynucleotidyl transferase (Amersham Biosciences) were incubated for 30 minutes at 37°C. The efficiency of the tailing reaction was verified by addition of radiolabeled dCTP to the reaction mix and running the products on agarose gels (data not shown).

The tailing reactions were PCR amplified using 0.75 μM primer A (5'-ACACAGGCGAACCAGAATGACGCTGCAGCCAAAGCA-3'), 1.0 μM primer B (CCCCC)$_3$, 320 μM dNTPs, 10x TAQ polymerase buffer and 2.5 U of TAQ polymerase by incubating for 2 min at 94°C, followed by 45 cycles of 45 seconds at 94°C, 45 seconds at 65°C and 70 seconds at 72°C. PCR amplified products were separated on a 1.2% agarose gel and non-tailed TRFs were amplified in parallel as negative control. Specific products were gel purified and sucloned into pGEM-T (Promega). Restriction digests were performed as described by manufacturers directions (New England Biolabs). Sequencing reactions were carried out by GeneWiz Inc (North Brunswick, NJ).

Rotating agarose gel electrophoresis

DNA agarose plugs were prepared as described by Navarro and Cross (55). Briefly, 2 x 10^8 cells were harvested, washed in Trypanosome Dilution Buffer (TDB), resuspended in 0.5 ml L-Buffer (0.1 M EDTA pH 8.0, 10 mM Tris-HCl pH 7.6, 20 mM NaCl) and incubated for 10 minutes at 42°C. 0.5 ml of 1.6% low gelling agarose (Sigma) in L-Buffer was added to 0.5 ml cells, mixed and poured into Plug Molds (Bio-Rad Laboratories). Plugs were treated in 3 ml L-Buffer for 2 days with 1 mg/ml proteinase K at 50°C. Upon washing twice for 15 minutes with L-Buffer, proteinase

K treatment and washing was repeated. Plugs were embedded in 0.8% Agarose in 0.5 x Tris-borate-EDTA gel. Megabase (MBC), intermediate (IC) and minichromosomes (MC) were separated under conditions previously described by Navarro and Cross (23). 1st window; linear ramp 100 - 300 seconds for 10 hours at 120 volts, 2nd window; 1000 – 2500 seconds for 80 hours at 50 volts. Gels were dried at room temperature and hybridized as described above. Separation of MC and IC took place at a rotation angle of 120° in 0.5x Tris-borate-EDTA at 12°C. The program consisted of one ramped pulse time of 60-s to 20-s at a constant voltage of 110 V for 60 h (Luisa Figueiredo, unpublished data). For in-gel hybridization with radiolabeled telomeric oligonucleotides, gels were dried at room temperature, denatured and neutralized; in-gel hybridization was performed as described previously (265). DNA was blotted onto a Hybond membrane, cross-linked in a UV-stratalinker 1800 (Stratagene), hybridized and washed as described. Signals were quantified using a phosphorimager screen and ImageQuant software (Molecular Dynamics).

To quantify the extent of MC loss, PFGE gels were run in duplicates: Gel 1 was in-gel hybridized using a radiolabelled $(TTAGGG)_4$ probe whereas Gel 2 was blotted onto Hybond N+ membrane and sequentially probed with 50-bp repeats, 177-bp repeat and individual *VSG* probes. MC 177 and 50-bp probes were obtained by PCR amplification from genomic DNA as previously described (246). Hybridized membranes were exposed to phosphorimager screens and signal intensity of individual bands was quantified using ImageQuant software. To analyze the reduction in MC 177-bp signal, 50-bp repeat and VSG probes were used to normalize loading.

Slot Blot hybridization

0.4 to 0.8 μg of DNA from wild-type and long term cultured TERT deficient strains was added to 6 x SSC (900 mM NaCl, 90 mM sodium citrate, pH 7.0), boiled for 10 minutes and placed on ice. 200 and 400 μl of denatured DNA were applied to manifold device containing a 6 x SSC equilibrated Hybond N+ membrane. By applying suction, the DNA was applied in duplicates onto the membrane. Upon

dismantling the apparatus, the membrane was cross-linked and hybridized with 177-bp and 50-bp repeat probes. Signal intensities were quantified using Phosphorimager screens (Molecular Dynamics).

Telomere size distribution analysis

Terminal restriction fragments containing specific *VSG* were detected by genomic blotting, hybridization and phosphorimaging (49). Using Image Quant software, all lanes were partitioned into 30 equally sized rectangles. The signal intensity in each rectangle was measured as a percentage of the total signal in the entire lane and graphically represented as a function of telomere length.

Long-range Southern blot

Digestion of DNA in genomic plugs was performed as recommended by the enzyme manufacturer (New England Biolabs). 60 Units of ApaI were incubated in NEB buffer 4 + 1x bovine serum albumin at 25°C overnight. Plugs were subsequently washed in TE (0.1 M EDTA pH 8.0, 10 mM Tris-HCl pH 7.6). Restriction fragments were separated on a 0.8% agarose gel in 0.5x TBE. We used a program consisting of a 1–12 sec linear ramp at a constant 150 v for 15 h at 12°C. The rotation angle was 120°.

Northern Blots and RT-PCR

T. brucei mRNA was isolated using RNAstat60, according to the manufacturer's protocol. The dominant *VSG* expressed by the population was cloned by RT-PCR using oligos against the conserved *T. brucei* spliced leader sequence (5´-GACTAGTTTCTGTACTATAT-3´ and a *VSG* C-terminal conserved region 5´-GACTAGTGTTAAAATATATCA-3´. Polymerase chain reaction was carried out for 30 cycles of 1 min at 94°C, 1 min at 40°C, 1 min at 72°C.

The detailed lineages of *T. brucei* cell lines used in these studies and by other laboratories are available at http://tryps.rockefeller.edu/trypanosome_pedigrees.html. The strain abbreviations used in this paper are indicated in parentheses.

T. brucei S42, 348 and *T. b. rhodesiense* s427 are isolates that have not been adapted for virulent growth. S42 (S42) was isolated from a female warthog, near Kirawira, Tanzania, on March 1966 (277). It was minimally passaged before being transmitted through tsetse in November 1974. STIB366D was derived from a single metacyclic cell and was minimally propagated before freezing as RUMP102, which we used as our source of S42 DNA. 246/STIB348U/MIAG106 (348) was isolated from a Hartebeest in Serengeti in 1971 (278). After growth in mice and rats for a total of ~6 weeks, it was transmitted through tsetse in July 1975. STIB348U was derived from a single metacyclic cell, and frozen as MIAG106 (our source of DNA) after passage through 2 irradiated mice. *T. b. rhodesiense* RUMP151 (151) is derived from the true s427, which was isolated in 1960 from a sheep in south-east Uganda (279). s427 was passaged through ~20 mice before being frozen as RUMP151, which is highly resistant to human serum (GAMC, unpublished data), consistent with its isolation from an area of epidemic human sleeping sickness ((279) and M.P. Cunningham, personal communication).

TREU927 (TREU927) was isolated in Kiboko, Kenya in 1969 or 1970, and preserved after 3–11 passages (280). The procyclic cells from which we isolated DNA had been propagated for at least thirty 2–3 day transfers in mice (92), before being differentiated to procyclic forms in the laboratory of Scott Landfear and further propagated for about 75 PD.

The origin of Lister 427 (427) is unknown. It is not related to s427, as originally thought, and was maintained by syringe passage during indeterminate intervals from 1961–1967. Lister 427 'single-marker' (SM) (259) bloodstream and 29-13 procyclic forms are extensively propagated laboratory-adapted clones with a low switching frequency of ~10^{-6}–10^{-7} / PD (74,82). The relative positions of RUMP150 and RUMP501 in the Lister 427 lineage are clear, and their genotypic identity has been

verified on several occasions (C.M.R. Turner and G.A.M. Cross, unpublished data). RUMP150 is genetically indistinguishable from single-marker bloodstream and 29-13 procyclic clones, but the degree of propagation of Lister 427 prior to its preservation as RUMP501 cannot be verified.

RUMP100 and RUMP502 are descendants of EATRO795, isolated from a Zebu cow in Kenya (Sept. 8th, 1964) (73,90,91,281), which has a high switching frequency. The ancestors of RUMP100 (100) were recloned several times, with minimal passaging, prior to infecting a mouse with a single metacyclic, yielding STIB367H, from which the RUMP100 population was frozen after one additional mouse passage. RUMP502 (502) is one passage removed from GUP2900 (GUG359). Although we lack documentation of the lineage prior to GUP2900, RUMP502 was recently verified to be genetically indistinguishable from EATRO795 (C. M. R. Turner, personal communication). DNA samples from paired samples of two other strains, before and after laboratory-adaptation, were kindly provided by C. M. R. Turner (Glasgow University). STIB247 (247) was isolated during the same expedition as STIB246/348 (see above) and probably also frozen after ~6 weeks of growth in mice and rats (278). Cloning of the population led to STIB247L (282) and 52 2-3 days syringe passages yielded GUTat 8.1 (283). Strain 386 (386) was isolated from a patient on the Ivory Coast in 1978 by members of the Bernhard-Nocht Institute, Hamburg (284). The detailed events between isolation and cloning of STIB386AA are unclear. DNA we obtained was before and after 52 passages in mice that led to dominant expression of GUTat 9.1 (283).

Cultivation of African wild-type strain isolates of T. brucei

African isolates strains were first grown in female CD-1 AKA ICR (Charles River) mice. After 3 days, approximately 10^8 cells were harvested from anesthetized mice by heart puncture and grown for 3 days in male Sprague Dawley rats (Charles River). Laboratory-adapted Lister 427 derivatives were cultured in HMI-9 at 37°C (274,275).

Cultivation of Leishmania and T. cruzi

Leishmania major Friedlin strain was cultured in M199 (GIBCO) plus supplements (40 mM HEPES, pH 7.4; 0.1 mM adenine; 1 μg/ml biotin; 5 μg/ml hemin; 1x Pen-strep (GIBCO); 10% bovine calf serum). *L. tarentolae* isolates were grown in brain-heart infusion medium (DIFCO) plus 10 mg/l hemin. A clone of *T. cruzi* Y strain epimastigotes containing FLAG-tagged gp72 (285) was grown in LDTN medium (286).

References

1.	Chappuis, F., Udayraj, N., Stietenroth, K., Meussen, A. and Bovier, P.A. (2005) Eflornithine is safer than melarsoprol for the treatment of second-stage T*rypanosoma brucei* gambiense human African trypanosomiasis. *Clin Infect Dis*, 41**,** 748-751.

2.	Hide, G. (1999) History of sleeping sickness in East Africa. *Clin Microbiol Rev*, 12**,** 112-125.

3.	Macarthur, W. (1955) An account of some of Sir David Bruce's researches, based on his own manuscript notes. *Trans R Soc Trop Med Hyg*, 49**,** 404-412.

4.	Vickerman, K. (1969) On the surface coat and flagellar adhesion in trypanosomes. *J Cell Sci*, 5**,** 163-193.

5.	Cross, G.A.M. (1975) Identification, purification and properties of clone-specific glycoprotein antigens constituting the surface coat of *Trypanosoma brucei*. *Parasitology*, 71**,** 393-417.

6.	Cross, G.A. (1977) Isolation, structure and function of variant-specific surface antigens. *Ann Soc Belg Med Trop*, 57**,** 389-402.

7.	Freymann, D., Down, J., Carrington, M., Roditi, I., Turner, M. and Wiley, D. (1990) 2.9 A resolution structure of the N-terminal domain of a variant surface glycoprotein from *Trypanosoma brucei*. *J Mol Biol*, 216**,** 141-160.

8.	Ferguson, M.A., Homans, S.W., Dwek, R.A. and Rademacher, T.W. (1988) Glycosyl-phosphatidylinositol moiety that anchors *Trypanosoma brucei* variant surface glycoprotein to the membrane. *Science*, 239**,** 753-759.

9.	Chattopadhyay, A., Jones, N.G., Nietlispach, D., Nielsen, P.R., Voorheis, H.P., Mott, H.R. and Carrington, M. (2005) Structure of the C-terminal domain from *Trypanosoma brucei* variant surface glycoprotein MITat1.2. *J Biol Chem*, 280**,** 7228-7235.

10.	Miller, E.N., Allan, L.M. and Turner, M.J. (1984) Topological analysis of antigenic determinants on a variant surface glycoprotein of *Trypanosoma brucei*. *Mol Biochem Parasitol*, 13**,** 67-81.

11.   van der Ploeg, L.H., Valerio, D., de Lange, T., Bernards, A., Borst, P. and Grosveld, F.G. (1982) An analysis of cosmid clones of nuclear DNA from *Trypanosoma brucei* shows that the genes for variant surface glycoproteins are clustered in the genome. *Nucleic Acids Res*, 10**,** 5905-5923.

12.   Barry, J.D., Marcello, L., Morrison, L.J., Read, A.F., Lythgoe, K., Jones, N., Carrington, M., Blandin, G., Bohme, U., Caler, E. et al. (2005) What the genome sequence is revealing about trypanosome antigenic variation. *Biochem Soc Trans*, 33**,** 986-989.

13.   Borst, P., Fase-Fowler, F. and Gibson, W.C. (1981) Quantitation of genetic differences between *Trypanosoma brucei gambiense*, *rhodesiense* and *brucei* by restriction enzyme analysis of kinetoplast DNA. *Mol Biochem Parasitol*, 3**,** 117-131.

14.   Van der Ploeg, L.H., Schwartz, D.C., Cantor, C.R. and Borst, P. (1984) Antigenic variation in *Trypanosoma brucei* analyzed by electrophoretic separation of chromosome-sized DNA molecules. *Cell*, 37**,** 77-84.

15.   Melville, S.E., Leech, V., Navarro, M. and Cross, G.A. (2000) The molecular karyotype of the megabase chromosomes of *Trypanosoma brucei* stock 427. *Mol Biochem Parasitol*, 111**,** 261-273.

16.   Melville, S.E., Leech, V., Gerrard, C.S., Tait, A. and Blackwell, J.M. (1998) The molecular karyotype of the megabase chromosomes of *Trypanosoma brucei* and the assignment of chromosome markers. *Mol Biochem Parasitol*, 94**,** 155-173.

17.   Weiden, M., Osheim, Y.N., Beyer, A.L. and Van der Ploeg, L.H. (1991) Chromosome structure: DNA nucleotide sequence elements of a subset of the minichromosomes of the protozoan *Trypanosoma brucei*. *Mol Cell Biol*, 11**,** 3823-3834.

18.   Wickstead, B., Ersfeld, K. and Gull, K. (2004) The small chromosomes of *Trypanosoma brucei* involved in antigenic variation are constructed around repetitive palindromes. *Genome Res*, 14**,** 1014-1024.

19. Zomerdijk, J.C., Kieft, R. and Borst, P. (1992) A ribosomal RNA gene promoter at the telomere of a mini-chromosome in *Trypanosoma brucei*. *Nucleic Acids Res*, 20**,** 2725-2734.

20. Alsford, S., Wickstead, B., Ersfeld, K. and Gull, K. (2001) Diversity and dynamics of the minichromosomal karyotype in *Trypanosoma brucei*. *Mol. Biochem. Parasitol.*, 113**,** 79-88.

21. De Lange, T. and Borst, P. (1982) Genomic environment of the expression-linked extra copies of genes for surface antigens of *Trypanosoma brucei* resembles the end of a chromosome. *Nature*, 299**,** 451-453.

22. Cully, D.F., Ip, H.S. and Cross, G.A. (1985) Coordinate transcription of variant surface glycoprotein genes and an expression site associated gene family in *Trypanosoma brucei*. *Cell*, 42**,** 173-182.

23. Navarro, M. and Cross, G.A.M. (1996) DNA rearrangements associated with multiple consecutive directed antigenic switches in *Trypanosoma brucei*. *Mol. Cell. Biol.*, 16**,** 3615-3625.

24. Vanhamme, L., Poelvoorde, P., Pays, A., Tebabi, P., Van Xong, H. and Pays, E. (2000) Differential RNA elongation controls the variant surface glycoprotein gene expression sites of *Trypanosoma brucei*. *Mol Microbiol*, 36**,** 328-340.

25. Kooter, J.M., van der Spek, H.J., Wagter, R., d'Oliveira, C.E., van der Hoeven, F., Johnson, P.J. and Borst, P. (1987) The anatomy and transcription of a telomeric expression site for variant-specific surface antigens in *T. brucei*. *Cell*, 51**,** 261-272.

26. Zomerdijk, J.C., Ouellette, M., ten Asbroek, A.L., Kieft, R., Bommer, A.M., Clayton, C.E. and Borst, P. (1990) The promoter for a variant surface glycoprotein gene expression site in *Trypanosoma brucei*. *EMBO J*, 9**,** 2791-2801.

27. Cully, D.F., Gibbs, C.P. and Cross, G.A. (1986) Identification of proteins encoded by variant surface glycoprotein expression site-associated genes in *Trypanosoma brucei*. *Mol Biochem Parasitol*, 21**,** 189-197.

28. Bitter, W., Gerrits, H., Kieft, R. and Borst, P. (1998) The role of transferrin-receptor variation in the host range of *Trypanosoma brucei*. *Nature*, 391**,** 499-502.

29. Pays, E., Tebabi, P., Pays, A., Coquelet, H., Revelard, P., Salmon, D. and Steinert, M. (1989) The genes and transcripts of an antigen gene expression site from *T. brucei*. *Cell*, 57**,** 835-845.

30. Ross, D.T., Raibaud, A., Florent, I.C., Sather, S., Gross, M.K., Storm, D.R. and Eisen, H. (1991) The trypanosome VSG expression site encodes adenylate cyclase and a leucine-rich putative regulatory gene. *Embo J*, 10**,** 2047-2053.

31. Hoek, M., Zanders, T. and Cross, G.A. (2002) *Trypanosoma brucei* expression-site-associated-gene-8 protein interacts with a Pumilio family protein. *Mol Biochem Parasitol*, 120**,** 269-283.

32. Gottesdiener, K.M. (1994) A new VSG expression site-associated gene (ESAG) in the promoter region of *Trypanosoma brucei* encodes a protein with 10 potential transmembrane domains. *Mol Biochem Parasitol*, 63**,** 143-151.

33. Schell, D., Evers, R., Preis, D., Ziegelbauer, K., Kiefer, H., Lottspeich, F., Cornelissen, A.W. and Overath, P. (1991) A transferrin-binding protein of *Trypanosoma brucei* is encoded by one of the genes in the variant surface glycoprotein gene expression site. *Embo J*, 10**,** 1061-1066.

34. Salmon, D., Geuskens, M., Hanocq, F., Hanocq-Quertier, J., Nolan, D., Ruben, L. and Pays, E. (1994) A novel heterodimeric transferrin receptor encoded by a pair of VSG expression site-associated genes in *T. brucei*. *Cell*, 78**,** 75-86.

35. Gerrits, H., Mussmann, R., Bitter, W., Kieft, R. and Borst, P. (2002) The physiological significance of transferrin receptor variations in *Trypanosoma brucei*. *Mol Biochem Parasitol*, 119**,** 237-247.

36. van Luenen, H.G., Kieft, R., Mussmann, R., Engstler, M., ter Riet, B. and Borst, P. (2005) Trypanosomes change their transferrin receptor expression to allow effective uptake of host transferrin. *Mol Microbiol*, 58**,** 151-165.

37. Borst, P., Bitter, W., Blundell, P.A., Chaves, I., Cross, M., Gerrits, H., van Leeuwen, F., McCulloch, R., Taylor, M. and Rudenko, G. (1998) Control of

VSG gene expression sites in *Trypanosoma brucei*. *Mol Biochem Parasitol*, 91**,** 67-76.

38. Kratz, E., Dugas, J.C. and Ngai, J. (2002) Odorant receptor gene regulation: implications from genomic organization. *Trends Genet*, 18**,** 29-34.

39. Chess, A., Simon, I., Cedar, H. and Axel, R. (1994) Allelic inactivation regulates olfactory receptor gene expression. *Cell*, 78**,** 823-834.

40. Lane, R.P., Cutforth, T., Young, J., Athanasiou, M., Friedman, C., Rowen, L., Evans, G., Axel, R., Hood, L. and Trask, B.J. (2001) Genomic analysis of orthologous mouse and human olfactory receptor loci. *Proc Natl Acad Sci U S A*, 98**,** 7390-7395.

41. Munoz-Jordan, J.L., Davies, K.P. and Cross, G.A. (1996) Stable expression of mosaic coats of variant surface glycoproteins in *Trypanosoma brucei*. *Science*, 272**,** 1795-1797.

42. Serizawa, S., Ishii, T., Nakatani, H., Tsuboi, A., Nagawa, F., Asano, M., Sudo, K., Sakagami, J., Sakano, H., Ijiri, T. et al. (2000) Mutually exclusive expression of odorant receptor transgenes. *Nat Neurosci*, 3**,** 687-693.

43. Gottschling, D.E., Aparicio, O.M., Billington, B.L. and Zakian, V.A. (1990) Position effect at *S. cerevisiae* telomeres: reversible repression of Pol II transcription. *Cell*, 63**,** 751-762.

44. Boulton, S.J. and Jackson, S.P. (1998) Components of the Ku-dependent non-homologous end-joining pathway are involved in telomeric length maintenance and telomeric silencing. *Embo J*, 17**,** 1819-1828.

45. Renauld, H., Aparicio, O.M., Zierath, P.D., Billington, B.L., Chhablani, S.K. and Gottschling, D.E. (1993) Silent domains are assembled continuously from the telomere and are defined by promoter distance and strength, and by SIR3 dosage. *Genes Dev*, 7**,** 1133-1145.

46. Mishra, K. and Shore, D. (1999) Yeast Ku protein plays a direct role in telomeric silencing and counteracts inhibition by rif proteins. *Curr Biol*, 9**,** 1123-1126.

47. Pryde, F.E. and Louis, E.J. (1999) Limitations of silencing at native yeast telomeres. *Embo J*, 18**,** 2538-2550.

48.   Fourel, G., Revardel, E., Koering, C.E. and Gilson, E. (1999) Cohabitation of insulators and silencing elements in yeast subtelomeric regions. *Embo J*, 18**,** 2522-2537.

49.   Horn, D. and Cross, G.A.M. (1997) Position-dependent and promoter-specific regulation of gene expression in *Trypanosoma brucei. EMBO J*, 16**,** 7422-7431.

50.   Glover, L. and Horn, D. (2006) Repression of polymerase I-mediated gene expression at *Trypanosoma brucei* telomeres. *EMBO Rep*, 7**,** 93-99.

51.   Janzen, C.J., Lander, F., Dreesen, O. and Cross, G.A. (2004) Telomere length regulation and transcriptional silencing in KU80-deficient *Trypanosoma brucei. Nucleic Acids Res*, 32**,** 6575-6584.

52.   Chaves, I., Zomerdijk, J., Dirks-Mulder, A., Dirks, R.W., Raap, A.K. and Borst, P. (1998) Subnuclear localization of the active variant surface glycoprotein gene expression site in *Trypanosoma brucei. Proc Natl Acad Sci U S A*, 95**,** 12328-12333.

53.   Rudenko, G., Bishop, D., Gottesdiener, K. and Van der Ploeg, L.H. (1989) Alpha-amanitin resistant transcription of protein coding genes in insect and bloodstream form *Trypanosoma brucei. EMBO J*, 8**,** 4259-4263.

54.   Kooter, J.M., De Lange, T. and Borst, P. (1984) Discontinuous synthesis of mRNA in trypanosomes. *EMBO J*, 3**,** 2387-2392.

55.   Navarro, M. and Cross, G.A.M. (1998) In situ analysis of a variant surface glycoprotein expression-site promoter region in *Trypanosoma brucei. Mol Biochem Parasitol*, 94**,** 53-66.

56.   Navarro, M. and Gull, K. (2001) A pol I transcriptional body associated with VSG mono-allelic expression in *Trypanosoma brucei. Nature*, 414**,** 759-763.

57.   Pays, E., Delauw, M.F., Laurent, M. and Steinert, M. (1984) Possible DNA modification in GC dinucleotides of Trypanosoma brucei telomeric sequences; relationship with antigen gene transcription. *Nucleic Acids Res*, 12**,** 5235-5247.

58. Bernards, A., van Harten-Loosbroek, N. and Borst, P. (1984) Modification of telomeric DNA in *Trypanosoma brucei*; a role in antigenic variation? *Nucleic Acids Res*, 12**,** 4153-4170.

59. Gommers-Ampt, J.H., Van Leeuwen, F., de Beer, A.L., Vliegenthart, J.F., Dizdaroglu, M., Kowalak, J.A., Crain, P.F. and Borst, P. (1993) beta-D-glucosyl-hydroxymethyluracil: a novel modified base present in the DNA of the parasitic protozoan *T. brucei*. *Cell*, 75**,** 1129-1136.

60. van Leeuwen, F., Wijsman, E.R., Kieft, R., van der Marel, G.A., van Boom, J.H. and Borst, P. (1997) Localization of the modified base J in telomeric VSG gene expression sites of *Trypanosoma brucei*. *Genes Dev*, 11**,** 3232-3241.

61. Cross, M., Kieft, R., Sabatini, R., Wilm, M., de Kort, M., van der Marel, G.A., van Boom, J.H., van Leeuwen, F. and Borst, P. (1999) The modified base J is the target for a novel DNA-binding protein in kinetoplastid protozoans. *EMBO J*, 18**,** 6573-6581.

62. DiPaolo, C., Kieft, R., Cross, M. and Sabatini, R. (2005) Regulation of trypanosome DNA glycosylation by a SWI2/SNF2-like protein. *Mol Cell*, 17**,** 441-451.

63. Pays, E., Lheureux, M. and Steinert, M. (1981) Analysis of the DNA and RNA changes associated with the expression of isotypic variant-specific antigens of trypanosomes. *Nucleic Acids Res*, 9**,** 4225-4238.

64. Greaves, D.R. and Borst, P. (1987) Trypanosoma brucei variant-specific glycoprotein gene chromatin is sensitive to single-strand-specific endonuclease digestion. *J Mol Biol*, 197**,** 471-483.

65. Gross, D.S. and Garrard, W.T. (1988) Nuclease hypersensitive sites in chromatin. *Annu Rev Biochem*, 57**,** 159-197.

66. Williams, R.O., Young, J.R. and Majiwa, P.A. (1979) Genomic rearrangements correlated with antigenic variation in *Trypanosoma brucei*. *Nature*, 282**,** 847-849.

67.   Hoeijmakers, J.H., Frasch, A.C., Bernards, A., Borst, P. and Cross, G.A. (1980) Novel expression-linked copies of the genes for variant surface antigens in trypanosomes. *Nature*, 284**,** 78-80.

68.   Bernards, A., Van der Ploeg, L.H., Frasch, A.C., Borst, P., Boothroyd, J.C., Coleman, S. and Cross, G.A. (1981) Activation of trypanosome surface glycoprotein genes involves a duplication-transposition leading to an altered 3' end. *Cell*, 27**,** 497-505.

69.   Pays, E., Van Meirvenne, N., Le Ray, D. and Steinert, M. (1981) Gene duplication and transposition linked to antigenic variation in Trypanosoma brucei. *Proc Natl Acad Sci U S A*, 78**,** 2673-2677.

70.   Rudenko, G., McCulloch, R., Dirks-Mulder, A. and Borst, P. (1996) Telomere exchange can be an important mechanism of variant surface glycoprotein gene switching in *Trypanosoma brucei*. *Mol Biochem Parasitol*, 80**,** 65-75.

71.   Pays, E., Van Assel, S., Laurent, M., Darville, M., Vervoort, T., Van Meirvenne, N. and Steinert, M. (1983) Gene conversion as a mechanism for antigenic variation in trypanosomes. *Cell*, 34**,** 371-381.

72.   Myler, P.J., Allison, J., Agabian, N. and Stuart, K. (1984) Antigenic variation in African trypanosomes by gene replacement or activation of alternate telomeres. *Cell*, 39**,** 203-211.

73.   Robinson, N.P., Burman, N., Melville, S.E. and Barry, J.D. (1999) Predominance of duplicative VSG gene conversion in antigenic variation in African trypanosomes. *Mol Cell Biol*, 19**,** 5839-5846.

74.   Lamont, G.S., Tucker, R.S. and Cross, G.A. (1986) Analysis of antigen switching rates in *Trypanosoma brucei*. *Parasitology*, 92 (Pt 2)**,** 355-367.

75.   McCulloch, R., Rudenko, G. and Borst, P. (1997) Gene conversions mediating antigenic variation in *Trypanosoma brucei* can occur in variant surface glycoprotein expression sites lacking 70-base-pair repeat sequences. *Mol Cell Biol*, 17**,** 833-843.

76.   Davies, K.P., Carruthers, V.B. and Cross, G.A. (1997) Manipulation of the vsg co-transposed region increases expression-site switching in *Trypanosoma brucei*. *Mol Biochem Parasitol*, 86**,** 163-177.

77. Michels, P.A., Van der Ploeg, L.H., Liu, A.Y. and Borst, P. (1984) The inactivation and reactivation of an expression-linked gene copy for a variant surface glycoprotein in *Trypanosoma brucei*. *Embo J*, 3**,** 1345-1351.

78. Cross, M., Taylor, M.C. and Borst, P. (1998) Frequent loss of the active site during variant surface glycoprotein expression site switching in vitro in *Trypanosoma brucei*. *Mol Cell Biol*, 18**,** 198-205.

79. Barry, J.D. (1997) The relative significance of mechanisms of antigenic variation in African trypanosomes. *Parasitol Today*, 13**,** 212-218.

80. Valdes, J., Taylor, M.C., Cross, M.A., Ligtenberg, M.J., Rudenko, G. and Borst, P. (1996) The viral thymidine kinase gene as a tool for the study of mutagenesis in Trypanosoma brucei. *Nucleic Acids Res*, 24**,** 1809-1815.

81. Aitcheson, N., Talbot, S., Shapiro, J., Hughes, K., Adkin, C., Butt, T., Sheader, K. and Rudenko, G. (2005) VSG switching in *Trypanosoma brucei*: antigenic variation analysed using RNAi in the absence of immune selection. *Mol. Microbiol*, 57**,** 1608-1622.

82. Horn, D. and Cross, G.A.M. (1997) Analysis of *Trypanosoma brucei VSG* expression site switching *in vitro*. *Mol Biochem Parasitol*, 84**,** 189-201.

83. Chaves, I., Rudenko, G., Dirks-Mulder, A., Cross, M. and Borst, P. (1999) Control of variant surface glycoprotein gene-expression sites in Trypanosoma brucei. *Embo J*, 18**,** 4846-4855.

84. Ulbert, S., Chaves, I. and Borst, P. (2002) Expression site activation in Trypanosoma brucei with three marked variant surface glycoprotein gene expression sites. *Mol Biochem Parasitol*, 120**,** 225-235.

85. Conway, C., McCulloch, R., Ginger, M.L., Robinson, N.P., Browitt, A. and Barry, J.D. (2002) Ku is important for telomere maintenance, but not for differential expression of telomeric VSG genes, in African trypanosomes. *J Biol Chem*, 277**,** 21269-21277.

86. Robinson, N.P., McCulloch, R., Conway, C., Browitt, A. and Barry, J.D. (2002) Inactivation of Mre11 does not affect VSG gene duplication mediated by homologous recombination in *Trypanosoma brucei*. *J Biol Chem*, 277**,** 26185-26193.

87.   Shinohara, A., Ogawa, H. and Ogawa, T. (1992) Rad51 protein involved in repair and recombination in *S. cerevisiae* is a RecA-like protein. *Cell*, 69**,** 457-470.

88.   McCulloch, R. and Barry, J.D. (1999) A role for RAD51 and homologous recombination in *Trypanosoma brucei* antigenic variation. *Genes Dev*, 13**,** 2875-2888.

89.   Proudfoot, C. and McCulloch, R. (2005) Distinct roles for two RAD51-related genes in *Trypanosoma brucei* antigenic variation. *Nucleic Acids Res*, 33**,** 6906-6919.

90.   Turner, C.M. (1997) The rate of antigenic variation in fly-transmitted and syringe-passaged infections of *Trypanosoma brucei*. *FEMS Microbiol Lett*, 153**,** 227-231.

91.   Turner, C.M. and Barry, J.D. (1989) High frequency of antigenic variation in *Trypanosoma brucei rhodesiense* infections. *Parasitology*, 99 Pt 1**,** 67-75.

92.   van Deursen, F.J., Shahi, S.K., Turner, C.M., Hartmann, C., Guerra-Giraldez, C., Matthews, K.R. and Clayton, C.E. (2001) Characterisation of the growth and differentiation in vivo and in vitro-of bloodstream-form *Trypanosoma brucei* strain TREU 927. *Mol Biochem Parasitol*, 112**,** 163-171.

93.   Sunkin, S.M. and Stringer, J.R. (1996) Translocation of surface antigen genes to a unique telomeric expression site in *Pneumocystis carinii*. *Mol Microbiol*, 19**,** 283-295.

94.   Barbour, A.G. and Garon, C.F. (1987) Linear plasmids of the bacterium *Borrelia burgdorferi* have covalently closed ends. *Science*, 237**,** 409-411.

95.   Scherf, A., Figueiredo, L.M. and Freitas-Junior, L.H. (2001) Plasmodium telomeres: a pathogen's perspective. *Curr Opin Microbiol*, 4**,** 409-414.

96.   Linardopoulou, E.V., Williams, E.M., Fan, Y., Friedman, C., Young, J.M. and Trask, B.J. (2005) Human subtelomeres are hot spots of interchromosomal recombination and segmental duplication. *Nature*, 437**,** 94-100.

97.   Blackburn, E.H. and Gall, J.G. (1978) A tandemly repeated sequence at the termini of the extrachromosomal ribosomal RNA genes in *Tetrahymena*. *J Mol Biol*, 120**,** 33-53.

98.	Blackburn, E.H. and Challoner, P.B. (1984) Identification of a telomeric DNA sequence in *Trypanosoma brucei*. *Cell*, 36**,** 447-457.

99.	Moyzis, R.K., Buckingham, J.M., Cram, L.S., Dani, M., Deaven, L.L., Jones, M.D., Meyne, J., Ratliff, R.L. and Wu, J.R. (1988) A highly conserved repetitive DNA sequence, (TTAGGG)n, present at the telomeres of human chromosomes. *Proc Natl Acad Sci U S A*, 85**,** 6622-6626.

100.	Griffith, J.D., Comeau, L., Rosenfield, S., Stansel, R.M., Bianchi, A., Moss, H. and de Lange, T. (1999) Mammalian telomeres end in a large duplex loop. *Cell*, 97**,** 503-514.

101.	Munoz-Jordan, J.L., Cross, G.A.M., de Lange, T. and Griffith, J.D. (2001) t-loops at trypanosome telomeres. *EMBO J*, 20**,** 579-588.

102.	Murti, K.G. and Prescott, D.M. (1999) Telomeres of polytene chromosomes in a ciliated protozoan terminate in duplex DNA loops. *Proc Natl Acad Sci USA*, 96**,** 14436-14439.

103.	Cesare, A.J., Quinney, N., Willcox, S., Subramanian, D. and Griffith, J.D. (2003) Telomere looping in *P. sativum* (common garden pea). *Plant J*, 36**,** 271-279.

104.	Griffith, J., Bianchi, A. and de Lange, T. (1998) TRF1 promotes parallel pairing of telomeric tracts in vitro. *J Mol Biol*, 278**,** 79-88.

105.	Stansel, R.M., de Lange, T. and Griffith, J.D. (2001) T-loop assembly in vitro involves binding of TRF2 near the 3' telomeric overhang. *EMBO J*, 20**,** 5532-5540.

106.	van Steensel, B., Smogorzewska, A. and de Lange, T. (1998) TRF2 protects human telomeres from end-to-end fusions. *Cell*, 92**,** 401-413.

107.	de Lange, T. (2002) Protection of mammalian telomeres. *Oncogene*, 21**,** 532-540.

108.	de Lange, T. (2004) T-loops and the origin of telomeres. *Nat. Rev. Mol. Cell. Biol.*, 5**,** 323-329.

109.	Wellinger, R.J., Wolf, A.J. and Zakian, V.A. (1993) Saccharomyces telomeres acquire single-strand TG1-3 tails late in S phase. *Cell*, 72**,** 51-60.

110. McElligott, R. and Wellinger, R.J. (1997) The terminal DNA structure of mammalian chromosomes. *EMBO J*, 16**,** 3705-3714.

111. Makarov, V.L., Hirose, Y. and Langmore, J.P. (1997) Long G tails at both ends of human chromosomes suggest a C strand degradation mechanism for telomere shortening. *Cell*, 88**,** 657-666.

112. Watson, J.D. (1972) Origin of concatemeric T7 DNA. *Nat New Biol*, 239**,** 197-201.

113. Olovnikov, A.M. (1973) A theory of marginotomy. The incomplete copying of template margin in enzymic synthesis of polynucleotides and biological significance of the phenomenon. *J Theor Biol*, 41**,** 181-190.

114. Harley, C.B., Futcher, A.B. and Greider, C.W. (1990) Telomeres shorten during ageing of human fibroblasts. *Nature*, 345**,** 458-460.

115. Cooke, H.J. and Smith, B.A. (1986) Variability at the telomeres of the human X/Y pseudoautosomal region. *Cold Spring Harb Symp Quant Biol*, 51 Pt 1**,** 213-219.

116. Huffman, K.E., Levene, S.D., Tesmer, V.M., Shay, J.W. and Wright, W.E. (2000) Telomere shortening is proportional to the size of the G-rich telomeric 3'-overhang. *J Biol Chem*, 275**,** 19719-19722.

117. Wright, W.E., Tesmer, V.M., Huffman, K.E., Levene, S.D. and Shay, J.W. (1997) Normal human chromosomes have long G-rich telomeric overhangs at one end. *Genes Dev*, 11**,** 2801-2809.

118. Karlseder, J., Smogorzewska, A. and de Lange, T. (2002) Senescence induced by altered telomere state, not telomere loss. *Science*, 295**,** 2446-2449.

119. Wellinger, R.J., Ethier, K., Labrecque, P. and Zakian, V.A. (1996) Evidence for a new step in telomere maintenance. *Cell*, 85**,** 423-433.

120. Larrivee, M., LeBel, C. and Wellinger, R.J. (2004) The generation of proper constitutive G-tails on yeast telomeres is dependent on the MRX complex. *Genes Dev*, 18**,** 1391-1396.

121. Lundblad, V. and Szostak, J.W. (1989) A mutant with a defect in telomere elongation leads to senescence in yeast. *Cell*, 57**,** 633-643.

122. Singer, M.S. and Gottschling, D.E. (1994) TLC1: template RNA component of *Saccharomyces cerevisiae* telomerase. *Science*, 266, 404-409.

123. Levis, R.W., Ganesan, R., Houtchens, K., Tolar, L.A. and Sheen, F.M. (1993) Transposons in place of telomeric repeats at a *Drosophila* telomere. *Cell*, 75, 1083-1093.

124. Greider, C.W. and Blackburn, E.H. (1985) Identification of a specific telomere terminal transferase activity in *Tetrahymena* extracts. *Cell*, 43, 405-413.

125. Greider, C.W. and Blackburn, E.H. (1987) The telomere terminal transferase of *Tetrahymena* is a ribonucleoprotein enzyme with two kinds of primer specificity. *Cell*, 51, 887-898.

126. Greider, C.W. and Blackburn, E.H. (1989) A telomeric sequence in the RNA of *Tetrahymena* telomerase required for telomere repeat synthesis. *Nature*, 337, 331-337.

127. Lingner, J., Hendrick, L.L. and Cech, T.R. (1994) Telomerase RNAs of different ciliates have a common secondary structure and a permuted template. *Genes Dev*, 8, 1984-1998.

128. Romero, D.P. and Blackburn, E.H. (1991) A conserved secondary structure for telomerase RNA. *Cell*, 67, 343-353.

129. Chen, J.L., Blasco, M.A. and Greider, C.W. (2000) Secondary structure of vertebrate telomerase RNA. *Cell*, 100, 503-514.

130. Blasco, M.A., Funk, W., Villeponteau, B. and Greider, C.W. (1995) Functional characterization and developmental regulation of mouse telomerase RNA. *Science*, 269, 1267-1270.

131. Fulton, T.B. and Blackburn, E.H. (1998) Identification of *Kluyveromyces lactis* telomerase: discontinuous synthesis along the 30-nucleotide-long templating domain. *Mol Cell Biol*, 18, 4961-4970.

132. Zappulla, D.C. and Cech, T.R. (2004) Yeast telomerase RNA: a flexible scaffold for protein subunits. *Proc Natl Acad Sci U S A*, 101, 10024-10029.

133. Lin, J., Ly, H., Hussain, A., Abraham, M., Pearl, S., Tzfati, Y., Parslow, T.G. and Blackburn, E.H. (2004) A universal telomerase RNA core structure

includes structured motifs required for binding the telomerase reverse transcriptase protein. *Proc Natl Acad Sci U S A*, 101**,** 14713-14718.

134. Dandjinou, A.T., Levesque, N., Larose, S., Lucier, J.F., Abou Elela, S. and Wellinger, R.J. (2004) A phylogenetically based secondary structure for the yeast telomerase RNA. *Curr Biol*, 14**,** 1148-1158.

135. Zuker, M. (2003) Mfold web server for nucleic acid folding and hybridization prediction. *Nucleic Acids Res*, 31**,** 3406-3415.

136. Seto, A.G., Livengood, A.J., Tzfati, Y., Blackburn, E.H. and Cech, T.R. (2002) A bulged stem tethers Est1p to telomerase RNA in budding yeast. *Genes Dev*, 16**,** 2800-2812.

137. Stellwagen, A.E., Haimberger, Z.W., Veatch, J.R. and Gottschling, D.E. (2003) Ku interacts with telomerase RNA to promote telomere addition at native and broken chromosome ends. *Genes Dev*, 17**,** 2384-2395.

138. Marrone, A., Walne, A. and Dokal, I. (2005) Dyskeratosis congenita: telomerase, telomeres and anticipation. *Curr Opin Genet Dev*, 15**,** 249-257.

139. Vulliamy, T., Marrone, A., Goldman, F., Dearlove, A., Bessler, M., Mason, P.J. and Dokal, I. (2001) The RNA component of telomerase is mutated in autosomal dominant dyskeratosis congenita. *Nature*, 413**,** 432-435.

140. Lingner, J. and Cech, T.R. (1996) Purification of telomerase from *Euplotes aediculatus*: requirement of a primer 3' overhang. *Proc Natl Acad Sci U S A*, 93**,** 10712-10717.

141. Prescott, D.M. (2000) Genome gymnastics: unique modes of DNA evolution and processing in ciliates. *Nat Rev Genet*, 1**,** 191-198.

142. Klobutcher, L.A., Swanton, M.T., Donini, P. and Prescott, D.M. (1981) All gene-sized DNA molecules in four species of hypotrichs have the same terminal sequence and an unusual 3' terminus. *Proc Natl Acad Sci U S A*, 78**,** 3015-3019.

143. Lingner, J., Hughes, T.R., Shevchenko, A., Mann, M., Lundblad, V. and Cech, T.R. (1997) Reverse transcriptase motifs in the catalytic subunit of telomerase. *Science*, 276**,** 561-567.

144. Nakamura, T.M., Morin, G.B., Chapman, K.B., Weinrich, S.L., Andrews, W.H., Lingner, J., Harley, C.B. and Cech, T.R. (1997) Telomerase catalytic subunit homologs from fission yeast and human. *Science*, 277**,** 955-959.

145. Meyerson, M., Counter, C.M., Eaton, E.N., Ellisen, L.W., Steiner, P., Caddle, S.D., Ziaugra, L., Beijersbergen, R.L., Davidoff, M.J., Liu, Q. et al. (1997) hEST2, the putative human telomerase catalytic subunit gene, is up-regulated in tumor cells and during immortalization. *Cell*, 90**,** 785-795.

146. Armbruster, B.N., Banik, S.S., Guo, C., Smith, A.C. and Counter, C.M. (2001) N-terminal domains of the human telomerase catalytic subunit required for enzyme activity in vivo. *Mol Cell Biol*, 21**,** 7775-7786.

147. Lai, C.K., Mitchell, J.R. and Collins, K. (2001) RNA binding domain of telomerase reverse transcriptase. *Mol Cell Biol*, 21**,** 990-1000.

148. Wenz, C., Enenkel, B., Amacker, M., Kelleher, C., Damm, K. and Lingner, J. (2001) Human telomerase contains two cooperating telomerase RNA molecules. *EMBO J*, 20**,** 3526-3534.

149. Beattie, T.L., Zhou, W., Robinson, M.O. and Harrington, L. (2001) Functional multimerization of the human telomerase reverse transcriptase. *Mol Cell Biol*, 21**,** 6151-6160.

150. Arai, K., Masutomi, K., Khurts, S., Kaneko, S., Kobayashi, K. and Murakami, S. (2002) Two independent regions of human telomerase reverse transcriptase are important for its oligomerization and telomerase activity. *J Biol Chem*, 277**,** 8538-8544.

151. Kelleher, C., Teixeira, M.T., Forstemann, K. and Lingner, J. (2002) Telomerase: biochemical considerations for enzyme and substrate. *Trends Biochem Sci*, 27**,** 572-579.

152. Kim, N.W., Piatyszek, M.A., Prowse, K.R., Harley, C.B., West, M.D., Ho, P.L., Coviello, G.M., Wright, W.E., Weinrich, S.L. and Shay, J.W. (1994) Specific association of human telomerase activity with immortal cells and cancer. *Science*, 266**,** 2011-2015.

153. Greider, C.W. (1991) Telomerase is processive. *Mol Cell Biol*, 11**,** 4572-4580.

154. de Lange, T. (1994) Activation of telomerase in a human tumor. *Proc Natl Acad Sci U S A*, 91**,** 2882-2885.

155. Sharpless, N.E. and DePinho, R.A. (2004) Telomeres, stem cells, senescence, and cancer. *J Clin Invest*, 113**,** 160-168.

156. Bodnar, A.G., Ouellette, M., Frolkis, M., Holt, S.E., Chiu, C.P., Morin, G.B., Harley, C.B., Shay, J.W., Lichtsteiner, S. and Wright, W.E. (1998) Extension of life-span by introduction of telomerase into normal human cells. *Science*, 279**,** 349-352.

157. Hahn, W.C., Counter, C.M., Lundberg, A.S., Beijersbergen, R.L., Brooks, M.W. and Weinberg, R.A. (1999) Creation of human tumour cells with defined genetic elements. *Nature*, 400**,** 464-468.

158. Hanahan, D. and Weinberg, R.A. (2000) The hallmarks of cancer. *Cell*, 100**,** 57-70.

159. Hahn, W.C., Stewart, S.A., Brooks, M.W., York, S.G., Eaton, E., Kurachi, A., Beijersbergen, R.L., Knoll, J.H., Meyerson, M. and Weinberg, R.A. (1999) Inhibition of telomerase limits the growth of human cancer cells. *Nat Med*, 5**,** 1164-1170.

160. Damm, K., Hemmann, U., Garin-Chesa, P., Hauel, N., Kauffmann, I., Priepke, H., Niestroj, C., Daiber, C., Enenkel, B., Guilliard, B. et al. (2001) A highly selective telomerase inhibitor limiting human cancer cell proliferation. *EMBO J*, 20**,** 6958-6968.

161. White, L.K., Wright, W.E. and Shay, J.W. (2001) Telomerase inhibitors. *Trends Biotechnol*, 19**,** 114-120.

162. Marcand, S., Gilson, E. and Shore, D. (1997) A protein-counting mechanism for telomere length regulation in yeast. *Science*, 275**,** 986-990.

163. Marcand, S., Brevet, V. and Gilson, E. (1999) Progressive cis-inhibition of telomerase upon telomere elongation. *EMBO J*, 18**,** 3509-3519.

164. Teixeira, M.T., Arneric, M., Sperisen, P. and Lingner, J. (2004) Telomere length homeostasis is achieved via a switch between telomerase- extendible and -nonextendible states. *Cell*, 117**,** 323-335.

165. Krauskopf, A. and Blackburn, E.H. (1996) Control of telomere growth by interactions of RAP1 with the most distal telomeric repeats. *Nature*, 383**,** 354-357.

166. Barnett, M.A., Buckle, V.J., Evans, E.P., Porter, A.C., Rout, D., Smith, A.G. and Brown, W.R. (1993) Telomere directed fragmentation of mammalian chromosomes. *Nucleic Acids Res*, 21**,** 27-36.

167. Chong, L., van Steensel, B., Broccoli, D., Erdjument-Bromage, H., Hanish, J., Tempst, P. and de Lange, T. (1995) A human telomeric protein. *Science*, 270**,** 1663-1667.

168. Bianchi, A., Stansel, R.M., Fairall, L., Griffith, J.D., Rhodes, D. and de Lange, T. (1999) TRF1 binds a bipartite telomeric site with extreme spatial flexibility. *EMBO J*, 18**,** 5735-5744.

169. Ye, J.Z., Donigian, J.R., van Overbeek, M., Loayza, D., Luo, Y., Krutchinsky, A.N., Chait, B.T. and de Lange, T. (2004) TIN2 Binds TRF1 and TRF2 Simultaneously and Stabilizes the TRF2 Complex on Telomeres. *J Biol Chem*, 279**,** 47264-47271.

170. Ye, J.Z., Hockemeyer, D., Krutchinsky, A.N., Loayza, D., Hooper, S.M., Chait, B.T. and de Lange, T. (2004) POT1-interacting protein PIP1: a telomere length regulator that recruits POT1 to the TIN2/TRF1 complex. *Genes Dev*, 18**,** 1649-1654.

171. Loayza, D. and De Lange, T. (2003) POT1 as a terminal transducer of TRF1 telomere length control. *Nature*, 423**,** 1013-1018.

172. Zhu, X.D., Kuster, B., Mann, M., Petrini, J.H. and de Lange, T. (2000) Cell-cycle-regulated association of RAD50/MRE11/NBS1 with TRF2 and human telomeres. *Nat Genet*, 25**,** 347-352.

173. van Steensel, B. and de Lange, T. (1997) Control of telomere length by the human telomeric protein TRF1. *Nature*, 385**,** 740-743.

174. Smith, S., Giriat, I., Schmitt, A. and de Lange, T. (1998) Tankyrase, a poly(ADP-ribose) polymerase at human telomeres. *Science*, 282**,** 1484-1487.

175. Smith, S. and de Lange, T. (2000) Tankyrase promotes telomere elongation in human cells. *Curr Biol*, 10**,** 1299-1302.

176. Chang, W., Dynek, J.N. and Smith, S. (2003) TRF1 is degraded by ubiquitin-mediated proteolysis after release from telomeres. *Genes Dev*, 17**,** 1328-1333.

177. Kim, S.H., Kaminker, P. and Campisi, J. (1999) TIN2, a new regulator of telomere length in human cells. *Nat Genet*, 23**,** 405-412.

178. Ye, J.Z. and de Lange, T. (2004) TIN2 is a tankyrase 1 PARP modulator in the TRF1 telomere length control complex. *Nat Genet*, 36**,** 618-623.

179. Price, C.M. and Cech, T.R. (1987) Telomeric DNA-protein interactions of Oxytricha macronuclear DNA. *Genes Dev*, 1**,** 783-793.

180. Baumann, P. and Cech, T.R. (2001) Pot1, the putative telomere end-binding protein in fission yeast and humans. *Science*, 292**,** 1171-1175.

181. Kelleher, C., Kurth, I. and Lingner, J. (2005) Human protection of telomeres 1 (POT1) is a negative regulator of telomerase activity in vitro. *Mol Cell Biol*, 25**,** 808-818.

182. Garvik, B., Carson, M. and Hartwell, L. (1995) Single-stranded DNA arising at telomeres in cdc13 mutants may constitute a specific signal for the RAD9 checkpoint. *Mol Cell Biol*, 15**,** 6128-6138.

183. Nugent, C.I., Hughes, T.R., Lue, N.F. and Lundblad, V. (1996) Cdc13p: a single-strand telomeric DNA-binding protein with a dual role in yeast telomere maintenance. *Science*, 274**,** 249-252.

184. Grandin, N., Damon, C. and Charbonneau, M. (2001) Ten1 functions in telomere end protection and length regulation in association with Stn1 and Cdc13. *EMBO J*, 20**,** 1173-1183.

185. Pennock, E., Buckley, K. and Lundblad, V. (2001) Cdc13 delivers separate complexes to the telomere for end protection and replication. *Cell*, 104**,** 387-396.

186. Qi, H. and Zakian, V.A. (2000) The Saccharomyces telomere-binding protein Cdc13p interacts with both the catalytic subunit of DNA polymerase alpha and the telomerase-associated est1 protein. *Genes Dev*, 14**,** 1777-1788.

187. Taggart, A.K., Teng, S.C. and Zakian, V.A. (2002) Est1p as a cell cycle-regulated activator of telomere-bound telomerase. *Science*, 297**,** 1023-1026.

188. Spellman, P.T., Sherlock, G., Zhang, M.Q., Iyer, V.R., Anders, K., Eisen, M.B., Brown, P.O., Botstein, D. and Futcher, B. (1998) Comprehensive identification of cell cycle-regulated genes of the yeast *Saccharomyces cerevisiae* by microarray hybridization. *Mol Biol Cell*, 9**,** 3273-3297.

189. Marcand, S., Brevet, V., Mann, C. and Gilson, E. (2000) Cell cycle restriction of telomere elongation. *Curr Biol*, 10**,** 487-490.

190. Peterson, S.E., Stellwagen, A.E., Diede, S.J., Singer, M.S., Haimberger, Z.W., Johnson, C.O., Tzoneva, M. and Gottschling, D.E. (2001) The function of a stem-loop in telomerase RNA is linked to the DNA repair protein Ku. *Nat Genet*, 27**,** 64-67.

191. Fisher, T.S., Taggart, A.K. and Zakian, V.A. (2004) Cell cycle-dependent regulation of yeast telomerase by Ku. *Nat Struct Mol Biol*, 11**,** 1198-1205.

192. Smogorzewska, A., Karlseder, J., Holtgreve-Grez, H., Jauch, A. and de Lange, T. (2002) DNA ligase IV-dependent NHEJ of deprotected mammalian telomeres in G1 and G2. *Curr Biol*, 12**,** 1635-1644.

193. Karlseder, J., Broccoli, D., Dai, Y., Hardy, S. and de Lange, T. (1999) p53- and ATM-dependent apoptosis induced by telomeres lacking TRF2. *Science*, 283**,** 1321-1325.

194. Reddel, R.R. (2003) Alternative lengthening of telomeres, telomerase, and cancer. *Cancer Lett*, 194**,** 155-162.

195. Lundblad, V. (2002) Telomere maintenance without telomerase. *Oncogene*, 21**,** 522-531.

196. Maringele, L. and Lydall, D. (2004) Telomerase- and recombination-independent immortalization of budding yeast. *Genes Dev*, 18**,** 2663-2675.

197. Nakamura, T.M., Cooper, J.P. and Cech, T.R. (1998) Two modes of survival of fission yeast without telomerase. *Science*, 282**,** 493-496.

198. Bryan, T.M., Englezou, A., Gupta, J., Bacchetti, S. and Reddel, R.R. (1995) Telomere elongation in immortal human cells without detectable telomerase activity. *EMBO J*, 14**,** 4240-4248.

199.   Dunham, M.A., Neumann, A.A., Fasching, C.L. and Reddel, R.R. (2000) Telomere maintenance by recombination in human cells. *Nat Genet*, 26**,** 447-450.

200.   Cesare, A.J. and Griffith, J.D. (2004) Telomeric DNA in ALT cells Is characterized by free telomeric circles and heterogeneous t-loops. *Mol Cell Biol*, 24**,** 9948-9957.

201.   Wang, R.C., Smogorzewska, A. and de Lange, T. (2004) Homologous recombination generates T-loop-sized deletions at human telomeres. *Cell*, 119**,** 355-368.

202.   Bernards, A., Michels, P.A., Lincke, C.R. and Borst, P. (1983) Growth of chromosome ends in multiplying trypanosomes. *Nature*, 303**,** 592-597.

203.   Pays, E., Laurent, M., Delinte, K., Van Meirvenne, N. and Steinert, M. (1983) Differential size variations between transcriptionally active and inactive telomeres of *Trypanosoma brucei*. *Nucleic Acids Res*, 11**,** 8137-8147.

204.   Van der Ploeg, L.H., Liu, A.Y. and Borst, P. (1984) Structure of the growing telomeres of Trypanosomes. *Cell*, 36**,** 459-468.

205.   Li, B. and Lustig, A.J. (1996) A novel mechanism for telomere size control in *Saccharomyces cerevisiae*. *Genes Dev*, 10**,** 1310-1326.

206.   Myler, P.J., Aline, R.F., Jr., Scholler, J.K. and Stuart, K.D. (1988) Changes in telomere length associated with antigenic variation in *Trypanosoma brucei*. *Mol Biochem Parasitol*, 29**,** 243-250.

207.   Van der Werf, A., Van Assel, S., Aerts, D., Steinert, M. and Pays, E. (1990) Telomere interactions may condition the programming of antigen expression in *Trypanosoma brucei*. *EMBO J*, 9**,** 1035-1040.

208.   Chiurillo, M.A., Peralta, A. and Ramirez, J.L. (2002) Comparative study of *Trypanosoma rangeli* and *Trypanosoma cruzi* telomeres. *Mol Biochem Parasitol*, 120**,** 305-308.

209.   Cano, M.I., Dungan, J.M., Agabian, N. and Blackburn, E.H. (1999) Telomerase in kinetoplastid parasitic protozoa. *Proc Natl Acad Sci U S A*, 96**,** 3616-3621.

210. Chiurillo, M.A., Santos, M.R., Franco Da Silveira, J. and Ramirez, J.L. (2002) An improved general approach for cloning and characterizing telomeres: the protozoan parasite *Trypanosoma cruzi* as model organism. *Gene*, 294**,** 197-204.

211. Conte, F.F. and Cano, M.I. (2005) Genomic organization of telomeric and subtelomeric sequences of *Leishmania (Leishmania) amazonensis*. *Int J Parasitol*, 35**,** 1435-1443.

212. Chiurillo, M.A., Beck, A.E., Devos, T., Myler, P.J., Stuart, K. and Ramirez, J.L. (2000) Cloning and characterization of *Leishmania donovani* telomeres. *Exp Parasitol*, 94**,** 248-258.

213. Chiurillo, M.A. and Ramirez, J.L. (2002) Characterization of *Leishmania major* Friedlin telomeric terminus. *Mem Inst Oswaldo Cruz*, 97**,** 343-346.

214. Fu, G. and Barker, D.C. (1998) Characterisation of Leishmania telomeres reveals unusual telomeric repeats and conserved telomere-associated sequence. *Nucleic Acids Res*, 26**,** 2161-2167.

215. Freitas-Junior, L.H., Porto, R.M., Pirrit, L.A., Schenkman, S. and Scherf, A. (1999) Identification of the telomere in *Trypanosoma cruzi* reveals highly heterogeneous telomere lengths in different parasite strains. *Nucleic Acids Res*, 27**,** 2451-2456.

216. Chiurillo, M.A., Cano, I., Da Silveira, J.F. and Ramirez, J.L. (1999) Organization of telomeric and sub-telomeric regions of chromosomes from the protozoan parasite *Trypanosoma cruzi*. *Mol Biochem Parasitol*, 100**,** 173-183.

217. Gatbonton, T., Imbesi, M., Nelson, M., Akey, J.M., Ruderfer, D.M., Kruglyak, L., Simon, J.A. and Bedalov, A. (2006) Telomere Length as a Quantitative Trait: Genome-Wide Survey and Genetic Mapping of Telomere Length-Control Genes in Yeast. *PLoS Genet*, 2**,** e35.

218. Hemann, M.T. and Greider, C.W. (2000) Wild-derived inbred mouse strains have short telomeres. *Nucleic Acids Res*, 28**,** 4474-4478.

219. Eid, J.E. and Sollner-Webb, B. (1995) ST-1, a 39-kilodalton protein in *Trypanosoma brucei*, exhibits a dual affinity for the duplex form of the 29-

base-pair subtelomeric repeat and its C-rich strand. *Mol Cell Biol*, 15, **389-** 397.

220. Eid, J.E. and Sollner-Webb, B. (1997) ST-2, a telomere and subtelomere duplex and G-strand binding protein activity in *Trypanosoma brucei*. *J Biol Chem*, 272, **14927-14936.**

221. Field, H. and Field, M.C. (1996) Leptomonas seymouri, *Trypanosoma brucei*: a method for isolating trypanosomatid nuclear factors which bind T. brucei single-stranded g-rich telomere sequence. *Exp Parasitol*, 83, **155-158.**

222. Berberof, M., Vanhamme, L., Alexandre, S., Lips, S., Tebabi, P. and Pays, E. (2000) A single-stranded DNA-binding protein shared by telomeric repeats, the variant surface glycoprotein transcription promoter and the procyclin transcription terminator of *Trypanosoma brucei*. *Nucleic Acids Res*, 28, **597-** 604.

223. Cano, M.I., Blake, J.J., Blackburn, E.H. and Agabian, N. (2002) A *Trypanosoma brucei* protein complex that binds G-overhangs and co-purifies with telomerase activity. *J Biol Chem*, 277, **896-906.**

224. Fernandez, M.F., Castellari, R.R., Conte, F.F., Gozzo, F.C., Sabino, A.A., Pinheiro, H., Novello, J.C., Eberlin, M.N. and Cano, M.I. (2004) Identification of three proteins that associate in vitro with the *Leishmania (Leishmania) amazonensis* G-rich telomeric strand. *Eur J Biochem*, 271, **3050-3063.**

225. Boulton, S.J. and Jackson, S.P. (1996) Identification of a *Saccharomyces cerevisiae* Ku80 homologue: roles in DNA double strand break rejoining and in telomeric maintenance. *Nucleic Acids Res*, 24, **4639-4648.**

226. Downs, J.A. and Jackson, S.P. (2004) A means to a DNA end: the many roles of Ku. *Nat Rev Mol Cell Biol*, 5, **367-378.**

227. Gravel, S., Larrivee, M., Labrecque, P. and Wellinger, R.J. (1998) Yeast Ku as a regulator of chromosomal DNA end structure. *Science*, 280, **741-744.**

228. Laroche, T., Martin, S.G., Gotta, M., Gorham, H.C., Pryde, F.E., Louis, E.J. and Gasser, S.M. (1998) Mutation of yeast Ku genes disrupts the subnuclear organization of telomeres. *Curr Biol*, 8, **653-656.**

229. Galy, V., Olivo-Marin, J.C., Scherthan, H., Doye, V., Rascalou, N. and Nehrbass, U. (2000) Nuclear pore complexes in the organization of silent telomeric chromatin. *Nature*, 403**,** 108-112.

230. Li, B., Espinal, A. and Cross, G.A. (2005) Trypanosome telomeres are protected by a homologue of mammalian TRF2. *Mol Cell Biol*, 25**,** 5011-5021.

231. Horn, D., Spence, C. and Ingram, A.K. (2000) Telomere maintenance and length regulation in *Trypanosoma brucei*. *EMBO J*, 19**,** 2332-2339.

232. Munoz, D.P. and Collins, K. (2004) Biochemical properties of *Trypanosoma cruzi* telomerase. *Nucleic Acids Res*, 32**,** 5214-5222.

233. Stevens, J.R. and Gibson, W. (1999) The molecular evolution of trypanosomes. *Parasitol Today*, 15**,** 432-437.

234. Cimino-Reale, G., Pascale, E., Alvino, E., Starace, G. and D'Ambrosio, E. (2003) Long telomeric C-rich 5'-tails in human replicating cells. *J Biol Chem*, 278**,** 2136-2140.

235. Riha, K., McKnight, T.D., Fajkus, J., Vyskot, B. and Shippen, D.E. (2000) Analysis of the G-overhang structures on plant telomeres: evidence for two distinct telomere architectures. *Plant J*, 23**,** 633-641.

236. Wong, K.K., Maser, R.S., Bachoo, R.M., Menon, J., Carrasco, D.R., Gu, Y., Alt, F.W. and DePinho, R.A. (2003) Telomere dysfunction and Atm deficiency compromises organ homeostasis and accelerates ageing. *Nature*, 421**,** 643-648.

237. Chen, Q., Ijpma, A. and Greider, C.W. (2001) Two survivor pathways that allow growth in the absence of telomerase are generated by distinct telomere recombination events. *Mol Cell Biol*, 21**,** 1819-1827.

238. Teng, S.C. and Zakian, V.A. (1999) Telomere-telomere recombination is an efficient bypass pathway for telomere maintenance in *Saccharomyces cerevisiae*. *Mol Cell Biol*, 19**,** 8083-8093.

239. McEachern, M.J. and Haber, J.E. (2006) Break-Induced Replication and Recombinational Telomere Elongation in Yeast. *Annu Rev Biochem*.

240. Alsford, N.S., Navarro, M., Jamnadass, H.R., Dunbar, H., Ackroyd, M., Murphy, N.B., Gull, K. and Ersfeld, K. (2003) The identification of circular extrachromosomal DNA in the nuclear genome of *Trypanosoma brucei*. *Mol. Microbiol*, 47**,** 277-289.

241. Myler, P.J., Aline, R.F., Jr., Scholler, J.K. and Stuart, K.D. (1988) Multiple events associated with antigenic switching in *Trypanosoma brucei*. *Mol Biochem Parasitol*, 29**,** 227-241.

242. Melville, S.E., Gerrard, C.S. and Blackwell, J.M. (1999) Multiple causes of size variation in the diploid megabase chromosomes of African trypanosomes. *Chromosome Res*, 7**,** 191-203.

243. Miller, K.M., Rog, O. and Cooper, J.P. (2006) Semi-conservative DNA replication through telomeres requires Taz1. *Nature*, 440**,** 824-828.

244. Forstemann, K., Hoss, M. and Lingner, J. (2000) Telomerase-dependent repeat divergence at the 3' ends of yeast telomeres. *Nucleic Acids Res*, 28**,** 2690-2694.

245. te Vruchte, D., Aitcheson, N. and Rudenko, G. (2003) Downregulation of *Trypanosoma brucei* VSG expression site promoters on circular bacterial artificial chromosomes. *Mol Biochem Parasitol*, 128**,** 123-133.

246. Ersfeld, K. and Gull, K. (1997) Partitioning of large and minichromosomes in *Trypanosoma brucei*. *Science*, 276**,** 611-614.

247. Gull, K., Alsford, S. and Ersfeld, K. (1998) Segregation of minichromosomes in trypanosomes: implications for mitotic mechanisms. *Trends Microbiol*, 6**,** 319-323.

248. Chung, H.M., Shea, C., Fields, S., Taub, R.N., Van der Ploeg, L.H. and Tse, D.B. (1990) Architectural organization in the interphase nucleus of the protozoan *Trypanosoma brucei*: location of telomeres and mini-chromosomes. *EMBO J*, 9**,** 2611-2619.

249. Chikashige, Y., Ding, D.Q., Funabiki, H., Haraguchi, T., Mashiko, S., Yanagida, M. and Hiraoka, Y. (1994) Telomere-led premeiotic chromosome movement in fission yeast. *Science*, 264**,** 270-273.

250. Chikashige, Y., Ding, D.Q., Imai, Y., Yamamoto, M., Haraguchi, T. and Hiraoka, Y. (1997) Meiotic nuclear reorganization: switching the position of centromeres and telomeres in the fission yeast *Schizosaccharomyces pombe*. *EMBO J*, 16**,** 193-202.

251. Cooper, J.P., Watanabe, Y. and Nurse, P. (1998) Fission yeast Taz1 protein is required for meiotic telomere clustering and recombination. *Nature*, 392**,** 828-831.

252. Szostak, J.W. and Blackburn, E.H. (1982) Cloning yeast telomeres on linear plasmid vectors. *Cell*, 29**,** 245-255.

253. Murray, A.W. and Szostak, J.W. (1983) Pedigree analysis of plasmid segregation in yeast. *Cell*, 34**,** 961-970.

254. Lowell, J.E., Roughton, A.I., Lundblad, V. and Pillus, L. (2003) Telomerase-independent proliferation is influenced by cell type in *Saccharomyces cerevisiae*. *Genetics*, 164**,** 909-921.

255. Henson, J.D., Neumann, A.A., Yeager, T.R. and Reddel, R.R. (2002) Alternative lengthening of telomeres in mammalian cells. *Oncogene*, 21**,** 598-610.

256. Tomaska, L., McEachern, M.J. and Nosek, J. (2004) Alternatives to telomerase: keeping linear chromosomes via telomeric circles. *FEBS Lett*, 567**,** 142-146.

257. Perrem, K., Colgin, L.M., Neumann, A.A., Yeager, T.R. and Reddel, R.R. (2001) Coexistence of alternative lengthening of telomeres and telomerase in hTERT-transfected GM847 cells. *Mol Cell Biol*, 21**,** 3862-3875.

258. Cerone, M.A., Autexier, C., Londono-Vallejo, J.A. and Bacchetti, S. (2005) A human cell line that maintains telomeres in the absence of telomerase and of key markers of ALT. *Oncogene*, 24**,** 7893-7901.

259. Wirtz, E., Leal, S., Ochatt, C. and Cross, G.A.M. (1999) A tightly regulated inducible expression system for conditional gene knock-outs and dominant-negative genetics in *Trypanosoma brucei*. *Mol Biochem Parasitol*, 99**,** 89-101.

260. Smogorzewska, A. and de Lange, T. (2004) Regulation of telomerase by telomeric proteins. *Annu Rev Biochem*, 73**,** 177-208.

261. Rudenko, G. and Van der Ploeg, L.H. (1989) Transcription of telomere repeats in protozoa. *EMBO J*, 8**,** 2633-2638.

262. Kraus, E., Leung, W.Y. and Haber, J.E. (2001) Break-induced replication: a review and an example in budding yeast. *Proc Natl Acad Sci U S A*, 98**,** 8255-8262.

263. Holmes, A.M. and Haber, J.E. (1999) Double-strand break repair in yeast requires both leading and lagging strand DNA polymerases. *Cell*, 96**,** 415-424.

264. Rudenko, G., Chaves, I., Dirks-Mulder, A. and Borst, P. (1998) Selection for activation of a new variant surface glycoprotein gene expression site in *Trypanosoma brucei* can result in deletion of the old one. *Mol Biochem Parasitol*, 95**,** 97-109.

265. Dreesen, O., Li, B. and Cross, G.A.M. (2005) Telomere structure and shortening in telomerase-deficient *Trypanosoma brucei*. *Nucleic Acids Res*, 33**,** 4536-4543.

266. Lustig, A.J. (2003) Clues to catastrophic telomere loss in mammals from yeast telomere rapid deletion. *Nat Rev Genet*, 4**,** 916-923.

267. Kyrion, G., Boakye, K.A. and Lustig, A.J. (1992) C-terminal truncation of RAP1 results in the deregulation of telomere size, stability, and function in Saccharomyces cerevisiae. *Mol Cell Biol*, 12**,** 5159-5173.

268. Tan, K.S., Leal, S.T. and Cross, G.A. (2002) Trypanosoma brucei MRE11 is non-essential but influences growth, homologous recombination and DNA double-strand break repair. *Mol Biochem Parasitol*, 125**,** 11-21.

269. Aparicio, O.M., Billington, B.L. and Gottschling, D.E. (1991) Modifiers of position effect are shared between telomeric and silent mating-type loci in *S. cerevisiae*. *Cell*, 66**,** 1279-1287.

270. Zhang, J.R., Hardham, J.M., Barbour, A.G. and Norris, S.J. (1997) Antigenic variation in Lyme disease borreliae by promiscuous recombination of VMP-like sequence cassettes. *Cell*, 89**,** 275-285.

271. Kitten, T. and Barbour, A.G. (1990) Juxtaposition of expressed variable antigen genes with a conserved telomere in the bacterium *Borrelia hermsii*. *Proc Natl Acad Sci U S A*, 87**,** 6077-6081.

272. Vuk-Pavlovic, Z., Standing, J.E., Crouch, E.C. and Limper, A.H. (2001) Carbohydrate recognition domain of surfactant protein D mediates interactions with *Pneumocystis carinii* glycoprotein A. *Am J Respir Cell Mol Biol*, 24**,** 475-484.

273. Angus, C.W., Tu, A., Vogel, P., Qin, M. and Kovacs, J.A. (1996) Expression of variants of the major surface glycoprotein of *Pneumocystis carinii*. *J. Exp. Med.*, 183**,** 1229-1234.

274. Doyle, J.J., Hirumi, H., Hirumi, K., Lupton, E.N. and Cross, G.A.M. (1980) Antigenic variation in clones of animal-infective *Trypanosoma brucei* derived and maintained in vitro. *Parasitology*, 80**,** 359-369.

275. Hirumi, H. and Hirumi, K. (1989) Continuous cultivation of *Trypanosoma brucei* blood stream forms in a medium containing a low concentration of serum protein without feeder cell layers. *J Parasitol*, 75**,** 985-989.

276. de Lange, T. (1992) Human telomeres are attached to the nuclear matrix. *EMBO J*, 11**,** 717-724.

277. Baker, J.R., Sachs, R. and Laufer, I. (1967) Trypanosomes of wild mammals in an area northwest of the Sergenti National Park, Tanzania. *Z Tropenmed Parasitol*, 18**,** 280-284.

278. Geigy, R. and Kauffmann, M. (1973) Sleeping sickness survey in the Serengeti area (Tanzania) 1971. I. Examination of large mammals for trypanosomes. *Acta Trop*, 30**,** 12-23.

279. Cunningham, M.P. and Vickerman, K. (1962) Antigenic analysis in the *Trypanosoma brucei* group, using the agglutination reaction. *Trans R Soc Trop Med Hyg*, 56**,** 48-59.

280. Goedbloed, E., Ligthart, G.S., Minter, D.M., Wilson, A.J., Dar, F.K. and Paris, J. (1973) Serological studies of trypanosomiasis in East Africa. II. Comparisons of antigenic types of *Trypanosoma brucei* subgroup organisms isolated from wild tsetse flies. *Ann Trop Med Parasitol*, 67**,** 31-43.

281. Onyango, R.J., Van Hoeve, K. and De Raadt, P. (1966) The epidemiology of *Trypanosoma rhodesiense* sleeping sickness in Alego location, Central

Nyanza, Kenya. I. Evidence that cattle may act as reservoir hosts of trypanosomes infective to man. *Trans R Soc Trop Med Hyg*, 60**,** 175-182.

282. Jenni, L., Marti, S., Schweizer, J., Betschart, B., Le Page, R.W., Wells, J.M., Tait, A., Paindavoine, P., Pays, E. and Steinert, M. (1986) Hybrid formation between African trypanosomes during cyclical transmission. *Nature*, 322**,** 173-175.

283. Turner, C.M., Aslam, N., Smith, E., Buchanan, N. and Tait, A. (1991) The effects of genetic exchange on variable antigen expression in *Trypanosoma brucei*. *Parasitology*, 103 Pt 3**,** 379-386.

284. Felgner, P., Brinkmann, U., Zillmann, U., Mehlitz, D. and Abu-Ishira, S. (1981) Epidemiological studies on the animal reservoir of gambiense sleeping sickness. Part II. Parasitological and immunodiagnostic examination of the human population. *Tropenmed Parasitol*, 32**,** 134-140.

285. Haynes, P.A., Russell, D.G. and Cross, G.A. (1996) Subcellular localization of *Trypanosoma cruzi* glycoprotein Gp72. *J Cell Sci*, 109 (Pt 13)**,** 2979-2988.

286. Tyler, K.M. and Engman, D.M. (2000) Flagellar elongation induced by glucose limitation is preadaptive for *Trypanosoma cruzi* differentiation. *Cell Motil Cytoskeleton*, 46**,** 269-278.